University of Alberta

Mathematical Models for Cell Movement: Chemotaxis and Transport Models

by
Zhian Wang

A thesis submitted to the Faculty of Graduate Studies and Research
in partial fulfillment of the requirements for the degree of

Doctor of Philosophy

in

Applied Mathematics

Department of Mathematical and Statistical Sciences

Edmonton, Alberta

Fall 2007

Your file Votre référence
ISBN: 978-0-494-33090-6
Our file Notre référence
ISBN: 978-0-494-33090-6

Abstract

In this thesis, we study chemotaxis models and mesenchymal transport models. By a novel choice of the so called squeezing probability, we try to incorporate the semi-elastic properties of cells into the volume filling chemotaxis model and establish the global existence of solutions. For this choice of squeezing probability, we examine the stability of homogeneous equilibrium and analyze the underlying bifurcations. In addition, we present one-dimensional numerical simulations and observe merging and emerging process of pattern formation. For a chemotaxis model without diffusion of the chemical signal, we study the shock structures for both the attractive and the repulsive case. We show the existence of travelling waves and furthermore prove that the traveling speed is identical to the shock speed. Then we prove that the traveling waves converge to the shock waves when the viscosity of the system vanishes, which implies that the shock wave admits a structure. For the one-dimensional mesenchymal motion transport models, we provide a detailed analysis for the qualitative behavior of solutions. We establish the global existence of classical solutions and show the existence of weak limits of solutions to the parabolic and hyperbolic rescaled models. Moreover, we establish the existence of traveling wave solutions and nonexistence of pattern formation. Some new questions and research directions are proposed in the thesis.

Acknowledgements

I am deeply indebted to my supervisor, professor Thomas Hillen, for his strong support, continuous encouragement and invaluable advice throughout my Ph.D study in Edmonton. His constant passion for mathematics, nice personality and optimistic attitude deeply infected me and have maintained my enthusiasm for mathematics. I am very grateful to him for patiently reading and revising my thesis and unstinting enthusiasm toward my research and result. Without his help and support, I would not have been able to achieve all that I have over the past four years. It was my fortunate to have professor Thomas Hillen as my supervisor. I heartfelt appreciate him.

The Center for Mathematical Biology (CMB), founded by professor Mark Lewis, has proved a particularly enjoyable and friendly atmosphere in which to work. I have benefitted from many very thoughtful discussion with the CMB visitors and their excellent talks in the seminar of mathematical biology. I thank everybody in the CMB, in particular: Mark Lewis, Gerda de Vries, Cecilia Hutchinson, Marjorie Wonham, Caroline Bampfylde, Andria Dawson, Alex Potapov and Jung min Lee, Frank Hilker.

I especially thank professor Angela Steven and Dr. Yasmin Dolak for kindly inviting me to visit Max Plank Institute at Leipzig and University of Vienna in Austria. I sincerely appreciate them for their hospitality and financial support. I greatly appreciate professor Angela Stevens for her constant support and encourage which I treasured.

I am grateful to Dr. Kevin Painter at the Heriot-Watt University who generously provided some numerical codes for me. I also thank him for many stimulating discussion on my research and study. I thank Dr. Peter Hinow at the Vanderbilt University for very helpful discussion about mesenchymal transport models. I am grateful to Dr. Dariusz Wrzosek at the Warsaw University for remarks about *fast diffusion* problems.

I would like to extend my thanks to many visitors who give me many useful suggestions and comments on my research, including Rebacca Tyson, Michael Ward, Mark Chaplain, Benoît Perthema, Chris Cosner, Stephen Cantrell and Karl Hadeler.

I also would like to express my sincere appreciation to the faculty and staff of the Department of Mathematical and Statistical Science for providing me with ev-

erything I could ask for in the way of support. Special thank is due to professor Yanping Lin for his invaluable support and encouragement he offered, and for his unfailing willingness to help. I also appreciate professor William Page in the Department of Biology for spending much time in talking the modeling of chemotactic movement of A. vinelandii.

I wish to express my gratitude to many friends, Guangrui Li, Hongbin Guo, Jia Liu, Jingjing Wu, Jiafen Gong, Hong Sang, Matthew Emmett and Shawn Desaulniers, whose company is always a joy and an inspiration. I will miss the days when I stayed with them.

Finally, none of this would have been possible without the enduring love and faith of my parents and my two sisters. To them this work is dedicated.

TABLE OF CONTENTS

LIST OF FIGURES

Chapter 1

INTRODUCTION

A characteristic feature of living organisms is that they sense the environment in which they reside and response to it. The response generally involves movement toward or away from an external signal (stimulus), and such a response is called *taxis*, which originates from the Greek *taxis*, meaning to *arrange*. The purpose of taxis ranges from movement toward food and avoidance of noxious substances to large-scale aggregation for the purpose of survival. There are many types of taxis such as aerotaxis, chemotaxis, geotaxis, haptotaxis, and others (see [95]). Any taxis involves two major components: (1) an external signal and (2) the response of the organism to this signal. The response, in turn, involves two major steps: (i) detection of the signal and (ii) transduction of the external signal into an internal signal that controls the pattern of movement. In this thesis, I am primarily concerned with chemotaxis, which describes the characteristic movement or orientation of an organism or cell along a chemical concentration gradient. Depending on whether it is toward or away from the external signal that affects the pattern of movement, the external signal is characterized as chemoattractant or chemorepellent. The characteristic consequences of chemotaxis are cell aggregation and pattern formation. There are two major chemotaxis models. One is called Patlak-Keller-Segel (PKS) model due to the pioneering works by Patlak [101] as well as Keller and Segel [67, 68]. The other is called kinetic transport model which was proposed by Alt [2, 3] and further developed by Othmer *et al* [93]. The PKS type model is based on macroscopic scales and describes the collective behavior of particles which interact with external signals. The kinetic transport model, which describes the behavior of individual cells, can incorporate microscopic level information on cell signal transduction. These two type models have most extensively been studied in the literature of chemotaxis. The primary part of my thesis will be focused on some existing PKS type chemotaxis models and mesenchymal transport models, which were established in the literature [98, 95, 75, 47].

1.1 Main Results of the Thesis

This thesis is focused on the study of analytical and numerical properties of PKS type chemotaxis models and mesenchymal transport models. The organization of this thesis is as follows.

Chapter 1. This is an introductory chapter where I briefly discuss the motivation of the study and the main results obtained for each chapter. Also I make a survey of chemotaxis models and transport models, of some results already obtained for these models, and of the techniques involved.

Chapter 2. This chapter deals with the volume filling chemotaxis mode which incorporate the elastic properties of cells. The finite blow-up phenomenon of classical the PKS model has been widely studied in the literature, as seen in the next section. However, the blow-up solution is not consistent with pattern formation by bacteria and have limited biological relevance although it is of interest mathematically. It is therefore desirable to study biologically relevant and mathematically useful modifications of the classical chemotaxis model that allow the global existence of solutions. There are numerous mechanisms developed toward this end, including saturation effects (e.g. Othmer and Stevens [95], Rivero *et al,* [106], Aida *et al.* [1]), cell kinetics (e.g. Mimura and Tsujikawa [81], Osaki *et al.* [91]), attraction-repulsion mechanism (e.g. Luca *et al.* [78] and Hillen *et al* [55]), volume filling effect (e.g. Painter and Hillen [51, 98]), finite sampling radius (e.g. Hillen *et al.* [53]), nonlinear motility parameter and nonlinear chemosensitivity (e.g. Hortsmann [59]) and nonlinear diffusion rate (see [70]). In Chapter 2, I will develop the volume filling chemotaxis model proposed in [51, 98] further. The fundamental standing point of the volume filling effect is that cells have a finite volume and can't move into regions which are already filled by other cells. Hence the probability of making a jump by a cell depends upon the availability of space into which it can move. The global existence and asymptotic behavior of solution as well as pattern formation have been studied in the literature [27, 51, 98, 124, 125] for a very general volume filling chemotaxis model. But in all these papers, the squeezing probability $q(u)$, the probability of a cell finding space at its neighboring site, is chosen with assumptions that cells behave like solid blocks. But cells are not solid blocks. They are elastic and can squeeze into open spaces. In this chapter, I include the elastic properties of cells into the model by means of a nonlinear squeezing probability function $q(u)$. I prove the global existence of classical solutions and study pattern formation of the resulting model. I give the general conditions for pattern formation and analyze the underlying bifurcations. Numerical simulations are presented and interesting merg-

ing (joining of two neighboring maxima) and emerging (insertion of new maxima between two local maxima)) patterning process are observed. These patterns are similar as patterns obtained in paper [98] and I conclude that merging and emerging process is a typical patterning process of the volume filling chemotaxis model.

Chapter 3. In Chapter 3, I continue to study the volume filling chemotaxis model with another novel choice for squeezing probability which still reflects the elastic properties of cells. But the nonlinear diffusion rate of the resulting model has a singularity at the crowding capacity and then the corresponding PDE theory used in Chapter 2 no longer applies. I call this a *fast* diffusion problem although it is slightly different from the conventional notion of fast diffusion (see, for example, [80]). As an open question, I leave the global existence of solutions to be studied in the future. In this chapter, I investigates pattern formation and the underlying bifurcation for the resulting chemotaxis model. The numerical simulations in one dimension for both zero kinetics and non-zero kinetics are presented. It turns out this novel choice of squeezing probability does not bring significant difference in pattern formation compared to the choice made in Chapter 2 and we still observe the typical merging and emerging patterning process. However mathematically this different choice raises an open question of global existence of solutions and bring new challenges to nonlinear analysis.

Chapter 4. This chapter treats another chemotaxis model without diffusion of external signal. In the literature, pattern formation and blow up phenomenon of the classical chemotaxis model are extensively studied. However, another phenomenon, i.e., shock formation, was rarely investigated except numerically in [95, 75]. Shock formation might indicate a propagating disturbance of cell movement which is generated by the interaction of cells with their environment. Due to the lack of food, adaption of environment and some other reasons, cells make a fast chemotactic aggregation and then collapse down to a lower level aggregation instead of blowing up. Mathematically this also leads to a new interesting direction which has never been investigated before. In this chapter, utilizing the theory of hyperbolic system of conservational laws, I study the shock structure for a chemotaxis model which was developed by Othmer and Stevens [95]. In this model, it is assumed that there is no diffusion (transport) of the chemical signal. I first establish the existence of shock waves for the model without viscosity. Then I prove that the traveling waves for both the attractive and the repulsive cases exist and that the traveling speed is identical to the shock speed. Eventually I show that traveling waves converge to the given shock waves as the viscosity vanishes. Furthermore, I explicitly find an entropy pair for the repulsive case, which thus ensures the uniqueness of the

weak solutions (shock solutions) for the repulsive chemotaxis model of Othmer and Stevens [95].

Chapter 5. In Chapter 5, I will turn to the study of transport models. The kinetic transport equation plays an essential role in bridging individual and population behavior in chemotaxis. By choosing appropriate multi-scales, I can integrate microscopic level information on signal transduction into population level or tissue level models. The turning kernel in this model plays a crucial role and determines the complexity and diversity that the macroscopic limit equation could have. There are many applications of kinetic transport equation in modeling cell movements such as mesenchymal motion [47] and motility of amoeboid cells [33]. This chapter is focused on the study of the mesenchymal motion models which were derived by Hillen [47] where the macroscopic limits and some applications are discussed as well. Numerical schemes and pattern formation in n-dimensions are studied by Painter [97]. In case of chemotaxis, a system of a transport equation and a parabolic equation for the chemical signal was studied by Chalub *et al.* [17] and Hwang *et al.* [63, 62]. Their arguments for the global existence of solutions as well as macroscopic limits are based on L^∞- estimates of the turning kernel. In the case of mesenchymal motion models, the turning kernel is given by the fibre distribution $q(t,x,\theta)$ which is allowed to be a delta distribution $q(\theta) = \delta_b(\theta)$ for a totally aligned tissue in direction of $b \in \mathbb{R}^n$. As a result, the fibre distribution is not necessarily bounded in L^∞. In particular, assumption (A0) in paper [17] does not apply and hence their results can not be applied directly to the case discussed here. The global existence analysis is quite technically involved and challenging. So far the global existence of solutions and convergence of macroscopic limits remains open. In this chapter, I give a detailed analysis for the one dimensional mesenchymal motion model and establish the global existence of classical solutions. In addition, I prove the existence of a weak limit of solutions for parabolic and hyperbolic scaled equations and prove the existence of traveling waves as well as nonexistence of pattern formation. Mathematically the high dimensional mesenchymal transport models have significant difference from the one dimensional case. The approaches used in this chapter for the one dimensional case is no longer valid for the higher dimensional case. In a collaboration [58] with T. Hillen and P. Hinow, the theory of semigroups of operators will be applied to show the global existence of solutions in a measurable Banach space for high dimensional mesenchymal transport models. The details will not be provided in this thesis.

Chapter 6. This is a discussion chapter. I briefly summarize the results obtained in this thesis and point out future research directions that I am going to pursue.

1.2 Introduction of the Models

1.2.1 Patlak-Keller-Segel Model (population level)

Let $u(t,x)$ and $v(x,t)$ denote the cell density and the concentration of the external signals (chemoattractant) at the position $x \in \Omega$ and time $t \geq 0$, respectively, then a simplified version of PKS model reads

$$\begin{cases} u_t = \nabla(D\nabla u - u\nabla\varphi(v)), \ (x,t) \in \Omega \times (0,\infty) \\ \tau v_t = k_c \triangle v + g(u,v), \\ \dfrac{\partial u}{\partial n} = \dfrac{\partial v}{\partial n} = 0, \ x \in \partial\Omega \\ u(x,0) = u_0(x), v(x,0) = v_0(x), \end{cases} \tag{1.2.1}$$

where Ω is a bounded domain of $\mathbb{R}^n (n \geq 1)$, $g(u,v)$ describes the production and degradation of external signal v and $\varphi(v)$ is called potential function describing the signal detection. The numerous results associated with various PKS type models are mostly summarized in three survey articles [60, 61, 52]. In the following, I briefly review some results regarding the finite time blow up solutions and global solutions to PKS type chemotaxis models.

Model (1.2.1) has been extensively studied in various aspects and a large number of results in the literature deal with the case where $\varphi(v) = \chi v$ and $g(u,v) = \alpha u - \gamma v$ with positive constants χ, γ and α, here χ is commonly called chemosensitivity. Najundiah [90] was first to suggest that aggregation of cells may eventually lead to the formation of a delta function in cell density, a phenomenon called chemotactic collapse in that paper. More often, it was referred as blow up in the literature. His argument, however, did not consider the possible dependence of such collapse on the dimension of the space in which aggregation happens. This viewpoint was developed by Childress and Percus [21, 20], who showed that singular behavior was not possible in one dimension. While in higher dimension ($n \geq 2$), they confirmed Nanjundiah's argument that collapse (blow up) can occur. They furthermore argued that, in two dimensions ($n = 2$), chemotactic blow up requires a threshold number of cell mass. Precisely, there exists two numbers c_* and c^* such that the solution exists globally in time if the initial mass $\|u_0\|_{L^1(\Omega)} \leq c_*$, and forms a δ-function singularity in finite time if $\|u_0\|_{L^1(\Omega)} \geq c^*$. However, these results are heuristic based on numerical computations for the steady states. Subsequently, for the parabolic-elliptic case ($\tau = 0$) Jäger and Luckhaus [65] proved that radially symmetric solutions in two dimensions can blow up for suitable initial data u_0 by constructing a radially symmetric lower solution for the first equation of PKS model. Precisely, they showed that there exists a critical number θ such that

(1) if $\int_\Omega u_0 dx < \theta$, the solution (u, v) exists globally in time, and

(2) if $\int_\Omega u_0 dx > \theta$, the solution u blows up in a finite time,

where Ω is a bounded domain in $\mathbb{R}^2$ with the C^1 boundary $\partial\Omega$. Furthermore, Nagai [83] refined the above work by identifying this critical number with $8\pi k_c/(\alpha\chi)$. He showed that blowup cannot occur if $n = 1$, or if $n = 2$ and Ω is a ball and $u_0(x)$ is radially symmetric such that $\int_\Omega u_0 dx < 8\pi k_c/(\alpha\chi)$, whereas blowup occurs if $\int_\Omega u_0 dx > 8\pi k_c/(\alpha\chi)$. Herrero and Velázquez [42, 43, 44] first considered the same v-equation ($\tau > 0$) as in [83] and showed that if Ω is an open ball in $\mathbb{R}^2$ with radius r, then one can obtain radial solutions $(u(r,t), v(r,t))$ such that $u(r,t)$ blows up exactly at the origin $r = 0$ at time $t = T > 0$ in such a way that $u(r,T) = \frac{8\pi k_c}{\alpha\chi}\delta(r) + f(r)$ as $r \to 0$ having a concentrated mass equal to $8\pi k_c/(\alpha\chi)$, where $\delta(r)$ is the Dirac measure centered at $r = 0$ and $f(r) = \frac{C}{r^2}e^{-2|\log(r)|^{1/2}}(1+o(1))$ with a positive constant C depending on χ. Global existence or blowup results for nonradial solutions or for general domain Ω can also be found in references [26, 85, 86, 87, 89], all of which deal with parabolic-elliptic versions ($\tau = 0$) of the PKS model with different sensitivity functions. There are many works devoted to analysis of steady states of the PKS model. The landmark in this direction was the paper by Najundiah [90] again, in which the Hopf's maximum principle was applied to the steady state system to derive the relation between u and v and consequently the steady state system was reduce to a scalar parameter-dependent elliptic problem. In [109], Schaaf showed that the stationary problem of more general PKS models than the cases studied by Najundiah can also be reduced to a scalar parameter-dependent elliptic equation. The linear and logarithmic chemotaxis sensitivity functions are considered there. Furthermore, Schaaf gave a stability analysis for the constant stationary solutions of the PKS model. Lin *et al* [77] established conditions with logarithmic sensitivity function for system to have both nonconstant and constant stationary solutions. Based on the variational techniques introduced by Struwe *et al* [118], Wang *et al* [122], Senba *et al* [111] and Hortsmann [59] independently proved the existence of nontrivial stationary solutions without symmetry assumptions. Coming to the full PKS model ($\tau > 0$), Nagai *et al* [89, 88] proved that radially symmetric solutions exist globally in time provided the initial mass satisfies $\|u_0\|_{L^1(\Omega)} < 8\pi k_c/(\alpha\chi)$. As for the general solutions (non-radial symmetric), they gave $\|u_0\|_{L^1(\Omega)} < 4\pi k_c/(\alpha\chi)$ as a criterion for the existence of global solutions. Biler [11] and Gajewski *et al* [39] independently obtained the same criterion as above for the global existence of non-radial solutions by constructing a Lyapunov function. Moreover, Gajewski *et al* [39] showed that the solutions asymptotically approximate stationary solutions for some sequence of time moments. The long time behavior of global in time solutions was

recently obtained by Feireisl *et al* [35]. It is clear that there is a discrepancy between the radial threshold $8\pi k_c/(\alpha\chi)$ and the non-radial threshold $(4\pi k_c/(\alpha\chi))$. This gap was filled by subsequent works [88, 85, 111, 110]. They showed that if there is a solution that blows up in finite time for $4\pi k_c/(\alpha\chi) < \|u_0\|_{L^1(\Omega)} < 8\pi k_c/(\alpha\chi)$, then the blowup (for u) has to happen at the boundary of the domain. Furthermore, in a book by Suzuki [119], when $n = 2$, the *quantized blow up* mechanism was discussed. It was shown that the solution will blow up in finite time if the initial mass $\|u_0\|_{L^1(\Omega)}$ is greater than a quantized mass $m_*(x_0)$ which is defined as

$$m_*(x_0) = \begin{cases} 8\pi k_c/\alpha\chi, & x_0 \in \Omega, \\ 4\pi k_c/\alpha\chi, & x_0 \in \partial\Omega, \end{cases}$$

where Ω is a bounded domain in $\mathbb{R}^2$. Beside the analysis of the PKS model on a bounded domain, Nagai [84] studied the problem on the whole space $\Omega = \mathbb{R}^2$. He showed that for $\|u_0\|_{L^1(\mathbb{R}^2)} < 4\pi k_c/(\alpha\chi)$, the solution exists globally in time using the Lyapunov function and furthermore found several decay properties of the solution.

Most of the studies mentioned above are focused on the two dimensional case. So what is known for the case $n = 1$ or $n \geq 3$? For the case $n = 1$, the paper by Osaki *et al* [92] and Hillen *et al* [54] filled the gap of the missing global existence proof using different approaches for the classical PKS model. For the case of higher space dimensions $n \geq 3$ and a bounded domain, the solution will blow up [83] if the initial data u_0 is radially symmetric and small. In [12], it was shown that if $n \geq 2$ and $\Omega \subset \mathbb{R}^n$ is a bounded star-shaped domain with respect to origin, then solutions blow up for sufficient large initial mass $\|u_0\|_{L^1(\Omega)}$. When $\Omega = \mathbb{R}^3$, for any $T > 0$ and constant $C > 0$, there exists a radial solution $(U(t,r), V(t,r))$ such that the radial solution blows up at the origin $r = 0$ and $t = T$ and $\int_{|x|\leq r} U(T,s)ds \to C$ (see [42, 43, 44]). For more detailed results about the PKS model, I refer to the survey articles [60, 61]. For $n \geq 3$ and non radial symmetric solutions with general bounded domain, Hillen *et al* [55] showed that L^p solutions $(p > 1 + n/2)$ globally exist when initial data $\|u_0\|_{L^p(\Omega)}$ is sufficient small. Recently, some interesting results about the unbounded domain for $n > 2$ are obtained. Corrias *et al* [23, 22] showed that in dimension $n > 2$, $L^{n/2}(\mathbb{R}^n)$ is the critical space: there exists a constant $K_1(n)$, such that when initial norms $\|u_0\|_{L^{n/2}(\mathbb{R}^n)} \leq K_1(n)$ there are global weak solutions and solutions decays to zero for the elliptic case $(\tau = 0)$, while solutions decay to $G(t) * u_0$ for the parabolic case $(\tau = 1)$, where $G(t,x)$ denotes the heat kernel. For large initial data $\|u_0\|_{L^{n/2}(\mathbb{R}^n)} \geq K_2(n)(>> K_1(n))$, the solutions blow up (see Perthame [103]). Clearly there is a gap between two thresholds $K_1(n)$ and $K_2(n)$,

which has not been filled yet so far.

1.2.2 Kinetic Transport Model (individual level)

Bacterial motility is commonly provided by flagella, which are long, spiral-shaped protein rods that stick out from the surface of the cell [108]. The examples of flagellated bacteria are enteric bacterium *E. coli*, bacterium *S. typhimurium* and soil bacterium *A. vinelandii*. The physical mechanism of movement of the flagellated bacteria is well known [9]. There are two models of movement pattern based on counterclockwise (CCW) and clockwise (CW) flagellar rotation. When the flagella turn counterclockwise, they join together and form a synchronous bundle that causes the flagella to point in one direction and pushes the body steadily forward. This forward motion is called 'run'. The speed of running is $s = 10 - 20\mu$m/sec. A clockwise rotation of each flagellum causes the bundle to come apart and the flagella turn independently, moving the cell body this way and that in a highly erratic manner. In this case, the cell is said to 'tumble'. I simply characterize these motions as "run and tumble". Tumbling reorients the cell so that it can move in a new direction when running starts again. The 'run and tumble' process is very similar to that of *scattering* for neutrons that 'run' along straight lines until they encounter an atom and then are 'scattered' in a new direction. The governing equation is therefore reminiscent to the Boltzmann equation [24, 102].

For *E. coli*, the duration of both run and tumble are exponentially distributed with means of 1 sec and 0.1 sec respectively if an extracellular chemical signal is not present [13]. Under the influence of an external signal (chemoattractant or noxious substance), the cell increases its time on running in a favorable direction. Since these bacteria are too small to detect spatial differences in the concentration of an external signal on the scale of a cell length, they choose a new direction essentially at random at the end of a tumble, although it has some bias in the direction of the preceding run [10, 31]. Therefore, from mathematical point of view, the movement of flagellated bacteria can be viewed as a biased random walk. As the mean time for tumbling is ten times smaller than the mean time of running, the tumbling time is negligible and consequently we can model the movement of the bacterium by a stochastic process called a velocity jump process which was introduced by Alt [2] and further developed in [93, 50, 94, 116]. A kinetic transport model to describe

this velocity jump process is as follows (see [93])

$$\begin{aligned} &\frac{\partial p}{\partial t} + v \cdot \nabla_x p = \mathcal{T}(S,p), \\ &\mathcal{T}(S,p) = \int_V (T(S;v,v')p(t,x,v') - T(S;v,v')p(t,x,v))dv', \end{aligned} \tag{1.2.2}$$

where $p(t,x,v)$ denotes the density of cells at position x, moving with velocity $v \in V \subset \mathbb{R}^n$ at time t. $\mathcal{T}$ is an operator modeling the change of direction of cells and turning kernel T, depending on the density S of external signal, gives the probability of a velocity jump from v' to v if a jump occurs. In [2, 3, 50, 94], it was shown that parabolic chemotaxis equation, such as the PKS model (1.2.1), can be obtained as the diffusion limit of the transport equation (1.2.2), thus allowing to determine the diffusion matrix D and the chemotactic sensitivity χ. The global existence, blow-up and macroscopic limits of the one-dimensional version of model (1.2.2) have been studied in [57, 56, 49, 64]. In higher dimension, the global existence of solutions and parabolic limits to equation (1.2.2) was given in [17] for a given S. When the equation for external signal S is coupled into transport equation (1.2.2), the rigorous proof of parabolic limits was subsequently supplied in [63, 62], where a more general turning kernel T was considered.

All of the above results either heuristically describe the macroscopic process, or, if using a transport model, assume that the turning kernel only depends on the signal concentration but not on its gradient, and not on internal variables. However, a bacteria population is comprised of millions of individual bacteria and collective behavior of the bacterial population involves individual-level response to signals. The machinery of signal transduction and adaption for some bacteria (*e.g., E. coli*) has been well characterized [7, 14, 115], which leads to the question of how to incorporate the individual behavioral rules into population level models. A significant progress on filling the gap between microscopic and macroscopic models has been made in [31, 32]. Assume that the internal variables $\xi \in Z \subset \mathbb{R}^n$ involved in the signal transduction evolve according to the equations

$$\frac{d\xi}{dt} = \eta(\xi, S(t,x(t))) \tag{1.2.3}$$

where $\eta(\cdot,S) : Z \to \mathbb{R}^m$ and $S(t,x)$ denotes the extracellular signal as above and $x(t)$ is the cell path. Then the governing equation with internal state variables in the jump velocity process is given by (see [31, 32])

$$\frac{\partial p}{\partial t} + v \cdot \nabla p + \nabla_\xi(\eta p) = -\lambda(\xi)p + \int_V \lambda(\xi)T(v,v',\xi)p(t,x,v',\xi)dv', \tag{1.2.4}$$

where $p(t, x, v, \xi)$ is the density of cells with internal state ξ at position $x \in \mathbb{R}^n$ with velocity $v \in V \subset \mathbb{R}^n$ at time $t \geq 0$. Here it is assumed that the random velocity changes follow a Poisson process with rate $\lambda(\xi)$ and the turning kernel satisfies the normalization condition $\int_V T(v, v', \xi)dv' = 1$. Applying the perturbation methods and moment closure approach, the authors of [31, 32] use a cartoon model for the internal state $\xi = (\xi_1, \xi_2)$

$$\frac{d\xi_1}{d\tau} = \frac{g(S(\tau)) - (\xi_1 + \xi_2)}{\tau_e}, \ \frac{d\xi_2}{d\tau} = \frac{g(S(\tau)) - \xi_2}{\tau_a}, \ \lambda(\xi) = \lambda_0 - b\xi_1. \tag{1.2.5}$$

as an example to show how aspects of the signal transduction and response explicitly enter into the macroscopic equations via chemotactic sensitivity function by studying the parabolic and hyperbolic limits of equation (1.2.4), where λ_0 is the basal turning frequency for a fully adapted cell and b is a positive constant. Their analysis showed how parameters that characterize signal transduction and response in individual cells are embedded in the macroscopic chemotaxis PKS model through the sensitivity function χ in. Specifically, they derive that the macroscopic density $\rho(t, x)$ evolves according to the following chemotaxis equation

$$\frac{\partial \rho}{\partial t} = \nabla \cdot (D\nabla\rho - \rho \cdot \chi(S)\nabla S)$$

where the macroscopic density $\rho(t, x)$ is defined by

$$\rho(t, x) = \int_Z \int_V p(t, x, v, \xi)dvd\xi,$$

and the diffusion rate and the chemosensitivity χ are given, respectively, as

$$D = \frac{s^2}{n\lambda_0}, \ \chi(S) = g'(S(x))\frac{bs^2\tau_a}{n\lambda_0(1 + \lambda_0\tau_a)(1 + \lambda_0\tau_e)},$$

Their argument was further developed in [33] for the more complex type of behavioral response characteristic of crawling cells, which detects a signal, extract directional information from a scaler concentration field, and change their motile behavior accordingly. The numerical approaches for solving (1.2.4) was explored in [30] and the global existence of solutions to equation (1.2.4) and (1.2.5) in one dimension coupled to the equation for external chemical $S(t, x)$ was obtained in [29]. In papers [2, 3, 31, 32, 33], the turning kernel T is assumed to be independent of internal or external variables due to the technical difficulty for deriving macroscopic limits. In the work [28], the authors studied the almost same model as (1.2.4) with a generalization that turning kernel T depends on the spatial and temporal gradient. By essentially assuming that the boundary condition $p(t, x, v, \xi) = 0$ for $\xi \in \partial Z$ and

applying moment closure method, the authors of [28] reduce equation (1.2.4) into the following two equations without the internal variable gradient

$$f_t + v \cdot \nabla f = \int_V (T[S]f' - T^*[S]f)dv', \tag{1.2.6}$$

$$(\tilde{\rho}z)_t + \nabla_x \cdot \left(z \int_V v f dv \right) = \tilde{\rho}\eta(z, S), \tag{1.2.7}$$

where

$$f(t,x,v) = \int_Z p(t,x,v,\xi)d\xi, \ \tilde{\rho}(t,x) = \int_V f(t,x,v)dv,$$

and $z(t,x)$ denotes the average values of the internal variables determined by

$$z(t,x) = \frac{1}{\tilde{\rho}} \int_V \int_Z \xi p(t,x,v,\xi)d\xi dv,$$

and turning kernel T is given by $T[S] = \varphi(S_t + v \cdot \nabla S)$ with an assumption that $\varphi : \mathbb{R} \to \mathbb{R}$ is a monotonically decreasing smooth function possessing positive lower and upper bound.

The hydrodynamic limits of equations (1.2.6) and (1.2.7) are rigorously derived in [28]). The numerical results for the macroscopic chemotaxis equations of models (1.2.6) and (1.2.7) were investigated as well.

Chapter 2

VOLUME FILLING CHEMOTAXIS MODEL WITH NONLINEAR SQUEEZING PROBABILITY[1]

2.1 Introduction

Chemotaxis is the characteristic movement or orientation of an organism or cell along a chemical concentration gradient either toward or away from the chemical stimulus. In the first case, the chemical is called a chemoattractant, and in the second case it is said to be a chemorepellent. The term chemotaxis is used broadly in the mathematical literature to describe general chemosensitive movement responses. Models for chemotaxis have been successfully applied to the aggregation patterns in bacteria [120, 121, 123], slime molds [37], skin pigmentation patterns [100], angiogenesis in tumour progression and wound healing [16] and many other examples. A classical and very important chemotaxis model was proposed by Keller and Segel [67] in 1970 to describe the aggregation process of cellular slime mold by chemical attraction. A special case of the Keller-Segel model reads

$$\begin{cases} u_t = \nabla(\nabla u - u\chi(v)\nabla v), \ (x,t) \in \Omega \times (0,\infty) \\ v_t = \varepsilon \triangle v + g(u,v), \\ \dfrac{\partial u}{\partial n} = \dfrac{\partial v}{\partial n} = 0, \\ u(x,0) = u_0(x), v(x,0) = v_0(x), \end{cases} \tag{2.1.1}$$

where Ω is a bounded domain of $\mathbb{R}^n$, $u(t,x)$ denotes the particle density and $v(t,x)$ stands for the concentration of chemoattractant, ε is a positive constant, χ is called chemosensitivity and $g(u,v)$ describes production and degradation of the chemoattractant.

Model (2.1.1) has been extensively studied in great detail in the literature (e.g., see the survey articles of Hortsmann [60, 61]). Of particular interest is the tendency of solutions to exhibit finite-time blow-up. It has been shown that possibility of blow-up of the solutions to system (2.1.1) essentially depends on the space dimension.

[1]The result in this chapter is a collaboration with Thomas Hillen and has been accepted for *Chaos*.

For constant chemosensitivity $\chi(v) = \chi$ and linear reproduction and degradation $g(u,v) = \nu u - \delta v$, finite-time blow-up never happens in 1-dimension (unless there is no diffusion of the chemoattractant v) but can occur in n-dimension for $n \geq 2$. The 2-dimensional case is important and several thresholds (for radially symmetric solutions and for non-symmetric solutions) were found. If the initial distribution exceeds this threshold, the solution will blow up in finite time. When the initial mass is below this threshold the solution exists globally.

There are various modifications of (2.1.1) which prevent blow up. For example, Mimura and Tsujikawa (1996) presented a chemotaxis-growth model which reads

$$\begin{cases} u_t = a\Delta u - \nabla(u\chi(v)\nabla v) + f(u) \quad \text{in } \Omega \times [0,\infty), \\ v_t = b\Delta v + \nu u - \delta v, \\ \frac{\partial u}{\partial n} = \frac{\partial v}{\partial n} = 0, \\ u(x,0) = u_0(x), v(0,x) = v_0(x), \end{cases} \tag{2.1.2}$$

where $f(u)$ is a smooth function of u such that $f(0) = 0$ and

$$f(u) = (-\xi u + \zeta)u \text{ for sufficiently large } u.$$

The function $f(u)$ describes cell proliferation and cell death. For space dimension $n = 1, 2$, Osaki *et al.*(2002) showed that the solutions of problem (2.1.2) exists globally due to the dissipativity of the growth of cells. Moreover, saturation effects in the chemotactic component $\chi(v)$ occur very naturally if cell surface receptor kinetics is taken into account. Chemotaxis models with saturation effects can prevent blow up and have been used in many applications (Biler [11], Ford *et al.* [19], Othmer and Stevens [95]). A chemotaxis model with finite sampling radius by incorporating a non-local sampling into the classical model was studied recently by Hillen *et al* [53]. The global existence of the solution for any space dimension and numerical simulation of pattern formation are shown in [53]. When cells demonstrate both chemoattraction and chemorepulsion according to multiple environmental signals, the classical model can be extended into an attraction-repulsion chemotaxis model. This type of model has been studied by a number of authors [78, 98, 99]. The general conditions for blow up or global existence to some specials cases of the attraction-repulsion model were identified in a recent work [55]. Other strategies of preventing blow up are reviewed in a forthcoming paper [52].

Painter and Hillen [98] introduced the mechanistic description of the volume filling effect. In the volume filling effect, it is assumed that particles have a finite volume and that cells can not move into regions which are already filled by other

cells. First we give a brief derivation of the model below. For a full derivation we refer to paper [98].

The derivation of the model begins with a master equation for a continuous-time and discrete-space random walk (Othmer and Stevens [95])

$$\frac{\partial u_i}{\partial t} = \mathcal{T}_{i-1}^{+} u_{i-1} + \mathcal{T}_{i+1}^{-} u_{i+1} - (\mathcal{T}_i^{+} + \mathcal{T}_i^{-}) u_i, \tag{2.1.3}$$

where u_i is defined to be the conditional probability of a walker at $i \in \mathbb{Z}$ at time t, conditioned at $i = 0$ at $t = 0$ and $\mathcal{T}_i^{\pm}$ are the transitional probabilities per unit of time for a one-step jump to $i \pm 1$.

In the volume filling approach, the probability of making a jump is assumed to depend on the availability of space into which cells can move. The transitional probability then takes the form

$$\mathcal{T}_i^{\pm} = q(u_{i\pm1})(\alpha + \beta[\tau(v_{i\pm1}) - \tau(v_i)]), \tag{2.1.4}$$

where $q(u)$ denotes the *squeezing probability* of a cell finding space at its neighboring location, α and β are constants and τ represents the mechanism of the signal detection. It was assumed that only a finite number of cells, say $\bar{u}$, can be accommodated at any site, and the function q is stipulated by the condition

$$q(\bar{u}) = 0, \quad \text{with} \quad 0 < q(u) \leq 1 \quad \text{for} \quad 0 \leq u < \bar{u}.$$

Moreover, the squeezing probability is zero when the cell density exceeds $\bar{u}$. A logical immediate choice for $q(u)$ is

$$q(u) = \begin{cases} 1 - \dfrac{u}{\bar{u}}, & 0 \leq u \leq \bar{u}, \\ 0, & u > \bar{u}, \end{cases} \tag{2.1.5}$$

which says that the probability of a cell finding a space at its neighboring site decreases linearly in the cell density at that site. The linear choice (2.1.5) for $q(u)$ says that the probability of a cell finding spaces is proportional to the number of occupants (see [118, 98, 104]). This corresponds to the situation where cells behave like solid blocks and are not squeezable. However, some cells are plastic and deformable and can change their shapes to squeeze into openings. Hence the probability $q(u)$ of a cell finding space should be a nonlinear function which is greater than a linear distribution as define by (2.1.5). Under this consideration, a more realistic form of squeezing probability $q(u)$ that takes into account the plastic properties of cells is

$$q(u) = \begin{cases} 1 - \left(\dfrac{u}{\bar{u}}\right)^{\gamma}, & 0 \leq u \leq \bar{u}, \\ 0, & u > \bar{u}, \end{cases} \tag{2.1.6}$$

where $\gamma \geq 1$ is called the *squeezing exponent* in this paper.

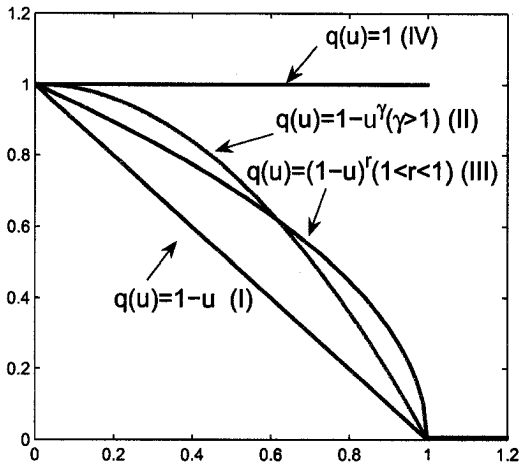

Figure 2.1: Illustration of linear and nonlinear squeezing probability $q(u)$, where we assume that $\bar{u} = 1$. Case (I) corresponds to the situation that cells are solid blocks and the probability of a cell finding space is proportional to the available space. Case (II) and (III) correspond to the case that cells are plastic and can deform to fit into open space. Hence the squeezing probability is pointwise larger than in the linear case (I). Case (IV) describes that a cell consists of a fluid that can fill all open space without restriction.

Substituting (2.1.4) into the master equation (2.1.3), applying Taylor expansion (see [98]), and converting the discrete equation into a continuous equation, we end up with the following equation

$$u_t = \nabla \cdot \big(d_1(q(u) - q'(u)u)\nabla u - q(u)u\chi(v)\nabla v\big), \tag{2.1.7}$$

where

$$d_1 = k\alpha, \ \chi(v) = 2k\beta\frac{d\tau(v)}{dv},$$

and k is a scaling constant.

Another possible choice of squeezing probability $q(u)$ which also reflect plastic cell property is given as

$$q(u) = \begin{cases} \left(1 - \dfrac{u}{\bar{u}}\right)^r, & 0 \leq u \leq \bar{u}, \\ 0, & u > \bar{u}, \end{cases} \tag{2.1.8}$$

with $0 < r < 1$. For this choice of $q(u)$, the derivative $q'(u) \to -\infty$ as $u \to \bar{u}$ (see Figure 2.1), which leads to a singularity in the diffusion coefficient (see (2.1.7)). In that case the model becomes a *fast diffusion* parabolic equation and the classical theory for global existence of nonlinear parabolic equations no longer applies. Hence we will use (2.1.6) as an example in the following analysis. We can, however, do a similar pattern formation analysis for (2.1.8) and also find merging and emerging dynamics similar as (2.1.6) does (shown in chapter 3).

There are some fluid cells that can unrestrictedly fill all open space. In this situation, the squeezing probability $q(u)$ is defined as follows

$$q(u) = \begin{cases} 1, & 0 \le u \le \bar{u}, \\ 0, & u > \bar{u}. \end{cases} \tag{2.1.9}$$

It is worthwhile to point out that all above choices for squeezing probability are made according to the biological relevance instead of mechanical justification. The graph for all these choices are plotted in Figure 2.1 and comparisons are given in the caption.

If we combine the chemotaxis equation (2.1.7) with the dynamic equation for the external signal and incorporate the birth and death dynamics of cells and external signals, denoted by $f(u,v)$ and $g(u,v)$, respectively, we obtain a formulation of the volume filling chemotaxis model

$$\begin{cases} u_t = \nabla \cdot \big(d_1(q(u) - q'(u)u)\nabla u - q(u)u\chi(v)\nabla v\big) + f(u,v), \\ v_t = d_2\Delta v + g(u,v), \end{cases} \tag{2.1.10}$$

on a bounded smooth domain Ω. Moreover, the zero-flux boundary conditions are prescribed as follows

$$\begin{gathered} \big(d_1(q(u) - q'(u)u)\nabla u\big) \cdot \mathbf{n} - q(u)u\chi(v)\nabla v \cdot \mathbf{n} = 0, \\ \nabla v \cdot \mathbf{n} = 0, \end{gathered} \tag{2.1.11}$$

where $\mathbf{n}$ denotes the unit outward normal vector at the boundary $\partial\Omega$.

The global existence of solutions to a volume filling chemotaxis model was first obtained in paper [51], where cell proliferation was not taken into account. Recently, Wrzosek [124] proved the global existence of the solution to system (2.1.10), (2.1.11) with cell kinetics and a smooth squeezing probability $q(u)$. Furthermore, he proved the existence of a global attractor of system (2.1.10), (2.1.11) in any space dimension $n \ge 1$ for the special linear form of $q(u)$ as in (2.1.5). In this paper, we consider a more realistic squeezing probability $q(u)$ which reflects the semi-plastic property of cells and more general kinetic forms f and g. We prove the global existence

of classical solutions and study pattern formation to system (2.1.10) and (2.1.11) under our novel choice of squeezing probability. For pattern formation, we extend the analysis in [98] by generalizing the squeezing probability function $q(u)$ to the form of (2.1.6) for $\gamma \geq 1$. It is worthwhile to note that the choice of (2.1.6) with $\gamma > 1$ in (2.1.10) results in density dependent diffusion (nonlinear diffusion) in the first equation of (2.1.10) , which is in contrast to choice (2.1.5) that results in a constant diffusion (linear diffusion).

The rest of paper is organized as follows. In section 2, we give the basic assumptions for squeezing probability $q(u)$ as well as the kinetic functions f and g and prove the global existence of classical solutions to the system (2.1.10), (2.1.11). The results are obtained based on Amann's theory of parabolic systems [5, 4, 6] by making a smooth extension for $q(u)$. In section 3, we will identify the conditions for pattern formation of the general system (2.1.10) with zero-flux boundary conditions (2.1.11) by performing the standard linear stability analysis. In section 4, we consider (2.1.6) and derive the dispersion relation. Based on this dispersion relation, we investigate the bifurcations of the chemosensitivity χ, the growth rate ν and the death rate δ of the chemoattractant. We also study the influence of crowding capacity γ on pattern formation. In section 5, we show numerical simulations for system (2.1.10) and (2.1.11) and compare the patterns obtained for the choice of (2.1.6) versus (2.1.5). We close with a discussion in section 6.

2.2 Global Existence

To study the local and global existence of the solutions to problem (2.1.10), (2.1.11), we assume that nonnegative initial data are given as

$$u(x,0) = u_0(x) \geq 0, \quad v(x,0) = v_0(x) \geq 0 \text{ for } x \in \Omega. \tag{2.2.1}$$

Moreover, we make the following assumptions.

(A1) d_1 and d_2 are positive constants, $\chi \in C^2(\mathbb{R}, \mathbb{R})$ and $\chi(v) > 0$.

(A2) The squeezing probability $q(u) \in C^3([0, \bar{u}))$ satisfies the following condition:

$$\begin{gathered}(1) \text{ there exists a critical number } \bar{u} \text{ such that} \\ q(0) = 1, q(\bar{u}) = 0, \text{ and} \\ 0 < q(u) < 1 \text{ for } u \in (0, \bar{u}) \text{ and } q(u) = 0 \text{ for all } u > \bar{u}. \\ (2)\ q(u) \text{ is nonincreasing, i.e., } q'(u) \leq 0. \text{ Moreover} \\ |q'(u)| \text{ is bounded and } q''(u) \leq 0 \text{ for all } u \in [0, \bar{u}].\end{gathered}$$

Hereafter we call $\bar{u}$ the *crowding capacity.*

(A3) $f \in C^2(\mathbb{R} \times \mathbb{R})$ satisfies the quasi-positivity condition, i.e., $f(0, v) \geq 0$ for $v \geq 0$. Moreover, there exists a constant $u_c > 0$ with $u_c < \bar{u}$ such that for all $v \geq 0$

$$f(u_c, v) = 0 \text{ and } f(u, v) < 0 \text{ for } u > u_c, \tag{2.2.2}$$

we call u_c the *carrying capacity.*

(A4) $g \in C^2(\mathbb{R} \times \mathbb{R})$ is bounded and satisfies the quasi-positivity condition: $g(u, 0) \geq 0$ for $u \geq 0$. In addition, there exists a constant $\bar{v} > 0$ such that

$$g(u, \bar{v}) < 0 \text{ for } 0 \leq u \leq \bar{u}. \tag{2.2.3}$$

Standard examples for q are (2.1.5) and (2.1.6). A typical choice for the cell kinetic function $f(u, v)$ is logistic growth $f(u, v) = \mu u(1 - u/u_c)$ and for g it is linear growth and death $g(u, v) = \nu u - \delta v$. A more general choice will be discussed later (see (2.2.4) and (2.2.5)).

Remark 2.2.1. *Here we assume that the crowding capacity $\bar{u}$ is larger than the carrying capacity u_c. The carrying capacity denotes a critical density beyond which there is not enough nutrients available to support further population growth, whereas the crowding capacity gives only a volume constraint of how many particles can be squeezed into a unit area (or volume). Hence it is reasonable to assume $\bar{u} > u_c$.*

Remark 2.2.2. *From assumption (A2), we see that the squeezing probability function $q(u)$ in not differentiable at $u = \bar{u}$. Later on, we will show that the solution u satisfies $0 \leq u \leq \bar{u}$. So here $q'(\bar{u})$ represents the left derivative of $q(u)$ at $u = \bar{u}$, i.e., $q'(\bar{u}) = \lim_{u \to \bar{u}^-} q'(u)$.*

Remark 2.2.3. *The condition $q''(u) < 0$ for $0 \leq u \leq \bar{u}$ means $q(u)$ is concave in $[0, \bar{u}]$. So $q(u)$ is pointwise larger than the linear case in (2.1.5) for $u \in [0, \bar{u}]$, which is used to reflect the plastic properties of cells. As the same reasons stated in Remark 2.2, here we define $q''(\bar{u})$ as the left derivative of $q'(u)$ at $u = \bar{u}$. Note that the condition $q''(u) < 0$ is sufficient but not necessary for global existence.*

Remark 2.2.4. *We now compare the above assumptions (A1)-(A4) with the conditions imposed by Wrzosek in [124]. In [124], $q(u) = \tilde{q}(u)(\bar{u} - u)$ and $\tilde{q}(u) > 0, \tilde{q}(u) \in C^3(\mathbb{R})$ for all $u \in \mathbb{R}$. Clearly our assumptions for $q(u)$ are different from the above assumptions given by Wrzosek. The argument applied in [124] can not be used directly here. Particularly $q(u)$ is allowed to be not differentiable at $u = \bar{u}$ in our assumption. Even in the domain $[0, \bar{u})$ in which $q(u)$ is smooth, our assumptions*

do not fulfill the assumptions in [124]. For example, the choice of (2.1.6) for γ being an integer greater than 1 satisfies both our assumptions and Wrzosek's assumptions for $u \in [0, \bar{u})$. However, when $\gamma > 1$ is not an integer, (2.1.6) can not be represented in the form in [124] even for $u \in [0, \bar{u})$.

For the cell kinetic term $f(u, v)$, in paper [124], $f(u, v) = uh(u)$ is independent of the chemoattractant concentration v where $h(u) \leq 0$ for $u \geq \bar{u}$. However, the cell kinetics might depend on the concentration of the signal. Many growth factors have been shown to stimulate such dual activity, for example, vascular endothelial growth factor (VEGF) mediates both endothelial cell proliferation and chemotaxis. An example from [98] for this behavior is

$$f(u, v) = ruv\left(1 - \frac{u}{u_c}\right), \tag{2.2.4}$$

where it is assumed that the chemical mediates both cell migration and cell proliferation, where $u_c < \bar{u}$. For the signal kinetics $g(u, v)$, in paper [124], $g(u, v) = g_1(u) - vg_2(v)$ where $g_1, g_2 \in C^2(\mathbb{R}), g_1 \geq 0, g_1(0) = 0, g_2 \geq 0$ and $\lim_{y \to +\infty} yg_2(y) = +\infty$. In fact, $g(u, v)$ can be more general and the conditions can be relaxed to (2.2.3). A standard example is of birth-death structure, i.e.,

$$g(u, v) = g_1(u, v)u - g_2(u, v)v, \tag{2.2.5}$$

with bounded birth rate $g_1 \geq 0$ and death rate $g_2 \geq \kappa$ for some positive constant κ. Then there exists a $\bar{v}$ such that $g(u, v)$ satisfies condition (2.2.3).

Under the assumption (A1)-(A4), we can immediately prove that v is nonnegative and bounded above by $\bar{v}$ if $0 \leq u \leq \bar{u}$. This is shown in the following Lemma.

Lemma 2.2.1. *Let assumption (A1)-(A4) hold and (u,v) be a solution of system (2.1.10), (2.1.11). If $0 \leq u \leq \bar{u}$, then it follows that $0 \leq v \leq \bar{v}$.*

Proof. We define an operator $\pounds$ by

$$\pounds v = v_t - d_2 \Delta v - g(u, v).$$

Then $\underline{v} = 0$ is a lower solution of the v-equation in (2.1.10) since for $0 \leq u \leq \bar{u}$

$$\pounds \underline{v} = -g_1(u, 0) \leq 0,$$

and $\bar{v}$ is a upper solution of the v-equation due to

$$\pounds \bar{v} = -g(u, \bar{v}) > 0.$$

Then it follows from the comparison principle that $0 \leq v \leq \bar{v}$.

□

In what follows, we are devoted to proving the global existence of classical solutions to system (2.1.10), (2.1.11). Note that $q(u)$ is not smooth at $u = \bar{u}$, which causes some trouble in applying the theory for nonlinear parabolic equations. Hence we first consider a smooth extension of $q(u)$ in the interval $[-\varepsilon, \bar{u}+\varepsilon]$ for some $\varepsilon > 0$, denoted by $\bar{q}(u)$, such that $\bar{q}(u)$ is concave and smooth at $u = 0$ and $u = \bar{u}$, and furthermore

$$\bar{q}(u) = \begin{cases} 1, & u < 0 \\ q(u), & 0 \leq u \leq \bar{u}. \\ < 0, & u > \bar{u}, \end{cases}$$

Then we consider the following auxiliary problem

$$\begin{cases} u_t = \nabla \cdot \left(d_1(\bar{q}(u) - \bar{q}'(u)u)\nabla u - u\bar{q}(u)\chi(v)\nabla v\right) + f(u,v), \\ v_t = d_2\Delta v + g(u,v), \end{cases} \tag{2.2.6}$$

Next, we will employ Amann's results [5, 4, 6] to prove the global existence of solutions to the auxiliary problem (2.2.6) and (2.1.11) and show that $0 \leq u \leq \bar{u}$ if $0 \leq u_0 \leq \bar{u}$. Since $q(u) = \bar{q}(u)$ for all $0 \leq u \leq \bar{u}$ and $0 \leq u \leq \bar{u}$ for $0 \leq u_0 \leq \bar{u}$, we automatically obtain the global existence of solutions for the original problem (2.1.10) and (2.1.11). The zero flux boundary condition (2.1.11) is equivalent to the Neumann boundary condition. Amann's results on global existence apply for both Dirichlet and Neumann boundary conditions. Hence for a given function $\eta \in C(\partial\Omega, \{0,1\})$, we consider more general conditions given by

$$\begin{aligned} \eta u + (1-\eta)\frac{\partial u}{\partial \mathbf{n}} &= 0 \text{ on } \partial\Omega, \\ \eta v + (1-\eta)\frac{\partial v}{\partial \mathbf{n}} &= 0 \text{ on } \partial\Omega, \end{aligned} \tag{2.2.7}$$

where $\mathbf{n}$ represents the outer unit normal vector on $\partial\Omega$.

Let $\rho \in (n, +\infty)$, then the space $W^{1,\rho}(\Omega;\mathbb{R}^2)$ is continuously embedded in the continuous function space $C(\Omega;\mathbb{R}^2)$. We define

$$W_b^{1,\rho} := \left\{ w \in W^{1,\rho}(\Omega;\mathbb{R}^2) \,\middle|\, \eta w|_{\partial\Omega} = 0 \right\},$$

By assumption (A2) and the definition of the extension $\bar{q}(u)$, we know that $d(u) = d_1(\bar{q}(u) - \bar{q}'(u)u) > 0$ and $d(u)$ is smooth for $u \in [-\varepsilon, \bar{u}+\varepsilon]$. Note that $\bar{q}(0) = 1$. Then it is easy to verify that

$$d(u) > d_1 \text{ for } u \in [-\varepsilon, \bar{u}+\varepsilon]. \tag{2.2.8}$$

Now we can choose an open subset $\mathcal{G} \subset \mathbb{R}^2$ such that

$$X_1 \subset \mathcal{G} \subset X_2,$$

where

$$X_1 = \{(u,v) \in \mathbb{R}^2 |\ 0 \le u \le \bar{u}, v \ge 0\}$$

and

$$X_2 = \{(u,v) \in \mathbb{R}^2 |\ -\varepsilon \le u \le \varepsilon + \bar{u}\}.$$

We consider the solution in the following solution space

$$X := \left\{ w = (u,v) \in W_b^{1,\rho} \middle|\ w(\overline{\Omega}) \in \mathcal{G} \right\}.$$

Under the above mathematical set up, we have the following local existence theorem.

Lemma 2.2.2. *Let Ω be a smooth bounded domain of $\mathbb{R}^n$ with boundary $\partial\Omega$ and the assumptions (A1)-(A4) be satisfied. Then we have*

(i) For any initial data $(u_0, v_0) \in X$, there exists a positive constant $T(u_0, v_0)$ depending on the initial data (u_0, v_0) such that problem (2.2.6), (2.2.1) and (2.2.7) has a unique maximal classical solution $(u(x,t), v(x,t))$ defined on $\Omega \times [0, T(u_0, v_0))$ satisfying

$$(u,v) \in C([0, T(u_0,v_0)); X) \cap C^{2,1}(\overline{\Omega} \times (0, T(u_0,v_0)); \mathbb{R}^2).$$

(ii) Let $\phi(t, (u_0, v_0))$ be the unique solution obtained above. Then ϕ is a $C^{0,1}$-map from the set $\{(t, (u,v)) | (u,v) \in X, 0 \le t \le T(u_0,v_0)\}$ to X.

(iii) If $u_0 \ge 0, v_0 \ge 0$, then $u \ge 0, v \ge 0$.

(iv) If $\|(u,v)(\cdot,t)\|_{L^\infty(\Omega)}$ is bounded away from the boundary of $\mathcal{G}$ for each time t with $0 < t \le T(u_0,v_0)$, then $T(u_0,v_0) = +\infty$, i.e., (u,v) is a global solution in time. Furthermore, $(u,v) \in C^\theta([0,+\infty); C^{2(1-\sigma)}(\overline{\Omega}))$ for any $0 \le \theta \le \sigma \le 1$.

Proof. The proof of local existence is similar to the proof in [59, 124]. Let $w = (u,v) \in \mathbb{R}^2$. Then (2.1.10), (2.2.1) and (2.2.7) can be rewritten as

$$\begin{cases} w_t = \nabla \cdot (a(w)\nabla w) + \mathcal{F}(w) & \text{in } \Omega \times [0,+\infty), \\ \mathcal{B}w = 0 & \text{on } \partial\Omega \times [0,+\infty), \\ w(\cdot,0) = (u_0, v_0) & \text{in } \Omega, \end{cases} \tag{2.2.9}$$

where

$$a(w) = \begin{pmatrix} d_1(\bar{q}(u) - \bar{q}'(u)u) & -u\chi(v)\bar{q}(u) \\ 0 & d_2 \end{pmatrix}$$

and

$$\mathcal{B}w = \eta w - (1-\eta)\frac{\partial w}{\partial \nu}.$$

Since for $(u,v) \in \mathcal{G}$, $d(u) = d_1(\bar{q}(u) - \bar{q}'(u)u) > 0$, the eigenvalues of $A(w)$ are positive. Therefore, (2.2.9) is normally elliptic [5]. Then (i) and (ii) follows from Thm. 7.3 and Corollary 9.3 in paper [5]. The positivity (iii) follows from Thm. 15.1 of [6]. Since (2.2.9) is a triangular system, (iv) follows from Thm. 5.2 of [4]. □

To obtain the global solution, from the results in (iv) of Lemma 2.7, it remains to prove that u, v are L^∞-bounded away from the boundary of $\mathcal{G}$. By the definition of $\mathcal{G}$, it suffices to show that u is bounded below by 0 and above by $\bar{u}$. In the following Lemma, we show that $0 \le u \le \bar{u}$ provided that $0 \le u_0 \le \bar{u}$.

Lemma 2.2.3. *Assume that $0 \le u_0 \le \bar{u}$. Let (u,v) be a solution obtained in Lemma 2.2.2 with zero flux boundary condition (2.1.11). Then it follows that $0 \le u \le \bar{u}$.*

Proof. We use a comparison principle for nonlinear parabolic equation to prove the existence of upper and lower bounds for u. Indeed, the lower bound 0 has been obtained in Lemma 2.2.2 (iii). We only need to show the existence of the upper bound $\bar{u}$. Given $v \in C^{2,1}(\overline{\Omega} \times (0, T(u_0, v_0)))$, we can easily verify from the first equation of system (2.2.6) that the operator P is uniformly parabolic (see [76]) on $\Gamma = \mathbb{R} \times \mathbb{R}^n \times \mathbb{R} \times \mathbb{R}$, where

$$\begin{aligned} Pu &= P(u, \nabla u, \triangle u, u_t) \\ &= u_t - \nabla \cdot \left(d_1(\bar{q}(u) - \bar{q}'(u)u)\nabla u - u\bar{q}(u)\chi(v)\nabla v\right) - f(u,v). \end{aligned}$$

For any solution (u,v) of system (2.2.6) obtained in Lemma 2.2.2, we have $Pu = 0$. However, for $u = \bar{u}$, we have from assumptions (A2) and (A3) that

$$P\bar{u} > 0.$$

On the boundary $\partial\Omega$, we have $\frac{\partial \bar{u}}{\partial \mathbf{n}} = 0$. Hence $u = \bar{u}$ is a supersolution of system (2.2.6) with Neumann boundary conditions. Following the comparison principle, we obtain that $u \le \bar{u}$. Together with the positivity property obtained in Lemma 2.2.2, one has $0 \le u \le \bar{u}$.

□

Note that we only can show the boundness of u for zero flux boundary condition. So the global existence of solutions to the auxiliary system (2.2.6) are obtained only for zero flux boundary condition. For $0 \le u \le \bar{u}$, we have $\bar{q}(u) = q(u)$. Then

combining Lemma 2.2.2, Lemma 2.2.3 and Lemma 2.2.4, we obtain the following global existence and boundedness theorem to system (2.1.10) with zero flux boundary condition (2.1.11).

Theorem 2.2.5. *For any $(u_0, v_0) \in X$ with $0 \leq u_0 \leq \bar{u}$, $0 \leq v_0 \leq \bar{v}$ on $\overline{\Omega}$, the initial-boundary value problem (2.1.10), (2.1.11) and (2.2.1) has a unique positive solution (u, v) satisfying*

(i) $(u, v) \in C([0, +\infty); X) \cap C^{2,1}(\overline{\Omega} \times (0, +\infty); \mathbb{R}^2)$.

(ii) $u(t, x)$ and $v(t, x)$ are bounded on $\overline{\Omega} \times [0, +\infty)$ with $0 \leq u \leq \bar{u}$, $0 \leq v \leq \bar{v}$.

(iii) The solution semigroup $\phi(t, (u_0, v_0))$ forms a semi-dynamical system on X.

2.3 Pattern Formation

Pattern formation in mathematics refers to the process that, by changing a bifurcation parameter, the spatially homogeneous steady states lose stability to spatially inhomogeneous perturbations, and stable inhomogeneous solutions arise. In this section, we investigate pattern formation for system (2.1.10). The approach applied here is very routine. We look for the spatial homogeneous steady states by setting the kinetics on the right hand side of (2.1.10) to be zero

$$f(u_s, v_s) = 0, \ g(u_s, v_s) = 0. \tag{2.3.1}$$

We suppose that (u_s, v_s) is a nonnegative solution of (2.3.1). That is, (u_s, v_s) is a homogeneous steady state of system (2.1.10). We assume that in the absence of any spatially variation the homogeneous steady state is linearly stable. We first determine the conditions for this to hold.

With no spatial variation, u and v satisfy

$$u_t = f(u, v), \ v_t = g(u, v). \tag{2.3.2}$$

The linearization of (2.3.2) at (u_s, v_s) is

$$w_t = Aw, \quad A = \begin{pmatrix} f_u & f_v \\ g_u & g_v \end{pmatrix} \tag{2.3.3}$$

where A is the community (Jacobian) matrix of system (2.3.2) at steady state (u_s, v_s). Hereafter, we shall take the partial derivative of f and g to be evaluated at the steady state unless stated otherwise. Then the conditions for which (u_s, v_s) is linearly stable can be easily determined by

$$trA = f_u + g_v < 0, \ |A| = f_u g_v - f_v g_u > 0. \tag{2.3.4}$$

If there are some parameters in f and g, then the steady states (u_s, v_s) are functions of these parameters. Hence inequalities (2.3.4) impose certain constraints on the parameters.

In what follows, we shall consider the full chemotaxis model (2.1.10). We examine small perturbations from the spatially homogeneous steady state (u_s, v_s) of the form

$$u = u_s + \epsilon\tilde{u}(x,t),\ v = v_s + \epsilon\tilde{v}(x,t), \tag{2.3.5}$$

where $\epsilon << 1$.

Substituting (2.3.5) into (2.1.10), we end up with

$$\begin{cases} \epsilon\tilde{u}_t = \epsilon\nabla\big(d_1(q(u_s+\epsilon\tilde{u}) - q'(u_s+\epsilon\tilde{u})(u_s+\epsilon\tilde{u}))\nabla u \\ \qquad\qquad -\epsilon(u_s+\epsilon\tilde{u})\chi(v_s+\epsilon\tilde{v})q(u_s+\epsilon\tilde{u})\nabla\tilde{v}\big) + f(u_s+\epsilon\tilde{u}, v_s+\epsilon\tilde{v}), \\ \epsilon\tilde{v}_t = \epsilon d_2\triangle\tilde{v} + g(u_s+\epsilon\tilde{u}, v_s+\epsilon\tilde{v}). \end{cases} \tag{2.3.6}$$

Equating first order terms with respect to ϵ, neglecting higher-order terms, and dropping the tilde for the convenience, we obtain the following linearized system for (2.1.10)

$$\begin{cases} u_t = d_1(q(u_s) - q'(u_s)u_s)\triangle u - u_s q(u_s)\chi(v_s)\triangle v + uf_u + vf_v, \\ v_t = d_2\triangle v + ug_u + vg_v. \end{cases} \tag{2.3.7}$$

Hereafter we abbreviate $\vartheta = q(u_s) - q'(u_s)u_s$ and $\varrho = -\chi(v_s)u_s q(u_s)$. The v_s in $\chi(v_s)$ will be often abbreviated for notational convenience unless stated otherwise, i.e., $\chi = \chi(v_s)$. Since we assume that $q'(u) < 0$ for $0 \le u \le \bar{u}$, we have $\vartheta > 0$. The chemotactic sensitivity χ is always assumed to be nonnegative and hence $\varrho < 0$.

In the following, we assume that the domain is a one dimensional bounded domain although all analysis still holds for any dimensional bounded domain. Then following the standard argument (*e.g.*, see [82]), the dispersion relation associated with system (2.3.7) can be determined as

$$\lambda^2 + a(k^2)\lambda + b(k^2) = 0, \tag{2.3.8}$$

where k is the spatial eigenvalue which is commonly referred to as the wavenumber and λ is the eigenvalue which determines temporal growth and depends on the wavenumber k. The $a(k^2)$ and $b(k^2)$ are given, respectively, as

$$\begin{aligned} a(k^2) &= (\vartheta d_1 + d_2)k^2 - (f_u + g_v), \\ b(k^2) &= \vartheta d_1 d_2 k^4 + (\varrho g_u - d_2 f_u - \vartheta d_1 g_v)k^2 + f_u g_v - f_v g_u. \end{aligned} \tag{2.3.9}$$

The dispersion relation (2.3.8) gives $\lambda(k)$ as a function of wavenumber k at steady state (u_s, v_s). For the steady state to be unstable, we require that $Re\lambda(k)$ is positive for some $k \neq 0$. Since $a(k^2) > 0$ due to (2.3.4), the instability can only occur if $b(k^2)$ becomes negative for some k so that equation (2.3.8) for λ has one positive and one negative root. Referring to (2.3.9), the condition $b(k^2) < 0$ requires that

$$\vartheta d_1 d_2 k^4 + (\varrho g_u - d_2 f_u - \vartheta d_1 g_v)k^2 + f_u g_v - f_v g_u < 0. \tag{2.3.10}$$

Since it is required in (2.3.4) that $|A| = f_u g_v - f_v g_u > 0$, a necessary condition for (2.3.10) is

$$\varrho g_u - d_2 f_u - \vartheta d_1 g_v < 0. \tag{2.3.11}$$

For (2.3.10) to be the case for some nonzero k, the discriminant of equation $b(k^2) = 0$ must be positive since the coefficient $\vartheta d_1 d_2$ of k^4 is positive. In other words, for the existence of an interval of unstable modes, we require that

$$(\varrho g_u - d_2 f_u - \vartheta d_1 g_v)^2 - 4\vartheta d_1 d_2 (f_u g_v - f_v g_u) > 0. \tag{2.3.12}$$

Applying (2.3.11), we obtain from (2.3.12) that

$$\varrho g_u - d_2 f_u - \vartheta d_1 g_v < -2\sqrt{\vartheta d_1 d_2 (f_u g_v - f_v g_u)}. \tag{2.3.13}$$

To recap, we have now obtained conditions for the generation of spatial patterns for the volume filling chemotaxis model (2.1.10) and (2.1.11). For the convenience we reproduce them here. Remembering that all derivatives are evaluated at the steady state (u_s, v_s), they are

$$\begin{gathered} f_u + g_v < 0,\ f_u g_v - f_v g_u > 0,\ \varrho g_u - d_2 f_u - \vartheta d_1 g_v < 0, \\ (\varrho g_u - d_2 f_u - \vartheta d_1 g_v)^2 - 4\vartheta d_1 d_2 (f_u g_v - f_v g_u) > 0, \end{gathered} \tag{2.3.14}$$

where $\vartheta = q(u_s) - q'(u_s)u_s$, $\varrho = -\chi(v_s)u_s q(u_s)$. The importance of the chemotaxis term in the chemotaxis model is that it leads to a Δv term in the u equation, so-called cross-diffusion. This removes the need for d_1 and d_2 to be sufficiently different in order to obtain spatial patterns. The strength of the chemotactic sensitivity χ plays a crucial role in pattern formation. Generally there exists a critical value χ_c such that there is no pattern formation if χ is below this critical value χ_c, while pattern formation can be expected if χ is larger than this critical value χ_c. In our problem, we can explicitly determine this critical value if all parameters are fixed in system (2.1.10) except for the chemotactic sensitivity χ. Indeed, from the foregoing analysis, we know that the bifurcation occurs when

$$\varrho g_u - d_2 f_u - \vartheta d_1 g_v = -2\sqrt{\vartheta d_1 d_2 (f_u g_v - f_v g_u)}. \tag{2.3.15}$$

Substituting $\varrho = -\chi u_s q(u_s)$ into (2.3.15) and solving the resulting equation for χ, we obtain the critical chemosensitivity χ_c

$$\chi_c = \frac{2\sqrt{\vartheta d_1 d_2 (f_u g_v - f_v g_u)} - d_2 f_u - \vartheta d_1 g_v}{g_u u_s q(u_s)}. \tag{2.3.16}$$

At this bifurcation value, the corresponding critical wavenumber is given by

$$k_c^2 = \frac{d_2 f_u + \vartheta d_1 g_v - \varrho g_u}{2\vartheta d_1 d_2}. \tag{2.3.17}$$

Whenever $b(k^2) < 0$, (2.3.8) has a solution λ which is positive for the range of wave numbers. When $\chi > \chi_c$, from (2.3.9), the range of unstable wave numbers $k_1^2 < k^2 < k_2^2$ is obtained from the zeros k_1^2 and k_2^2 of $b(k^2) = 0$ as

$$\begin{aligned} k_1^2 &= \frac{C - \{C^2 - 4\vartheta d_1 d_2 (f_u g_v - f_v g_u)\}^{1/2}}{2\vartheta d_1 d_2} < k^2 \\ &< k_2^2 = \frac{C + \{C^2 - 4\vartheta d_1 d_2 (f_u g_v - f_v g_u)\}^{1/2}}{2\vartheta d_1 d_2}, \end{aligned} \tag{2.3.18}$$

where $C = d_2 f_u + \vartheta d_1 g_v - \varrho g_u$ denotes the coefficient of k^2 in equation $b(k^2) = 0$.

Whenever conditions (2.3.14) are satisfied and there is a range of wavenumbers k lying within the bound defined by (2.3.18), then the corresponding spatial eigenfunctions are linearly unstable and pattern formation can be expected. It is worthwhile to point out that for an infinite domain there is always a spatial pattern if $0 < k_1^2 < k_2^2$ in (2.3.18). In this situation, conditions (2.3.14) are sufficient conditions for pattern formation to system (2.1.10) and (2.1.11). While for a finite domain, the possible wavenumbers k and corresponding spatial wavelengths are discrete and depend in part on the boundary conditions. If there does not exist discrete wavenumber k^2 lying between k_1^2 and k_2^2, then there is no spatial pattern formation even if (2.3.14) is satisfied. Some examples will be given in the forthcoming sections.

We summarize the main results obtained in this section in the following theorem.

Theorem 2.3.1. *Let (u_s, v_s) be a spatially homogeneous steady state of system (2.1.10). Let f_u, f_v and g_u, g_v denote the partial derivatives evaluated at steady state (u_s, v_s). Then pattern formation of system (2.1.10) with zero-flux boundary condition (2.1.11) is possible if (2.3.14) is satisfied. Furthermore, the critical chemosensitivity χ_c is determined by (2.3.16). When $\chi < \chi_c$, there is no spatial pattern, whereas pattern formation can be expected if $\chi > \chi_c$ and the range of unstable wavenumbers is given by (2.3.18).*

2.4 *Analysis for Nonlinear Squeezing Probability*

By the global existence and boundedness obtained in Theorem 2.4, we know that $0 \leq u \leq \bar{u}$ if $0 \leq u_0 \leq \bar{u}$. Then as we mentioned in the Introduction, a logical choice for the squeezing probability function $q(u)$ which reflects the plastic property of particles is

$$q(u) = 1 - \left(\frac{u}{\bar{u}}\right)^{\gamma}, \quad \gamma \geq 1, \quad 0 \leq u \leq \bar{u}. \tag{2.4.1}$$

In this section, we will discuss the dynamics of system (2.1.10) with $q(u)$ which has the nonlinear form (2.4.1). For simplicity, we suppose that the cell and chemoattractant kinetics have the following form extensively used in the literature (e.g., [98, 124])

$$f(u,v) = \mu u(1 - u/u_c), \quad g(u,v) = \nu u - \delta v, \tag{2.4.2}$$

where the cell kinetics follows the logistic growth with carrying capacity $0 < u_c \leq \bar{u}$ and $\mu > 0$, the chemoattractant grows with rate ν and decays with rate δ due to dilution. Applying (2.4.1), (2.4.2) into (2.1.10), (2.1.11), we obtain

$$\begin{cases} u_t = \nabla \cdot \big(D(u)\nabla u - \chi\varphi(u)\nabla v\big) + \mu u(1 - \frac{u}{u_c}), \\ v_t = d_2\Delta v + \nu u - \delta v, \\ \big(D(u)\nabla u - \chi\varphi(u)\nabla v\big) \cdot \mathbf{n} = 0, \ \nabla v \cdot \mathbf{n} = 0, \\ u(x,0) = u_0(x) \geq 0, \ v(x,0) = v_0(x) \geq 0, \end{cases} \tag{2.4.3}$$

where $\mathbf{n}$, as usual, denotes the unit outward normal vector at the boundary of the domain and $D(u)$ and $\varphi(u)$ are denoted by

$$D(u) = d_1\left[1 + (\gamma - 1)\left(\frac{u}{\bar{u}}\right)^{\gamma}\right], \ \varphi(u) = u\left[1 - \left(\frac{u}{\bar{u}}\right)^{\gamma}\right]. \tag{2.4.4}$$

As a special case of (2.1.10), the global existence and boundedness of the solution to (2.4.3) has been given by Theorem 2.4.

Clearly, the spatially homogeneous steady states of system (2.4.3) are $(0,0)$ and $(u_c, \nu u_c/\delta)$. Furthermore, by linearization, one can easily determine that the steady state $(0,0)$ is a saddle point and hence unstable, while the steady state $(u_c, \nu u_c/\delta)$ is stable to the corresponding homogeneous system of (2.4.3) with two negative eigenvalues $-\nu$ and $-\delta$. Therefore, we focus on the stable steady state $(u_s, v_s) = (u_c, \nu u_c/\delta)$ to study pattern formation for system (2.4.3). First we linearize the system (2.4.3) about the steady state $(u_c, \nu u_c/\delta)$ and obtain

$$\begin{cases} u_t = \nabla \cdot \big(D(u_c)\nabla u\big) - \nabla \cdot \big(\chi\varphi(u_c)\nabla v\big) - \mu u. \\ v_t = d_2\Delta v + \nu u - \delta v, \\ \big(D(u_c)\nabla u - \chi\varphi(u_c)\nabla v\big) \cdot \mathbf{n} = 0, \ \nabla v \cdot \mathbf{n} = 0, \\ u(x,0) = u_0(x) \geq 0, \ v(x,0) = v_0(x) \geq 0, \end{cases}$$

Performing the linear stability analysis as before, we find the corresponding dispersion relation

$$\begin{aligned} &\lambda^2 + a(k^2)\lambda + b(k^2) = 0, \\ &a(k^2) = (D(u_c) + d_2)k^2 + (\mu + \delta), \\ &b(k^2) = D(u_c)d_2k^4 + (\mu d_2 + \delta D(u_c) - \chi\nu\varphi(u_c))k^2 + \mu\delta. \end{aligned} \tag{2.4.5}$$

From the analysis in the previous section, the condition (2.3.14) has to be satisfied to obtain pattern formation. In the situation discussed in this section, we know that $f_u + g_v = -(\mu + \delta) < 0$ and $f_u g_v - f_v g_u = \mu\delta > 0$. Then we only need the third and fourth condition in (2.3.14) to hold. This requires that (see 2.3.13)

$$\mu d_2 + \delta D(u_c) - \chi\nu\varphi(u_c) < -2\sqrt{d_2\mu\delta D(u_c)}. \tag{2.4.6}$$

Then (2.4.6) gives a necessary condition for pattern formation of system (2.4.3). If we regard the wavenumber as a continuous variable in spite of the fact the wavenumber is discrete, (2.4.6) then gives a sufficient and necessary condition for pattern formation of system (2.4.3) with zero flux boundary condition.

In the remainder of this section, we will investigate the influence of the squeezing exponent γ, chemosensitivity χ, growth rate ν and death rate δ of chemoattractant on the pattern formation of (2.4.3).

2.4.1 Bifurcations with Chemotactic Sensitivity χ

From the previous analysis, if we think of the chemosensitivity χ as the bifurcation parameter, then the bifurcation value χ_c is determined by (see 2.3.16)

$$\chi_c = \frac{2\sqrt{d_2\mu\delta D(u_c)} + \mu d_2 + \delta D(u_c)}{\nu\varphi(u_c)}. \tag{2.4.7}$$

The corresponding critical wavenumber k_c is determined from (2.3.17) by

$$k_c^2 = \frac{-\mu d_2 - \delta D(u_c) + \chi_c\nu\varphi(u_c)}{2d_2D(u_c)}. \tag{2.4.8}$$

When $\chi > \chi_c$, we have $b(k^2) < 0$ for some wavenumbers k^2 and hence there exists a positive solution λ of (2.4.5) for some $k \neq 0$. Moreover, the range of unstable wave numbers $k_1^2 < k^2 < k_2^2$ can be obtained as

$$k_1^2 = \frac{S - \{S^2 - 4\mu\delta d_2D(u_c)\}^{1/2}}{2d_2D(u_c)}, \tag{2.4.9}$$

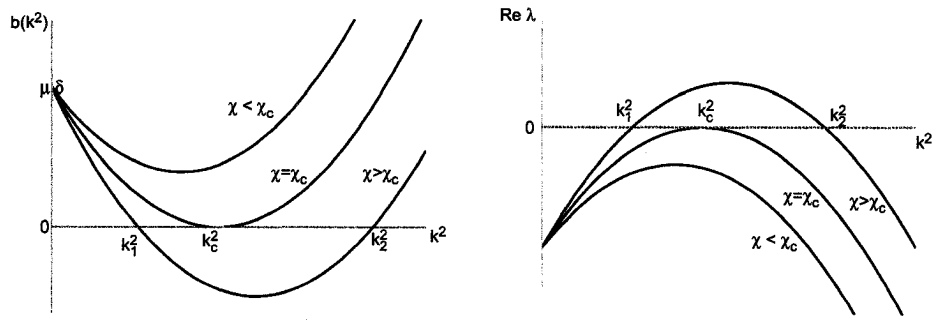

(a) (b)

Figure 2.2: (a) A sketch of $b(k^2)$ against k^2 defined by (2.4.5). When the chemosensitivity strength χ increases beyond the critical value χ_c, $b(k^2)$ becomes negative for a finite range of k^2. (b) Plot of the real part of eigenvalue $\lambda(k^2)$ as a function of k^2 defined in (2.4.5). When $\chi > \chi_c$, there is a range of wavenumbers $k_1^2 < k^2 < k_2^2$ such that the steady state is unstable. The parameters are chosen as $\gamma = 1, d_1 = 0.1,\ d_2 = 1.0, u_c = 2.0,\ \bar{u} = 4.0,\ \mu = 4.0,\ \nu = 5.0,\ \delta = 10.0$.

and

$$k_2^2 = \frac{S + \{S^2 - 4\mu\delta d_2 D(u_c)\}^{1/2}}{2d_2 D(u_c)}, \tag{2.4.10}$$

where $S = -\mu d_2 - \delta D(u_c) + \chi\nu\varphi(u_c)$.

Then the critical value is (k_c, χ_c) such that $b(k^2) > 0$ for all k^2 if $\chi < \chi_c$, however $b(k^2) < 0$ for a range of wavenumbers $k_1^2 < k^2 < k_2^2$ if $\chi > \chi_c$. Figure 2.2(a) shows how $b(k^2)$ varies as a function of k^2 for various χ and Figure 2.2(b) shows how the eigenvalue λ varies as a function of k^2 for various χ. A stability curve for $b(k^2) = 0$ for $\gamma = 2$ in Figure 2.3 immediately gives us some information we need to know. When $\chi \leq \chi_c$, $b(k^2) \geq 0$ and consequently no positive wavenumbers correspond to χ. As χ increases and exceeds the critical value χ_c, there must exist wavenumbers k between the two curves (dashed and solid portion of the curve in Figure 2.3). These wavenumbers define unstable modes.

As we mentioned in the previous section, the condition $\chi > \chi_c$ does not guarantee pattern formation since the allowable wavenumbers k are discrete for a finite domain. Generally the pattern formation can be achieved by increasing the domain size. So a question arises as how can a necessary and sufficient condition be derived to generate the spatial pattern for a fixed domain. Indeed, the bifurcation diagram Figure 2.3

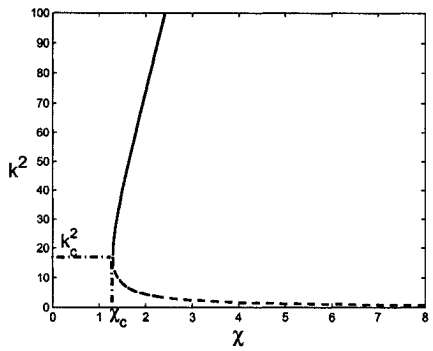

Figure 2.3: A sketch of $b(k^2) = 0$ in (2.4.5) in the (k^2, χ)-plane, where parameters are chosen as $\gamma = 2, d_1 = 0.1,\ d_2 = 1.0, u_c = 2.0,\ \bar{u} = 4.0,\ \mu = 4.0,\ \nu = 5.0,\ \delta = 10.0$ and consequently $k_c^2 = 17.889,\ \chi_c = 1.296$. The dashed portion denotes k_1^2 and solid portion represents k_2^2.

has given us some useful clues already. We study the difference for k_2^2 and k_1^2

$$\mathcal{K}(\chi, \nu, \delta) = k_2^2 - k_1^2 = \frac{\left[(\mu d_2 - \delta D(u_c) + \nu\chi\varphi(u_c))^2 - 4\mu\delta d_2 D(u_c)\right]^{1/2}}{d_2 D(u_c)}.$$

Here we consider the difference as a function of χ, ν and δ since we will investigate the influence of χ, ν and δ on the pattern formation in the following. It is easy to verify that $\mathcal{K}(\chi, \nu, \delta)$ is a increasing function of χ and ν. So pattern formation can be supported by increasing the valve of χ or ν. Biologically, we expect pattern formation if the growth rate ν of the chemoattractant or the chemosensitivity χ is big enough. On the other hand, $\mathcal{K}(\chi, \nu, \delta)$ is a decreasing function of δ. Hence pattern formation also can be supported by decreasing the decay rate δ of the signal.

We now derive a sufficient and necessary condition for the chemosensitivity χ for pattern formation in a one dimensional domain $[0, \ell]$. On $[0, \ell]$ with non flux boundary conditions, the corresponding wavenumbers k are given by $k = n\pi/\ell$, where $n = 0, \pm 1, \pm 2, \cdots$. The requirement (2.3.18) in terms of modes n becomes

$$n_1^2 < n^2 < n_2^2, \tag{2.4.11}$$

where $n_1 = k_1\ell/\pi$ and $n_2 = k_2\ell/\pi$. Now we want to find an appropriate value of χ such that there exists at least one integer n satisfying (2.4.11). Without loss of generality, we look at positive wavemodes only and other cases can be analyzed analogously. For $\chi = \chi_c$, we have $k_1 = k_2 = k_c$ and hence $k_1\ell/\pi = k_2\ell/\pi$. We can easily check that $k_1^2(\chi)$ as a function of χ is decreasing and that, $k_2^2(\chi)$ is

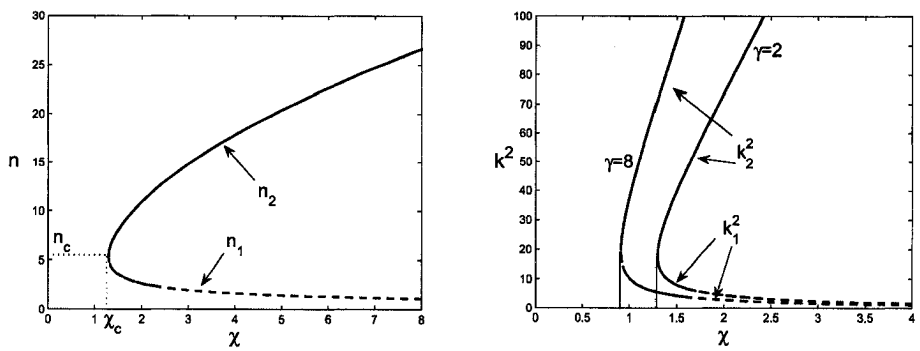

(a) (b)

Figure 2.4: (a) A sketch of $b(n^2\pi^2/\ell^2) = 0$ in (2.4.5) in the (n, χ)-plane, where the domain is chosen as $[0, \ell]$ with $\ell = 4$ and parameters are chosen as $\gamma = 2, d_1 = 0.1$, $d_2 = 1.0, u_c = 2.0$, $\bar{u} = 4.0$, $\mu = 4.0$, $\nu = 5.0$, $\delta = 10.0$ and consequently $n_c = 5.38$, $\chi_c = 1.296$. (b) A comparison of wavenumbers with respect to squeezing exponent γ. Parameters are chosen as in (a) except γ.

increasing. As a consequence, n_1 is decreasing (see dotted portion of the curve in Figure 2.4(a)) and n_2 is increasing (see solid portion of the curve in Figure 2.4(a)) as a function of χ. Now we look for the conditions such that there exists at least one integer n between n_1 and n_2. At the critical value χ_c as obtained above, we define $n_c := n_1(\chi_c) = n_2(\chi_c)$. Then we have two cases to consider.

Case (a). n_c is an integer. Then we increase χ from χ_c, and any increment of χ will lead to $n_1(\chi) < n_c < n_2(\chi)$ due to the monotonicity of n_1 and n_2. We immediately get an unstable mode $n = n_c$ (see Figure 2.4(a)). In this case, χ_c is a bifurcation value, such that pattern formation is obtained when $\chi > \chi_c$ and no pattern formation evolves when $\chi < \chi_c$.

Case (b). n_c is not an integer number. Since $n_1(\chi)$ is continuously decreasing with respect to χ and $n_2(\chi) \to \infty$ as $\chi \to \infty$, there must exist a minimum number of χ, denoted by χ_B, such that $\chi_B > \chi_c$ and $n_1(\chi_B)$, or $n_2(\chi_B)$, or both are integer. For $\chi > \chi_B$, we obtain an unstable mode n such that $n_1(\chi) < n < n_2(\chi)$.

We therefore end up with the following theorem.

Theorem 2.4.1. *Assume $\gamma \geq 1$. Let $\chi_B \geq \chi_c$ be the first number of χ such that either $k_1\ell/\pi$, or $k_2\ell/\pi$ is an integer. Then χ_B is a bifurcation number and $\chi > \chi_B$ is a necessary and sufficient condition for pattern formation of system (2.4.3).*

Next, we examine the relationship between the critical value χ_c and the crowding squeezing exponent γ, from which we can understand the influence of γ on the dynamics of system (2.4.3). We give the following theorem.

Theorem 2.4.2. *The critical value χ_c, as a function of squeezing exponent γ, is decreasing.*

Proof. For convenience, we denote $\sigma = u_c/\bar{u} < 1$ and $M(\gamma) = \frac{1}{1-(\frac{u_c}{\bar{u}})^\gamma} = \frac{1}{1-\sigma^\gamma} > 1$, then (2.4.7) can be rewritten as

$$\chi_c = \frac{1}{\nu u_c}\left(2\sqrt{\mu\delta d_1 d_2 M(\gamma)}\sqrt{1+\gamma\sigma^\gamma M(\gamma)} + \mu d_2 M(\gamma) + \delta d_1(1+\gamma\sigma^\gamma M(\gamma))\right) \tag{2.4.12}$$

Note that $0 < u_c/\bar{u} < 1$. Then function M is non-increasing with respect to γ. Next we prove that function $\gamma\sigma^\gamma M(\gamma)$ is a decreasing function of γ. To see this, we define $h(\gamma) = \gamma\sigma^\gamma M(\gamma)$. Then we have

$$\frac{dh}{d\gamma} = \frac{\sigma^\gamma(1-\sigma^\gamma+\gamma\ln\sigma)}{(1-\sigma^\gamma)^2}.$$

Since $\sigma < 1$, it is easy to verify that $1-\sigma^\gamma+\gamma\ln\sigma < 0$ for all $\gamma > 1$. So $h(\gamma)$ is decreasing with respect to γ. Consequently the critical chemosensitivity value χ_c is a decreasing function of squeezing exponent γ.

□

Remark 2.4.3. *Biologically, Theorem 4.2 tells us that cells are apt to aggregate when the squeezing exponent γ is increased since the squeezing probability $q(u)$ is increasing with respect to γ. When the squeezing probability is bigger, cells are more motile and hence pattern formation is easier to form.*

2.4.2 Bifurcation with Growth Rate ν

In this subsection, we consider growth rate ν as the bifurcation parameter, and therefore fix all other parameters in system (2.4.3). Note that varying ν affects the value of the steady state (u_s, v_s). We want to understand the influence of the dynamical parameter ν on pattern formation of system (2.4.3). The temporal eigenvalues λ of the linearization at (u_s, v_s) are the roots of equation (2.4.5).

We compute the critical value ν_c for ν from (2.4.5)

$$\nu_c = \frac{2\sqrt{d_2\mu\delta D(u_c)} + \mu d_2 + \delta D(u_c)}{\chi\varphi(u_c)} \tag{2.4.13}$$

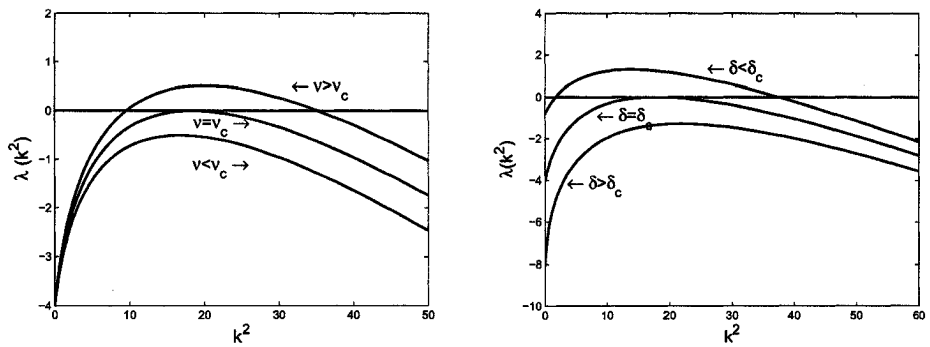

(a) (b)

Figure 2.5: (a). Dispersion relation (2.4.5) as the parameter ν passes through the bifurcation value $\nu_c = 10.18$, where $\gamma = 4, d_1 = 0.1, d_2 = 1.0, u_c = 2.0, \bar{u} = 4.0, \mu = 4.0, \delta = 10.0, \chi = 0.5$. (b) Dispersion relation (2.4.5) as the parameter δ passes through the bifurcation value $\delta_c = 4.04$, where $\gamma = 2, d_1 = 0.1, d_2 = 1.0, u_c = 2.0, \bar{u} = 4.0, \mu = 10, \nu = 20, \chi = 0.5$.

such that no unstable modes exist if ν is below this critical number ν_c, whereas unstable modes are possible when ν is beyond this critical value ν_c (see Figure 2.5(a) for the dispersion relation). Furthermore, if we consider ν_c as a function of γ and recall the proof of Theorem 4.2, we can show that the critical value ν_c of the growth rate decreases as the parameter γ increases. This outcome is consistent with the biological context that increasing the growth rate ν of chemoattractant, result in higher concentration of chemoattractant which makes the system more unstable.

Remember that the critical number ν_c is not necessary a bifurcation value due to the discrete nature of the unstable modes. But we can formally obtain the desired bifurcation value for ν by performing the same analysis as for χ in section 4.1 and obtain a bifurcation theorem similar with Theorem 4.1. To avoid repetition, we do not provide details here.

2.4.3 Bifurcation with Decay Rate δ

In the model (2.4.3), the parameter δ stands for the decay (degradation) rate of the chemoattractant, and the uniform steady state (u_s, v_s) depends on δ. If we perform the similar linear stability analysis as we did in previous sections, it is easy to derive a critical value for δ as

$$\delta_c = \frac{(\sqrt{\nu\chi\varphi(u_c)} - \sqrt{\mu d_2})^2}{d_1 D(u_c)}. \tag{2.4.14}$$

such that when $\delta > \delta_c$, there does not exist unstable modes, whereas unstable modes can be expected when $\delta < \delta_c$. Now if we regard the death rate δ as a dynamical parameter, the dispersion relation of (2.4.5) as δ passes through the critical value δ_c is shown in Figure 2.5(b). Here the plot of the dispersion relation for δ in Figure 2.5(b) has some difference in appearance compared to the plot of the dispersion relation for ν in Figure 2.5(a). From Figure 2.5(a), we see that all eigenvalues λ take the same value at $k^2 = 0$ for any dynamical parameter ν. However, Figure 2.5(b) shows that the eigenvalue λ has different value at $k^2 = 0$ for each different dynamical parameter δ. In fact, from equation (2.4.5), when $k^2 = 0$, we have

$$\lambda^2 + (\mu + \delta)\lambda + \mu + \delta = 0. \tag{2.4.15}$$

It is clear that equation (2.4.15) is independent of parameter ν but dependent on parameter δ.

Now we examine the relationship between the critical value δ_c and squeezing exponent γ. We still use the notation in Section 4.1 and rewrite (2.4.14) as follows

$$\delta_c^{1/2} = \sqrt{\frac{1}{d_1(1+\gamma\sigma^\gamma M(\gamma))}}\left(\sqrt{\nu\chi u_c} - \sqrt{\mu d_2 M(\gamma)}\right).$$

In section 4.1, we have shown that function $M(\gamma)$ and $\gamma\sigma^\gamma M(\gamma)$ are decreasing with respect to γ. Then it is easy to see that δ_c, as a function of γ, is increasing which is in contrast to the critical growth rate ν_c that is a decreasing function of γ. This is in agreement with the biological interpretation. When increasing the squeezing exponent, the critical death rate becomes larger and hence pattern formation can allow faster dilution of chemicals. As a consequence, pattern formation is easier to form.

2.5 Numerical Simulation in One-Dimension

In this section, we will numerically investigate pattern formation for model (2.4.3). The MATLAB PDE solver, pdepe, is a powerful tool to solve initial-boundary value problems for systems of nonlinear reaction diffusion type PDEs in the one space variable x and time t. The pdepe solver converts the PDEs to ODEs using a second-order accurate spatial discretization based on a set of nodes specified by the user. The discretization method is described in paper [112], where the consistency of the discretization can be adjusted by refining the mesh. The pdepe solver is applied here to solve the initial-boundary problem (2.4.3).

Unless stated otherwise, throughout this section, we assume zero flux boundary condition. For $\gamma = 1$, numerical solutions have been shown by Painter and Hillen

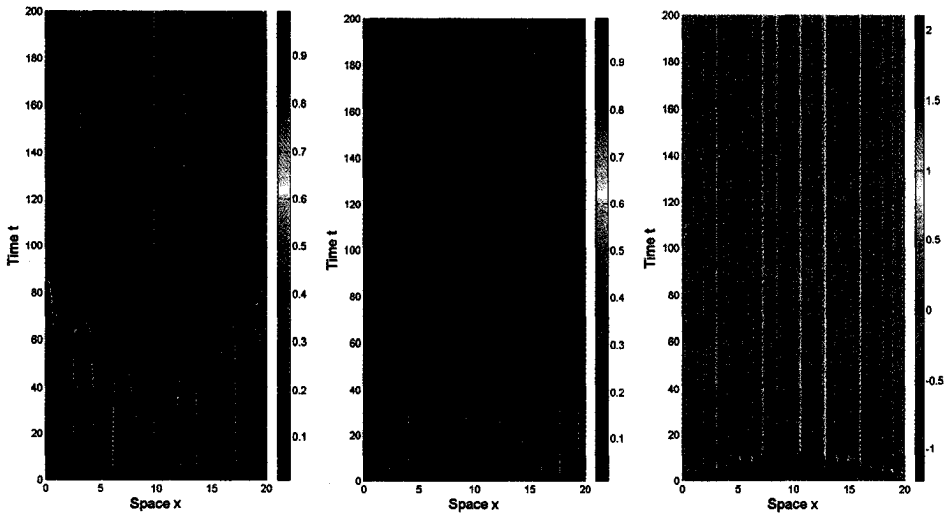

(a) (b) (c)

Figure 2.6: Space-time evolution of cell density for model (2.4.3) with zero-kinetics with initial value that is set as the small perturbation of the homogeneous solution $u_0 = 0.2$ and with $\delta = 10, \bar{u} = 1.0, u_c = 0.5, d_2 = 1.0$: (a) $\nu = 40, d_1 = 0.25, \gamma = 1, \chi = 2$. (b) $\nu = 40, d_1 = 0.25, \gamma = 2, \chi = 2$. (c) $\nu = 30, d_1 = 0.01, \gamma = 2, \chi = 1$.

in [98]. In the case of zero kinetics ($f(u, v) = 0$), Painter and Hillen found a typical behavior of merging of local peaks (also called coarsening process). In the paper by Potapov and Hillen [104], these local peaks were identified as metastable steady states and in the paper by Dolak and Schmeiser [27], a singular perturbation analysis around this transient patterns was given. These patterns are similar to coarsening patterns obtained for the Brusselator model [69], where a nonlinear stability analysis was performed. If cell kinetics are included into the model, in addition to the merging of peak patterns, the emerging of new local maxima was observed also by Painter and Hillen [98]. In this article, we particularly focus on the effect of nonlinear squeezing probability $q(u) = 1 - \left(\frac{u}{\bar{u}}\right)^{\gamma}$ through $\gamma > 1$ on the merging and emerging process. We obtain similar patterning process as the linear diffusion case ($\gamma = 1$) in [98] and our results confirm that merging and emerging processes are very typical patterning processes for volume filling chemotaxis model.

2.5.1 Zero Cell Kinetics

In this subsection, we will consider the nonlinear diffusion volume-filling chemotaxis model (2.1.10) with cell kinetics $f(u,v) = 0$ and $g(u,v) = \nu u - \delta v$ as well as nonlinear squeezing probability function $q(u) = 1 - (u/\bar{u})^\gamma$, $\gamma > 1$. Then the cell density is conserved due to no cell growth and death. Again, we look at the stability of the homogeneous steady state $(u_s, \nu u_s/\delta)$. Note that condition (2.3.4) is not satisfied in the case of $f = 0$. However the instability region can be explicitly determined by performing standard linear stability analysis as before:

$$\chi > \frac{\bar{u}^\gamma + (\gamma - 1)u_s^\gamma}{u_s \bar{u}^\gamma (\bar{u}^\gamma - u_s^\gamma)} \frac{d_1 \delta}{\nu}. \tag{2.5.1}$$

Under this condition, unstable wavemodes can be expected. From (2.5.1), we see that the cell density is crucial for pattern formation. At high or low initial cell density u_s, the system tends to be stable to spatial perturbations.

Some typical numerical simulation examples are shown in Figure 2.6. In Figure 2.6(a), we choose squeezing exponent $\gamma = 1$ and then the diffusion of the system (3.8) becomes linear. In Figure 2.6(b), we choose $\gamma = 2$ and the diffusion of the system (3.8) is then nonlinear. For both cases, we observe some initial merging process, which stops and a new time-independent peak pattern appears. Actually, similar merging dynamics appear for other crowding squeezing exponents $\gamma > 1$ (not shown).

In Figure 2.6(c), we significantly reduce the cell diffusion parameter d_1, which leads to a persistent steady state without observable merging dynamics.

2.5.2 Non-Zero Cell Kinetics

From the above numerical analysis, we see that without cell kinetics we obtain multiple aggregations which undergo a merging process. In this section, we include the effect of cell kinetics into the model and explore whether or not stable multi-peak aggregation patterns can develop. We suppose that cells follow logistic growth $f(u,v) = \mu u(1 - u/u_c)$. Production term $g(u,v)$ and squeezing probability $q(u)$ are chosen as before. Then the model is the same as (2.4.3).

The nontrivial uniform steady state of (2.4.3) is given by $(u_s, v_s) = (u_c, \nu u_c/\delta)$, and the instability region of this steady state is determined by condition (2.4.6). The graph of the dispersion relation now corresponds to Figure 2.2(a). Thus, low wave-modes might be stable to spatial perturbation, and higher wavemodes may develop multi-peak solutions, which is contrast to the case of zero kinetics where low wave-modes might be unstable. We choose a set of parameters such that the instability

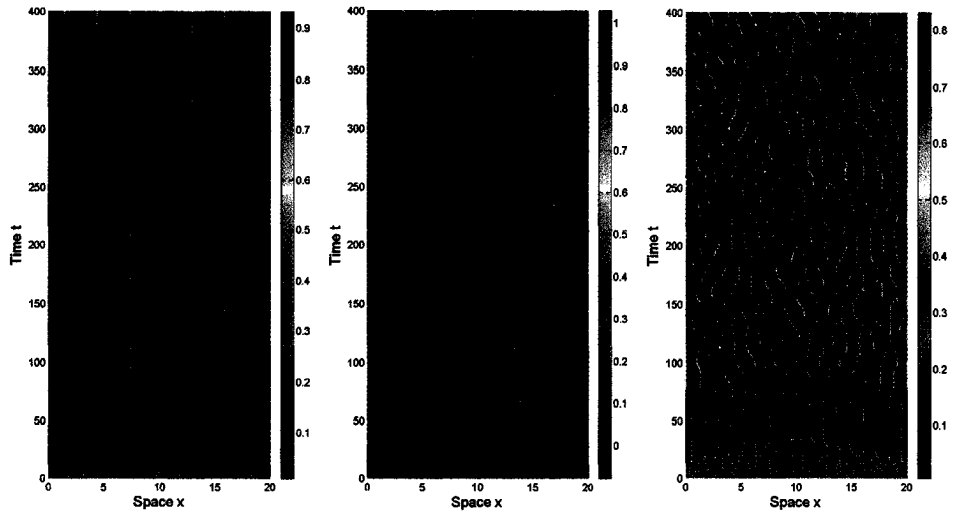

(a) (b) (c)

Figure 2.7: Space-time evolution of cell density for model (2.4.3) for different choices of parameters. (a) $d_1 = 0.25, d_2 = 1, \nu = 10, \delta = 10, \bar{u} = 1.0, u_c = 0.25, \mu = 0.5, \chi = 10, \gamma = 2$. Simulations indicate that a fixed spatial pattern exists as peaks persist and grow. Here are 7 peaks. (b) $d_1 = 0.25, d_2 = 1, \nu = 10, \delta = 10, \bar{u} = 1.0, u_c = 0.25, \mu = 0.5, \chi = 20, \gamma = 2$. (c)$d_1 = 0.01, d_2 = 1, \nu = 10, \delta = 10, \bar{u} = 1.0, u_c = 0.25, \mu = 0.5, \chi = 1, \gamma = 2$. In (b) and (c), typical merging and emerging patterns develop. The parameters chosen in (a) are closer to the stability region than those chosen in (b) and (c). All simulations use the domain size as [0 20].

condition (2.4.6) is satisfied and present the numerical simulation in Figure 2.7. We first choose parameters deep in the instability region and it was shown that multiple peaks develop and these peaks exist indefinitely (see Figure 2.7(b)-(c)). Numerical simulation shows that a time-independent persistent spatial pattern might not exist and patterns demonstrate an interesting pattern interaction process of merging and emerging, where neighboring aggregations join to form a single aggregation resulting in a large interval of low cell density. In the low density regions, new cell aggregations subsequently arise, which is in contrast to the zero kinetics case in which only merging process was observed. When the parameters are chosen close to the stability/instability boundary, solutions can stabilize into a time-independent spatial pattern (see Figure 2.7(a), where a seven peak pattern evolves). However, there are not local peaks emerging during the evolution. In Figure 2.7(c), we choose

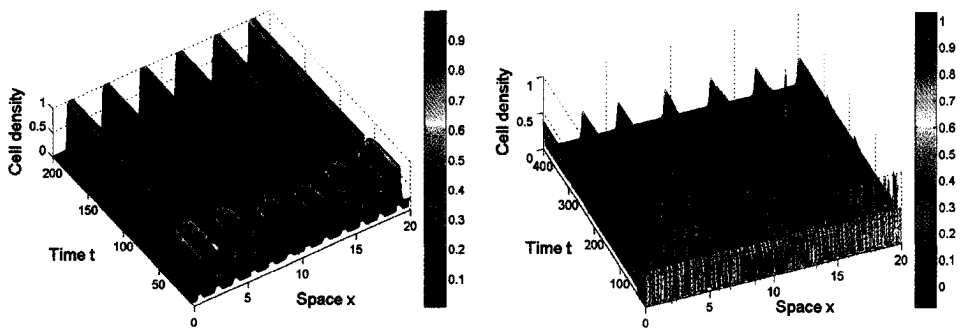

(a) (b)

Figure 2.8: Evolution of merging and emerging local peaks. (a) Zero cell kinetics, where $\nu = 40, \delta = 10, \bar{u} = 1.0, u_c = 0.5, d_1 = 0.25, d_2 = 1.0, \gamma = 1, \chi = 2$. (b) Nonzero cell kinetics, where $d_1 = 0.25, d_2 = 1, \nu = 10, \delta = 10, \bar{u} = 1.0, u_c = 0.25, \mu = 0.5, \chi = 20, \gamma = 2$.

very small diffusive rate d_1 and get more complex pattern due to high chemotactic effects.

The evolution of merging and emerging peak solutions is presented in Figure 2.8. We see that peaks are capped by the crowding capacity $\bar{u}$ due to the volume filling effects. For zero kinetics, (see Figure 2.8(a)), after some time, peaks merge into some stationary peaks. For nonzero kinetics case (see Figure 2.8(b)), we see that initially solution tends to blow up (very sharp) but the volume filling mechanism prevents blow up and then solutions stay bounded to form complex merging and emerging patterns.

2.6 Discussion

In this chapter, we include a nonlinear squeezing probability function $q(u)$, which reflects plastic properties of cells, into a volume filling chemotaxis model and prove the global existence of classical solutions to the resulting model. We show that the cell density will stay below the crowding capacity $\bar{u}$ if the initial cell density is less than this crowding capacity. We carry out conditions of pattern formation for the general volume filling chemotaxis model. Moreover, we apply a particular choice (2.4.1) of $q(u)$ into the model to perform the linear stability analysis and study the underlying bifurcation for different parameters. One dimensional numerical simulations are presented for both zero cell kinetics and nonzero cell kinetics. Merging

and emerging dynamics are observed under different parameter values. We find that the squeezing exponent γ has no huge effects on the spatio-temporal dynamics. The merging and emerging process can be observed for all values of $\gamma \geq 1$, the limit state, however, depends on γ.

The parameter γ has been included to describe plastic properties of cells. The case of $\gamma = 1$ corresponds to solid blocks (see the car-parking problem in [118]), whereas $\gamma \to \infty$ corresponds to cells being fluids which can fill all open space. The critical chemosensitivity χ_c is decreasing in γ, hence increasing γ is destabilizing the system. If γ is large, chemotaxis has a large effect and more cells can still enter into a crowded region and make chemotactic aggregation more pronounced.

The merging pattern formation had been experimentally observed in Dd (*Dictyostelium discoideum*) cell movement [36]. This patterning process describes the dynamics between cell aggregations. A cell aggregation is a swarm of individual cells. However merging pattern formation denotes two swarms merging to form one larger aggregation. This process is beneficial to particles for survival of harmful situations or avoiding predators. The emerging pattern formation is the insertion of a new aggregation into a free area triggered by cell kinetics, which is beneficial to optimally use available resources. These new aggregations can then merge with other neighboring aggregations to form stronger aggregations for some reasons described above. The emerging pattern formation is possibly related to the chemotactic pattern formation by motile *Azotobacter vinelandii* [96] although a final confirmation needs to be made.

Comparing Figure 2.8(a) and (b), we can conclude that the emerging process is due to cell growth. It is of interest to further study the merging and emerging process in more details. The merging and emerging patterns in Figure 2.7(b) seem to have a dominating wave length so that neither too many nor too few local maxima arise. In paper [104], some scaling analysis and numerical analysis were applied to describe the transition region and the local peaks were identified with metastable steady states. For the merging process (no kinetics), a qualitative analysis was given by Dolak and Schmeiser [27] using a singular perturbation argument. It would be interesting to apply their methods to study the merging-emerging process as observed above. A detailed analysis will be given in a forthcoming paper [48].

Chapter 3

PATTERN FORMATION FOR A VOLUME FILLING CHEMOTAXIS MODEL WITH FAST DIFFUSION

3.1 Introduction

Taking into account the plastic cell properties, $q(u)$ should be pointwise larger than the linear case. To do this, we make the assumption $q''(u) < 0$ and (2.1.6) and (2.1.8) are two explicit choices. In chapter 2, we study the case of (2.1.6). In this chapter, we continue to consider case (2.1.8). For convenience, we rewrite (2.1.8) again here

$$q(u) = \begin{cases} \left(1 - \dfrac{u}{\bar{u}}\right)^r, & 0 \le u \le \bar{u}, \\ 0, & u > \bar{u}, \end{cases} \tag{3.1.1}$$

Hereafter, we call the parameter r the *crowding exponent*. This chapter discusses the dynamics of system (2.1.9) with $q(u)$ which takes the nonlinear form (3.1.1). We still assume that the cell kinetics follows the logistic growth with carrying capacity $u_c \le \bar{u}$, the chemoattractant grows with rate ν and decays with rate δ as in Chapter 2. Then we obtain the following system with zero flux boundary conditions

$$\begin{cases} u_t = \nabla \cdot \left(d_1(1-\frac{u}{\bar{u}})^{r-1}(1-\frac{u(1-r)}{\bar{u}})\nabla u\right) - \nabla \cdot \left(u(1-\frac{u}{\bar{u}})^r \chi \nabla v\right) + \mu u(1-\frac{u}{u_c}), \\ v_t = d_2 \Delta v + \nu u - \delta v, \\ \left(d_1(1-\frac{u}{\bar{u}})^{r-1}(1-\frac{u(1-r)}{\bar{u}})\nabla u - \chi u(1-\frac{u}{\bar{u}})^r \nabla v\right) \cdot \mathbf{n} = 0, \ \nabla v \cdot \mathbf{n} = 0, \\ u(x,0) = u_0(x) \ge 0, \ v(x,0) = v_0(x) \ge 0, \end{cases} \tag{3.1.2}$$

where $(x,t) \in \Omega \times (0,\infty)$ and $\mathbf{n}$, as usual, denotes the unit outward normal vector at the boundary of the domain Ω.

It is easy to see that nonlinear diffusion function in the first equation of (3.1.2) tends to ∞ when $u \to \bar{u}$, which is called a *fast* diffusion problem although it is different from the conventional concept (see [80]), which refer to the following problem

$$p_i = \Delta u^{1+\delta}, -1 < \delta < 0,$$

When $\delta > 0$, the above problem is called *slow* diffusion problem. The case $\delta = 0$ is the linear heat equation. For *fast* diffusion the solution decays to zero in some

finite time which depends on the initial data, whereas the solution decays to zero in infinite time for *slow* diffusion. This is the essential difference between *fast* and *slow* diffusion. So far, we are not able to biologically explain why the choice (3.1.1) might result in a *fast* diffusion. But we expect that the solution is bounded away from $\bar{u}$ and then the *fast* diffusion might be avoided. However, this needs to be mathematically proven.

Amann's theory requires the diffusion function to be a C^2 function. Since $0 < r < 1, (1 - \frac{u}{\bar{u}})^{r-1} \to \infty$ as $u \to \bar{u}$ and the diffusion of the system (3.1.2) blows up at $u = \bar{u}$. Hence Amann's theory [5, 4, 6] as applied in Chapter 2 no longer applies here. The global existence of system (3.1.2) remains open and need to be explored in the future using new mathematical techniques. One of possible approaches is apply a mollifier to smooth diffusion with a small parameter ε and then prove the convergence of solutions as $\varepsilon \to 0$. However, we still can study pattern formation regardless of the open question of global existence.

In this Chapter, we will explicitly give the conditions for pattern formation of system (3.1.2) and find the critical values for various parameters in the system. Also we study the relation between those critical values and crowding exponent r. The numerical simulations in one dimension for both zero kinetics and non-zero kinetics are presented. It turns out the novel choice (3.1.1) of squeezing probability $q(u)$ does not bring significant difference in pattern formation compared to the choice made in Chapter 2. Here we still observe merging and emerging patterning process. The reason that we still study the pattern formation for the choice (3.1.1) is that we may that the singularity in diffusion might make a difference in pattern formation. But afterwards we know that there is no significant difference.

To investigate pattern formation of system (3.1.2), we need to find the homogeneous steady states of system (3.1.2), which are $(0, 0)$ and $(u_c, \nu u_c/\delta)$. Furthermore, by linearization, one can easily determine that the steady state $(0, 0)$ unstable, while the steady state $(u_c, \nu u_c/\delta)$ is stable to the corresponding homogeneous system of (3.1.2). Therefore, we take steady state $(u_s, v_s) = (u_c, \nu u_c/\delta)$ to study pattern formation for system (3.1.2). First we linearize system (3.1.2) about the steady state $(u_c, \nu u_c/\delta)$ and obtain

$$\begin{cases} u_t = \nabla \cdot \left(d_1(1 - \frac{u_c}{\bar{u}})^{r-1}(1 - \frac{u_c(1-r)}{\bar{u}})\nabla u\right) - \nabla \cdot \left(\chi u_c(1 - \frac{u_c}{\bar{u}})^r \nabla v\right) - \mu u, \\ v_t = d_2 \Delta v + \nu u - \delta v, \\ \left(d_1(1 - \frac{u_c}{\bar{u}})^{r-1}(1 - \frac{u_c(1-r)}{\bar{u}})\nabla u - \chi u_c(1 - \frac{u_c}{\bar{u}})^r \nabla v\right) \cdot \mathbf{n} = 0, \ \nabla v \cdot \mathbf{n} = 0, \\ u(x, 0) = u_0(x) \geq 0, \ v(x, 0) = v_0(x) \geq 0. \end{cases} \tag{3.1.3}$$

Then the temporal growth rate λ satisfies

$$\begin{vmatrix} \lambda+\mu+(1-\frac{u_c}{\bar{u}})^{r-1}(1-\frac{u_c(1-r)}{\bar{u}})d_1k^2 & -\chi u_c(1-\frac{u_c}{\bar{u}})^r k^2 \\ -\nu & \lambda+\delta+d_2k^2 \end{vmatrix} = 0 \tag{3.1.4}$$

and hence the corresponding dispersion relation is

$$\begin{aligned} &\lambda^2+a(k^2)\lambda+b(k^2)=0, \\ &a(k^2)=((1-\tfrac{u_c}{\bar{u}})^{r-1}(1-\tfrac{u_c(1-r)}{\bar{u}})d_1+d_2)k^2+(\mu+\delta), \\ &b(k^2)=(1-\tfrac{u_c}{\bar{u}})^{r-1}(1-\tfrac{u_c(1-r)}{\bar{u}})d_1d_2k^4 \\ &\qquad +(-\chi\nu u_c(1-\tfrac{u_c}{\bar{u}})^r+\mu d_2+(1-\tfrac{u_c}{\bar{u}})^{r-1}(1-\tfrac{u_c(1-r)}{\bar{u}})\delta d_1)k^2+\mu\delta. \end{aligned} \tag{3.1.5}$$

From the analysis in the previous Chapter, a necessary condition for pattern formation of system (3.1.2) is

$$\begin{aligned} &-\chi\nu u_c(1-\tfrac{u_c}{\bar{u}})^r+\mu d_2+\delta d_1(1-\tfrac{u_c}{\bar{u}})^{r-1}(1-\tfrac{u_c(1-r)}{\bar{u}}) \\ &<-2\sqrt{(1-\tfrac{u_c}{\bar{u}})^{r-1}(1-\tfrac{u_c(1-r)}{\bar{u}})d_1d_2\mu\delta}. \end{aligned} \tag{3.1.6}$$

If we regard the wavenumber as a continuous variable in spite of the fact the wavenumber is discrete, (3.1.6) then gives a sufficient and necessary condition for pattern formation of system (3.1.2) with zero flux boundary condition.

In the remainder of this Chapter, we will investigate the influence of the crowding exponent r, chemosensitivity χ, growth rate ν and death rate δ of chemoattractant on the pattern formation of system(3.1.2).

3.2 Bifurcation Analysis

3.2.1 Bifurcations with Chemotactic Sensitivity χ

From the previous analysis, if we think of the chemosensitivity χ as the bifurcation parameter, then the bifurcation value χ_c is determined by

$$\chi_c=\frac{2\sqrt{(1-\frac{u_c}{\bar{u}})^{r-1}(1-\frac{u_c(1-r)}{\bar{u}})d_1d_2\mu\delta}+\mu d_2+\delta d_1(1-\frac{u_c}{\bar{u}})^{r-1}(1-\frac{u_c(1-r)}{\bar{u}})}{\nu u_c(1-\frac{u_c}{\bar{u}})^r}. \tag{3.2.1}$$

The corresponding critical wavenumber k_c is determined (see (2.3.17)) by

$$k_c^2=\frac{-\mu d_2-\delta d_1(1-\frac{u_c}{\bar{u}})^{r-1}(1-\frac{u_c(1-r)}{\bar{u}})+\nu\chi u_c(1-\frac{u_c}{\bar{u}})^r}{2(1-\frac{u_c}{\bar{u}})^{r-1}(1-\frac{u_c(1-r)}{\bar{u}})d_1d_2}. \tag{3.2.2}$$

when $\chi > \chi_c$, we have $b(k^2) < 0$ and hence there exists a positive solution λ of (3.1.5) for some $k \neq 0$. Moreover, the range of unstable wave numbers $k_1^2 < k^2 < k_2^2$ can be obtained as

$$k_1^2 = \frac{S - \{S^2 - 4\mu\delta d_1 d_2(1 - \frac{u_c}{\bar{u}})^{r-1}(1 - \frac{u_c(1-r)}{\bar{u}})\}^{1/2}}{2(1 - \frac{u_c}{\bar{u}})^{r-1}(1 - \frac{u_c(1-r)}{\bar{u}})d_1 d_2}, \tag{3.2.3}$$

and

$$k_2^2 = \frac{S + \{S^2 - 4\mu\delta d_1 d_2(1 - \frac{u_c}{\bar{u}})^{r-1}(1 - \frac{u_c(1-r)}{\bar{u}})\}^{1/2}}{2(1 - \frac{u_c}{\bar{u}})^{r-1}(1 - \frac{u_c(1-r)}{\bar{u}})d_1 d_2}, \tag{3.2.4}$$

where $S = -\mu d_2 - \delta d_1(1 - \frac{u_c}{\bar{u}})^{r-1}(1 - \frac{u_c(1-r)}{\bar{u}}) + \nu\chi u_c(1 - \frac{u_c}{\bar{u}})^r$.

Then the bifurcation value is (k_c, χ_c) such that $b(k^2) > 0$ for all k^2 if $\chi < \chi_c$, however $b(k^2) < 0$ for a range of wavenumbers $k_1^2 < k^2 < k_2^2$ if $\chi > \chi_c$.

As we mentioned in the previous Chapter, the condition $\chi > \chi_c$ does not guarantee pattern formation since the allowable wavenumbers k are discrete for a finite domain. That is, the critical value χ_c is not necessary a bifurcation number. However, the bifurcation value of χ can be obtained as in Theorem 2.4.1 in the Chapter 2. To avoid repetition, we omit the details.

Next, we examine the relationship between the critical value χ_c and the crowding exponent r, from which we can understand the influence of r on the dynamics of system (3.1.2). Indeed, if we set $M = \frac{1}{1-\frac{u_c}{\bar{u}}} > 1$, then (3.2.1) can be rewritten as

$$\chi_c = \frac{1}{\nu u_c}\left(2\sqrt{\mu\delta d_1 d_2}\sqrt{M^r + \frac{u_c}{\bar{u}}rM^{r+1}} + \mu d_2 M^r + \delta d_1(1 + \frac{u_c}{\bar{u} - u_c}r)\right) \tag{3.2.5}$$

It is easy to see that χ_c, as a function of r, is an increasing function.

3.2.2 Bifurcation with Crowding Exponent r

In this subsection, we shall derive a condition on r such that pattern formation is possible. Toward this end, we rearrange inequality 3.1.6 and get

$$\begin{aligned}&(1 - \tfrac{u_c}{\bar{u}})^{r-1}(1 - \tfrac{u_c(1-r)}{\bar{u}})\delta d_1 + 2\sqrt{(1 - \tfrac{u_c}{\bar{u}})^{r-1}(1 - \tfrac{u_c(1-r)}{\bar{u}})d_1 d_2\mu\delta} \\ &< \chi\nu u_c(1 - \tfrac{u_c}{\bar{u}})^r - \mu d_2,\end{aligned} \tag{3.2.6}$$

which immediately requires that

$$\chi\nu u_c\left(1 - \frac{u_c}{\bar{u}}\right)^r > \mu d_2. \tag{3.2.7}$$

Since $u_c < \bar{u}$, we have that

$$1 - \frac{u_c(1-r)}{\bar{u}} = 1 - \frac{u_c}{\bar{u}} + \frac{u_c}{\bar{u}}r \geq 1 - \frac{u_c}{\bar{u}} \geq 0.$$

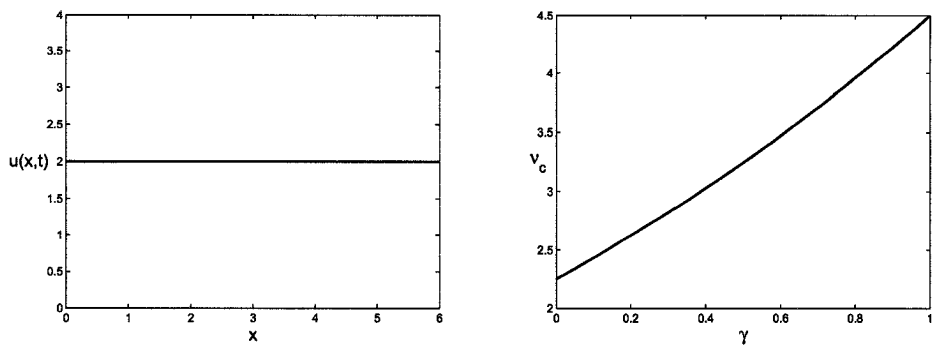

(a) (b)

Figure 3.1: (a) A plot of a stable solution of system (3.1.2), where parameters are chosen as $r = 0.02, d_1 = 0.1,\ d_2 = 10, u_c = 2.0,\ \bar{u} = 4.0,\ \mu = 4.0,\ \nu = 5.0,\ \delta = 10.0, \chi = 2.75$. (b) The plot of the critical number ν_c as a function of crowding exponent r. The figure shows that ν_c is an increasing function of r.

Applying the above inequality, we can derive the following inequality from (3.2.6)

$$\sqrt{(1-\frac{u_c}{\bar{u}})^r} > \frac{\sqrt{\mu\nu\chi u_c d_2} + \sqrt{\mu\delta d_1 d_2}}{\nu\chi u_c - \delta d_1}, \tag{3.2.8}$$

with a condition $\nu\chi u_c - \delta d_1 > 0$. It is easy to check that condition (3.2.8) covers condition (3.2.7).

Noting that the carrying capacity u_c is less than the crowding capacity $\bar{u}$, the function $(1-\frac{u_c}{\bar{u}})^r$ is decreasing with respect to r when $0 < r \leq 1$ and hence $\sqrt{1-\frac{u_c}{\bar{u}}} \leq \sqrt{(1-\frac{u_c}{\bar{u}})^r} \leq 1$. The inequality (3.2.8) immediately gives a necessary condition on parameters for pattern formation

$$\sqrt{\mu\nu\chi u_c d_2} + \sqrt{\mu\delta d_1 d_2} < \nu\chi u_c - \delta d_1.$$

If we fix all parameters in (3.2.8) except r, then we have the following possibilities to solve (3.2.8) for r.

(1). If $\sqrt{1-\frac{u_c}{\bar{u}}} > \frac{\sqrt{\mu\nu\chi u_c d_2}+\sqrt{\mu\delta d_1 d_2}}{\nu\chi u_c - \delta d_1}$, then (3.2.8) holds for any r with $0 < r \leq 1$. As a consequence, the pattern formation is possible.

(2). If $\sqrt{1-\frac{u_c}{\bar{u}}} < \frac{\sqrt{\mu\nu\chi u_c d_2}+\sqrt{\mu\delta d_1 d_2}}{\nu\chi u_c - \delta d_1} \leq 1$, then we can solve (3.2.8) for r to obtain that

$$r < \frac{2\ln\frac{\sqrt{\mu\nu\chi u_c d_2}+\sqrt{\mu\delta d_1 d_2}}{\nu\chi u_c - \delta d_1}}{\ln(1-\frac{u_c}{\bar{u}})}. \tag{3.2.9}$$

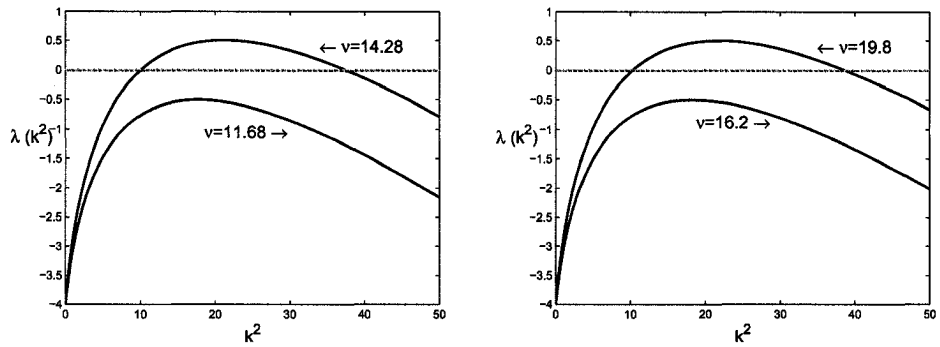

(a) $r = \frac{1}{2}$ (b) $r = 1$

Figure 3.2: (a) The plot of dispersion relation (3.1.5) with $\nu = 14.28$ and $\nu = 11.68$ for $r = 1/2$. (b) Dispersion relation (3.1.5) with $\nu = 19.8$ and $\nu = 16.2$ for $r = 1$. Where $d_1 = 0.1, d_2 = 1.0, u_c = 2.0, \bar{u} = 4.0, \mu = 4.0, \delta = 10.0, \chi = 0.5$.

We confirm our results by numerical simulations. In Figure 3.1(a), we choose appropriate parameter values such that

$$0.7071 = \sqrt{1 - \frac{u_c}{\bar{u}}} < \frac{\sqrt{\mu\nu\chi u_c d_2} + \sqrt{\mu\delta d_1 d_2}}{\nu\chi u_c - \delta d_1} = 0.9938 \leq 1$$

and $\dfrac{2\ln\frac{\sqrt{\mu\nu\chi u_c d_2}+\sqrt{\mu\delta d_1 d_2}}{\nu\chi u_c - \delta d_1}}{\ln(1-\frac{u_c}{\bar{u}})} = 0.0179$. From the above analysis, we know that if $r > 0.0179$, then the solution will be stable and no pattern formation is possible, as shown in Figure 3.1(a), where we chose $r = 0.02$.

In summary, we obtain the following theorem.

Theorem 3.2.1. *Let all parameters in (3.1.2) be fixed except for r. If $\delta d_1 - \nu\chi u_c < 0$, then we have the following results:*

(i). If parameters are chosen such that $\frac{\sqrt{\mu\nu\chi u_c d_2}+\sqrt{\mu\delta d_1 d_2}}{\nu\chi u_c - \delta d_1} > 1$, then there is no pattern formation for any r with $0 < r \leq 1$.

(ii). If $\sqrt{1 - \frac{u_c}{\bar{u}}} < \frac{\sqrt{\mu\nu\chi u_c d_2}+\sqrt{\mu\delta d_1 d_2}}{\nu\chi u_c - \delta d_1} \leq 1$. Then the following inequality gives a necessary condition for pattern formation of system (3.1.2)

$$r < \frac{2\ln(\sqrt{\mu\nu\chi u_c d_2} + \sqrt{\mu\delta d_1 d_2}\,) - 2\ln(\nu\chi u_c - \delta d_1)}{\ln(1 - \frac{u_c}{\bar{u}})}.$$

(iii). If $\sqrt{1 - \frac{u_c}{\bar{u}}} > \frac{\sqrt{\mu\nu\chi u_c d_2}+\sqrt{\mu\delta d_1 d_2}}{\nu\chi u_c - \delta d_1}$, then the pattern formation is possible for $r \in (0, 1]$.

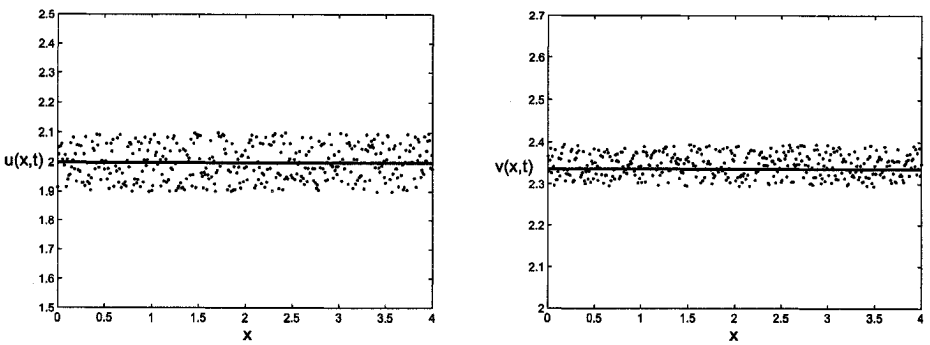

Figure 3.3: Evolution of the solution $(u(x,t), v(x,t))$ to system (3.1.2) with $r = 1/2$, $\nu = 11.68$ and $d_1 = 0.1, d_2 = 1.0, u_c = 2.0, \bar{u} = 4.0, \mu = 4.0, \delta = 10.0, \chi = 0.5$ by a random perturbation (denoted by the dots) of the stable steady state $(u_s, v_s) = (2, 3.336)$. The solid curves represents the solution $u(x,t)$ and $v(x,t)$ at $t = 4$.

3.2.3 Bifurcation with Growth Rate ν

In this subsection, we investigate the influence of the dynamical parameter ν on pattern formation of system (3.1.2). The temporal eigenvalues of the linearization at (u_s, v_s) are the roots of equation (3.1.5).

We visualize $\lambda(k^2)$ in Figure 3.2(a) for two particular values of the growth rate of chemoattractant, namely $\nu = 14.28$, for which we obtain a range of positive eigenvalues, and $\nu = 11.68$ for which all eigenvalues are negative, where we choose $r = 1/2$. In other words, the uniform steady state (u_s, v_s) obtained with $\nu = 14.28$ is unstable and pattern formation can be expected, whereas the uniform steady state (u_s, v_s) obtained with $\nu = 11.68$ is stable and no patterns evolve. Figure 3.2(b) plots the dispersion relation (3.1.5) with $r = 1$. When $r = 1$, then $\vartheta = 1$ and the first equation of (3.1.2) is significantly reduced and the diffusion of cells becomes linear. While, when $0 < r < 1$, the diffusion of cells is really nonlinear and has a singularity at $u = \bar{u}$. This means that cells will diffuse very fast when the cell density is high. Mathematically, the singularity might introduce different phenomena or mathematical difficulties, but here we observe not much difference compared to the linear case. We can understand this from both mathematical and biological point of view. Mathematically the diffusion is a stabilizing force in the chemotaxis model, the solution tends to be stable when the diffusion of cells is big. Biologically, when cells diffuse quickly, the possibility of cell aggregation is relatively small and the cell density will be controlled. Second, if we compare the dispersion

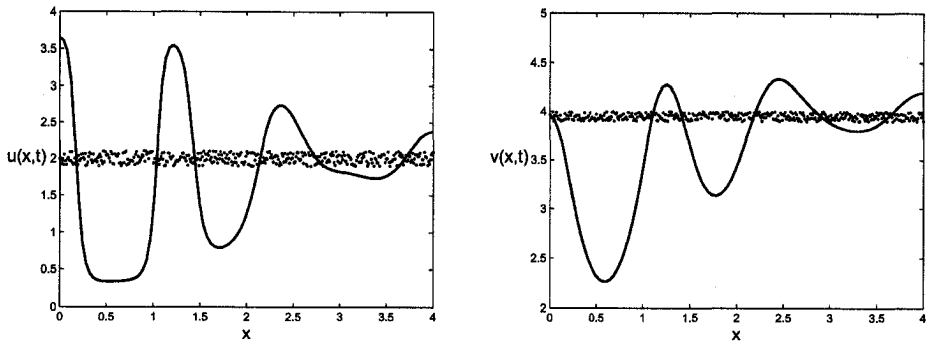

Figure 3.4: Evolution of the solution $(u(x,t), v(x,t))$ to system (3.1.2) with $r = 1/2$, $\nu = 20$ and $d_1 = 0.1, d_2 = 1.0, u_c = 2.0, \bar{u} = 4.0, \mu = 4.0, \delta = 10.0, \chi = 0.5$ by a random perturbation (denoted by the dots) of the unstable steady state $(u_s, v_s) = (2, 4)$. The solid curves represents the solution $u(x,t)$ and $v(x,t)$ at $t = 4$.

relation (3.1.5) as shown in Figure 3.2(a) and Figure 3.2(b), we find that there are no significant differences for both $r = 1$ and $r = \frac{1}{2}$. Actually, numerical plots show that the dispersion relation does not have significant differences for $r = 1$ or any other value of $r \in (0, 1)$ (not shown). The only difference we can see is in the possible bifurcation value of ν. We will examine the influence of r on the critical value of ν below.

For $\nu = 11.68$, we expect no pattern formation as shown in Figure 3.3. Although $\nu = 14.28$ satisfies the necessary condition for instability, there is no discrete wavenumber k which satisfies $k_1^2 < k^2 < k_2^2$ for the finite domain $[0, 4]$, where k_1^2 and k_2^2 are given by (3.2.3) and (3.2.4), respectively. Hence we observe no pattern formation for $\nu = 14.28$ (simulation not shown). However, it is easy to verify that the difference of k_2^2 and k_1^2 is increased by further increasing ν. In Figure 3.4, we choose $\nu = 20$ and we do observe pattern formation.

We now compute the critical value ν_c for ν from (3.1.5)

$$\nu_c = \frac{2\sqrt{(1-\frac{u_c}{\bar{u}})^{r-1}(1-\frac{u_c(1-r)}{\bar{u}})d_1 d_2 \mu\delta} + \mu d_2 + \delta d_1 (1-\frac{u_c}{\bar{u}})^{r-1}(1-\frac{u_c(1-r)}{\bar{u}})}{\chi u_c (1-\frac{u_c}{\bar{u}})^r}, \tag{3.2.10}$$

such that no unstable modes exist if ν is below this critical number ν_c, whereas unstable modes are possible when ν is beyond this critical value ν_c (see Figure 3.5(a) for the dispersion relation). Furthermore, if we consider ν_c as a function of r, we can show from (3.2.10) that $\nu_c'(r) > 0$. This implies that the critical value of

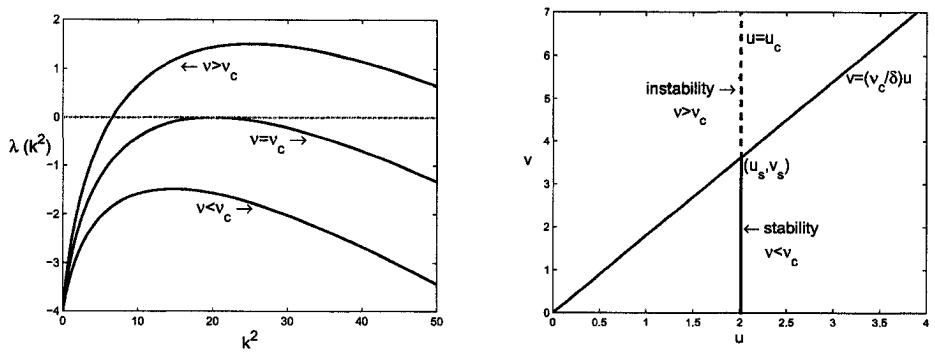

(a) (b)

Figure 3.5: (a). Dispersion relation (3.1.5) as the parameter ν passes through the bifurcation value $\nu_c = 12.98$, where $r = 1/2, d_1 = 0.1, d_2 = 1.0, u_c = 2.0, \bar{u} = 4.0, \mu = 4.0, \delta = 10.0, \chi = 0.5$. (b). Bifurcation diagram for the stability of the spatial homogeneous steady state (u_s, v_s) as the growth rate ν of chemoattractant varies. The solid portion of the line $u = u_c$ denotes the stable uniform steady states, and the dotted portion of the line $u = u_c$ represents the unstable uniform steady states. The intersection of two lines represents the uniform steady states at the bifurcation value ν_c.

the growth rate ν increases as the parameter r increases (see Figure 3.1(b)).

Remember that the critical number ν_c is not necessary a bifurcation value due to the discrete nature of the unstable modes. But we can formally obtain the desired bifurcation value for ν by performing the same analysis as for χ in section 4.1 and obtain a bifurcation theorem similar with Theorem 2.4.1. To avoid repetition, we do not provide details here. So we assume the bifurcation value is obtained and still denoted by ν_c, then the bifurcation diagram for the steady state (u_s, v_s) obtained from the intersection of line $u = u_c$ and line $v = \frac{\nu}{\delta}u$ is illustrated in Figure 3.5(b). When ν is small, the steady state is stable (denoted by the solid portion of the line $u = u_c$). The slope of line $v = \frac{\nu}{\delta}u$ increases as ν increases (or equivalently, increase as δ decreases), and as it passes through the value ν_c/δ, the resulting steady state becomes unstable (denoted by the dashed portion of the line $u = u_c$). This outcome is consistent with the biological context that increasing the growth rate ν of chemoattractant will result in higher concentration of chemoattractant which makes the system be more unstable.

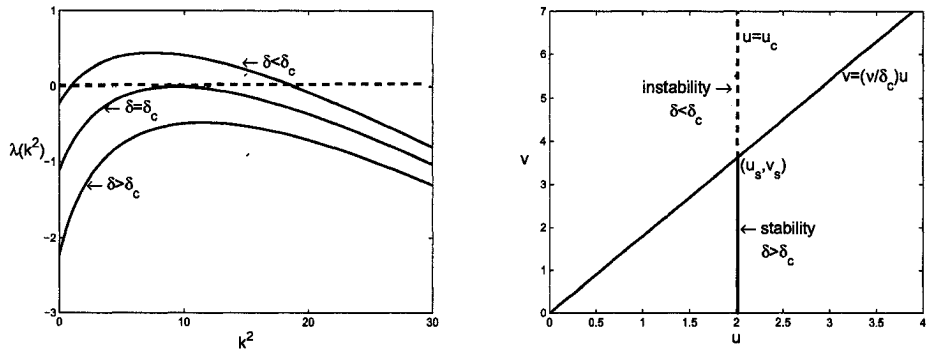

(a) (b)

Figure 3.6: (a). Dispersion relation (3.1.5) as the parameter δ passes through the bifurcation value $\delta_c = 29.22$, where $r = \frac{1}{2}, d_1 = 0.1, d_2 = 1.0, u_c = 2.0, \bar{u} = 4.0, \mu = 4.0, \nu = 20, \chi = 0.5$. (b). Bifurcation graph for the stability of the spatial homogeneous steady state (u_s, v_s) as the death rate δ of chemoattractant varies. The solid portion of the line $u = u_c$ denotes the stable uniform steady states, and the dotted portion of the line $u = u_c$ represents the unstable uniform steady states. The intersection of two lines represents the uniform steady states at the bifurcation value δ_c.

3.2.4 Bifurcation with Death Rate δ

In the model (3.1.2), the parameter δ stands for the death (degradation) rate of the chemoattractant, and the uniform steady state (u_s, v_s) depends on δ. So δ might be a potential dynamical parameter. In this section, we will understand the influence of the parameter δ on the pattern formation of system (3.1.2).

If we perform the similar linear analysis as we did in previous sections, it is easy to derive a critical value for δ

$$\delta_c = \frac{(\sqrt{\nu\chi u_c(1-u_c/\bar{u})^r} - \sqrt{\mu d_2})^2}{d_1(1-\frac{u_c}{\bar{u}})^{r-1}(1-\frac{u_c(1-r)}{\bar{u}})}. \tag{3.2.11}$$

such that when $\delta > \delta_c$, there does not exist unstable modes, whereas unstable modes can be expected when $\delta < \delta_c$. Now if we regard the death rate δ as a dynamical parameter, the dispersion relation of (3.1.5) as δ passes through the critical value δ_c is shown in Figure 3.6(a).

Now we examine the relationship between the critical value δ_c and crowing exponent r. For convenience we denote $\rho = 1 - u_c/\bar{u}$. Under condition (3.2.11), we

can rewrite (3.2.11) as follows

$$\delta_c^{1/2} = \sqrt{\frac{1}{d_1(\rho + \frac{u_c}{\bar{u}}r)}}\left(\sqrt{\nu\chi u_c\rho} - \sqrt{\frac{\mu d_2}{\rho^{r-1}}}\right).$$

Note that $0 < \rho < 1$ and hence ρ^{r-1} is decreasing with respect to r. Then it is easy to see that δ_c, as a function of r, is decreasing. Therefore, the critical death rate δ of chemoattractant decreases with respect to crowing exponent r. This is in contrast to the critical growth rate ν_c which is an increasing function of r.

Due to the discrete property of unstable modes, δ_c is not necessarily the bifurcation value which can be formally obtained such that either $k_1^2\ell/\pi^2$, or $k_2^2\ell/\pi^2$ reaches an integer number as a function of δ. We skip the detail since it uses the same argument as finding the bifurcation number for χ in section 4.1. If we still denote this bifurcation value by δ_c, the bifurcation diagram with respect to parameter δ for the steady state (u_s, v_s) can be graphed in Figure 3.6(b), which is in contrast to the case for parameter ν. When δ is small, the steady state is unstable (denoted by the dotted portion of the line $u = u_c$). The slope of line $v = \frac{\nu}{\delta}u$ decreases as δ increases, and as it passes through the value ν_c/δ, the resulting steady state becomes stable (denoted by the solid portion of the line $u = u_c$).

3.3 Numerical Simulation in One-Dimension

In this section, we will numerically investigate pattern formation for the model (3.1.2). We still use MATLAB PDE solver pdepe as we used in chapter 2 to solve the model (3.1.2). For $r = 1$, numerical solutions have been shown by Painter and Hillen in [98]. In case of zero kinetics ($f(u, v) = 0$), Painter and Hillen found a typical behavior of merging of local peaks (also called coarsening process). As before, we consider zero kinetics and non zero kinetics separately.

3.3.1 Zero Cell Kinetics

In this subsection, we will consider system (3.1.2) with cell kinetics ($\mu = 0$). Unless stated otherwise, throughout this section, we shall assume zero flux boundary condition. Initial conditions will be set as small perturbation of the homogeneous steady state. For initial conditions $u(x, 0) = u_s$ (constant), the instability region can be explicitly determined according to (3.1.6) by the following inequality

$$\chi > \frac{(\bar{u} - u_s)^r + ru_s\bar{u}^{-2}(\bar{u} - u_s)^{r-1}}{u_s(\bar{u} - u_s)^r}\frac{d_1\delta}{\nu}. \tag{3.3.1}$$

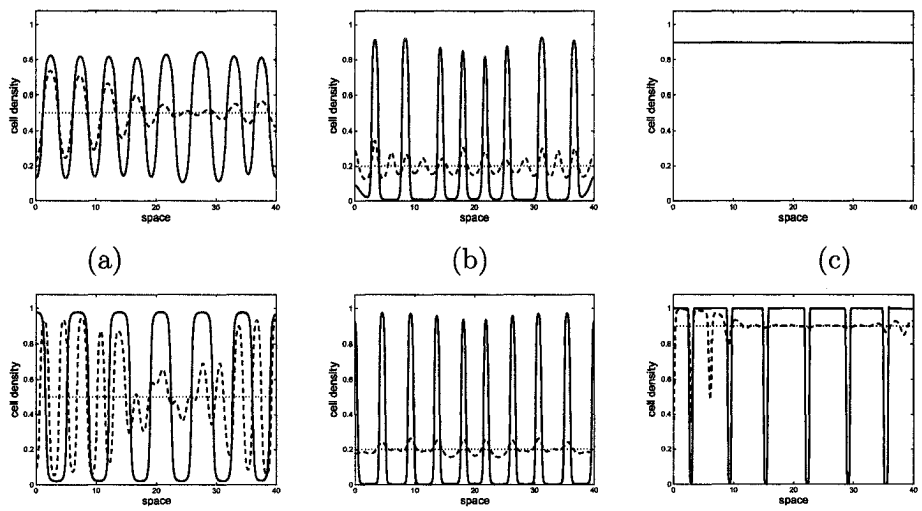

Figure 3.7: Early evolution of multiple-peak patterns for model (3.1.2) with zero cell kinetics $f(u,v) = 0$ and $g(u,v) = \nu u - \delta v$ and with different initial cell density. In (a), (b) and (c), we take $r = 1/2$ and diffusion is nonlinear. In (d), (e) and (f), we take $r = 1$ and diffusion is linear. (a) Initial cell density=0.5, at $T = 0$(dot), 150(dash) and 400(solid). (b) Initial cell density=0.2, at $T = 0$(dot), 320(dash) and 400(solid). (c) Initial cell density=0.9, no patterns form. (d) Initial cell density=0.5, at $T = 0$(dot), 50(dash) and 400(solid). (e) Initial cell density=0.2, at $T = 0$(dot), 400(dash) and 500(solid). (f) Initial cell density=0.9, at $T = 0$(dot), 30(dash) and 400(solid). Other parameters: $d_1 = 0.25, d_2 = 1, \nu = 50, \delta = 10, \bar{u} = 1.0; u_c = 0.5, \chi = 0.6$.

Under this condition, unstable wavemodes can be expected. From (3.3.1), we see that the cell density is crucial for pattern formation. At high or low initial cell density u_s, the system tends to be stable to spatial perturbations.

Typical numerical simulation examples are shown in Figure 3.7 (a-f) for a range of different initial cell densities. In these examples, we assume the crowding capacity $\bar{u}$ to be 1. As expected from the condition (3.3.1), for the initial density close to 0 or 1, there is no spatial patterning. In the region of instability a series of cell density peaks form. But the growth at the peak is capped due to the volume filling mechanism, which results in the formation of density plateaus. By varying the initial cell density of the cell population (as shown in Figure 3.7 for $u_s = 0.2, u_s = 0.5, u_s = 0.9$), the variation in the thickness and inter-width of these plateaus can be controlled. Hence the volume filling mechanism forms a robust approach of generating variations in

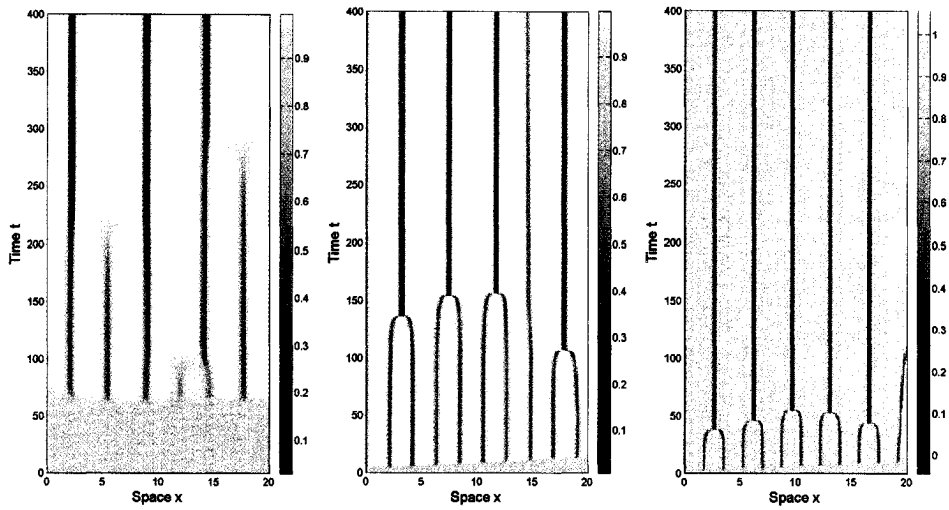

(a) (b) (c)

Figure 3.8: Space-time evolution of cell density for model (3.1.2) with zero-kinetics subject to different chemosensitivity χ. (a) $\chi = 1$. (b) $\chi = 2$. (c) $\chi = 3$. The other parameters are chosen as $\nu = 50, \delta = 10, u_m = 1.0, u_c = 0.5, u_0 = 0.9, d_1 = 0.25, d_2 = 1.0, r = 1/2$. Numerical simulations show that, when there is no cell kinetics, only a merging process is observed, whereas the emerging process does not appear. We also observe that for a larger chemosensitivity, there is more merging.

cell density of varying thickness. Comparing Figure 10(c) and Figure 3.7(f), we see the difference between linear cell diffusion and nonlinear cell diffusion. When the cell density is close to the crowding capacity, nonlinear cell diffusion will play a more crucial role than linear diffusion does and cells will not aggregate due to the high diffusion effect. In the simulations of Figure 3.8, we observe merging process at initial stage, which stops at a later stage and new time-independent persistent peak patterns appear subsequently. Also, we observe that the greater the chemosensitivity is, the earlier the peak patterns arise. This is not unexpected since biologically cells take a shorter time to aggregate when the external signals are stronger. Moreover, numerical simulations (see Figure 3.8) show that the number of peaks arising initially with larger chemosensitivity is larger than the number of peaks with smaller chemosensitivity. This is in agreement with our analysis obtained in section 4.1 since we would get more unstable modes by increasing χ. The number of unstable modes is proportional to the peak patterns developing initially. But

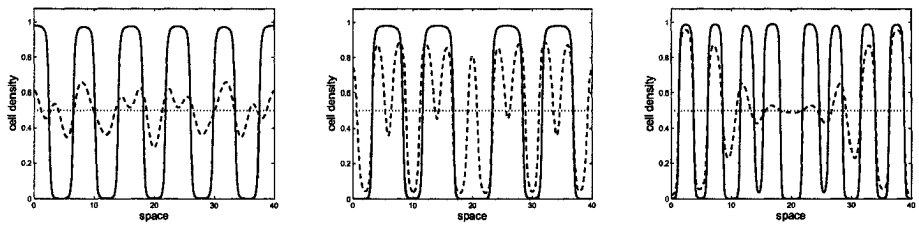

(a) (b) (c)

Figure 3.9: Early evolution of peak patterns for model (3.1.2) with zero cell kinetics ($\mu = 0$) for a range of r. (a) $r = 0.125$, at $T = 0$(dot), 150(dash) and 400(solid). (b) $r = 0.25$, at $T = 0$(dot), 300(dash) and 400(solid). (c) $r = 0.75$, at $T = 0$(dot), 30(dash) and 400(solid). Other parameters: $d_1 = 0.25, d_2 = 1, \nu = 1, \delta = 1, \bar{u} = 1.0; u_c = 0.5, \chi = 5$.

over time, the unstable modes will decrease due to the consumption of external chemicals and the number of peaks will decrease accordingly. As a consequence, merging process happens and solutions stabilize into a time-independent spatial patterns (a 5 peak pattern in Figure 3.8).

Figure 3.9 demonstrates the dynamics of pattern formation for different value of crowding exponent r. Since the cell kinetics is zero (or equivalently to say $\mu = 0$), the inequality (3.2.8) is satisfied. As expected from Theorem 4.2, spatial patterning is possible. In Figure 3.9, we choose parameters within the instability region and plot a time evolution of the peak patterns for a range of values of r. The dynamics of pattern formation can be simulated similarly for other parameters (ν and δ) but the numerical simulations are not shown here.

3.3.2 Non-Zero Cell Kinetics

In this section, we include the effect of cell kinetics into the model and explore whether stable multi-peak aggregation patterns can develop. We suppose that cells follow logistic growth $f(u, v) = \mu u(1 - u/u_c)$. Then the model is the same as (3.1.2).

The nontrivial uniform steady state of (3.1.2) is given by $(u_s, v_s) = (u_c, \nu u_c/\delta)$, and the instability region of this steady state is determined by condition (3.1.6). We choose a set of parameters such that the instability condition (3.1.6) is satisfied and plot the results in Figure 3.10. The time sequence plot shows that multiple peaks develop and numerical simulations indicate that these peaks exists indefinitely. Simulations also show that a time-independent persistent spatial pattern might not exist and solutions demonstrate an interesting pattern interaction process of merging

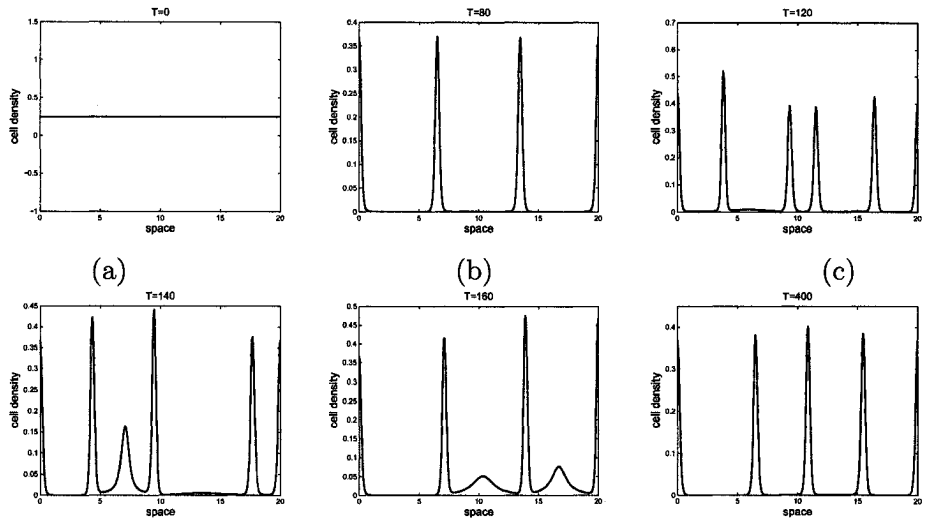

Figure 3.10: Time sequence showing cell density evolution for model (3.1.2) with $\mu \neq 0$, where $d_1 = 0.25, d_2 = 1, \nu = 1, \delta = 1, \bar{u} = 1.0, u_c = 0.5, \mu = 5, r = 1/4, \chi = 50$.

and emerging. Time evolution shows a temporarily oscillating pattern as some peaks collapse together (see $T = 120 - 160$) or new peaks arise (see $T = 160 - 400$). But when the parameters are chosen close to the stability/instability boundary, solutions can stabilize into a time-independent spatial pattern (see Figure 3.11(a), where a 7 peaks pattern evolves persistently). This might provide a mechanism to generate stripe pattern in two dimension. Examples for a variety of parameter values deep in the instability region are shown in Figure 3.11(b)-(c), where neighboring aggregations join to form a single aggregation resulting in a large space of low cell density. In the low density regions, new cell aggregations subsequently arise.

3.4 Discussion

In this chapter the volume filling chemotaxis model which including a different squeezing probability $q(u)$ than the one chosen in the previous chapter. The new choice of $q(u)$ leads to an unbounded diffusion rate when cell density approach the crowding capacity. From mathematical point of view, this behavior will make system more stable and the global in time solutions should exist although we are not able to prove this so far. However, we study the pattern formation for the resultant system.

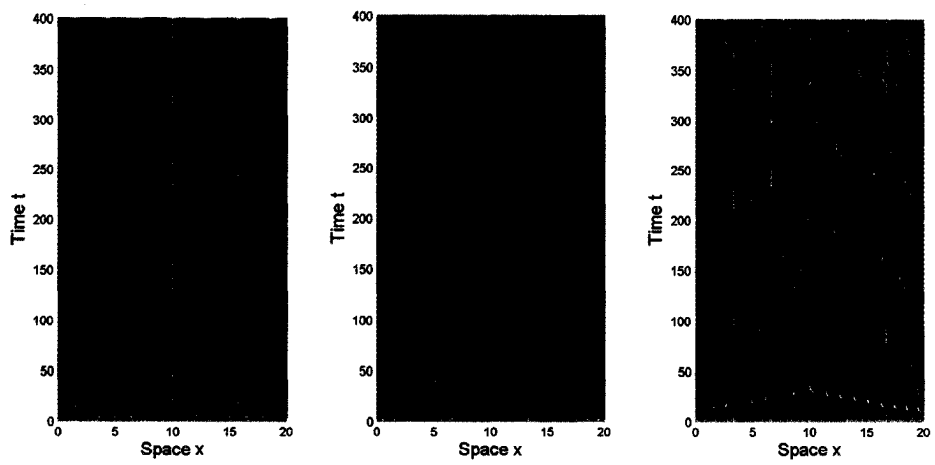

(a) (b) (c)

Figure 3.11: Space-time evolution of cell density for model (3.1.2) for different choices of parameters. (a) $d_1 = 0.25, d_2 = 1, \nu = 10, \delta = 10, \bar{u} = 1.0, u_c = 0.25, \mu = 0.5, \chi = 10, r = 1/2$. Simulations indicate that a fixed spatial pattern exists as peaks persist and grow. Here are 7 peaks. (b) $d_1 = 0.25, d_2 = 1, \nu = 10, \delta = 10, \bar{u} = 1.0, u_c = 0.25, \mu = 0.5, \chi = 20, r = 1/2$. (c)$d_1 = 0.01, d_2 = 1, \nu = 10, \delta = 10, \bar{u} = 1.0, u_c = 0.25, \mu = 0.5, \chi = 1.5, r = 1/2$. In (b) and (c), typical merging and emerging patterns develop. The parameters chosen in (a) are closer to the stability region than those chosen in (b) and (c). All simulations use the domain size as [0 20].

We observe similar patterning process as we had in chapter 2. In the case of zero kinetics, we find merging process, while we observe merging and emerging process for nonzero cell kinetics. This again confirms the conclusion that the emerging process is due to cell kinetics. For the case of zero cell kinetics, we find that initial cell density is important for pattern formation. There is no pattern formation for high or low cell density. Note that we observe very similar patterning process for the choices of squeezing probability $q(u)$ described in both chapter 2 and chapter 3. However critical values of chemosensitivity and growth and degradation rate on pattern formation are quite different, as we have seen from our analysis. Moreover, the choice of $q(u)$ in this chapter leads to an open question of *fast* diffusion problem, which is mathematically interesting and challenging.

Chapter 4

SHOCK FORMATION IN A CHEMOTAXIS MODEL [1]

4.1 Introduction

In many biological system, an organism navigates in response to a diffusible or otherwise transported signal. In its simplest form this can be modeled by diffusion equations with advection terms of the form first derived by Patlak [101]. However, other systems are more accurately modeled by random walkers that deposit a nondiffusible signal that modifies the local environment for succeeding passages and there is little or no transport of the modifying substance. Examples include myxobacteria which produce slime over which their cohorts can move more readily, and ants, which follow trails left by predecessors. In either case, the question arises as to whether aggregation is possible with such strictly local modification or whether some form of longer range communication is necessary. To answer this question, Othmer and Stevens [95] have developed a number of mathematical chemotaxis models. They illustrate that within the framework of partial differential equation models, stable aggregations can occur with local modulation of the transition rates, that is, without long range signaling via a diffusible chemical. One of these chemotaxis models in one-space dimension reads

$$\begin{cases} \dfrac{\partial p}{\partial t} = D\dfrac{\partial}{\partial x}\left(p\dfrac{\partial}{\partial x}\left(\ln\left(\dfrac{p}{\phi(w)}\right)\right)\right), \\ \dfrac{\partial w}{\partial t} = R(p,w), \end{cases} \tag{4.1.1}$$

with no-flux boundary condition

$$\frac{\partial}{\partial x}\left(\ln\left(\frac{p}{\phi(w)}\right)\right) = 0 \text{ at } x = 0,\ l, \tag{4.1.2}$$

as well as initial conditions

$$p(x,0) = p_0(x) \geq 0, w(x,0) = w_0(x) > 0 \text{ for } 0 \leq x \leq l. \tag{4.1.3}$$

[1] The result in this chapter is a collaboration with Thomas Hillen and has been published online in *Math. Methods. Appl. Sci.* at http://www3.interscience.wiley.com/cgi-bin/jissue/106560971.

Here $p(x,t)$ is the particle density of a particular species and $w(x,t)$ is the concentration of that active agent. The chemotactic potential ϕ and signal reproduction and decay term R are given as

$$\phi(w) = \left(\frac{w+\beta}{w+\gamma}\right)^{\alpha}, \quad R(p,w) = \frac{\lambda pw}{k_1+w} + \frac{\gamma_r p}{k_2+p} - \mu w, \tag{4.1.4}$$

were $\beta, \gamma, k, k_1, k_2, \lambda, \gamma_r, \mu$ and D are all nonnegative constants with D and λ being strictly positive and $\alpha \neq 0$. Here the definition for potential function $\phi(w)$ in (4.1.4) corresponds to a so called barrier mode which describe a saturation effect of external signals in the receptor binding reaction. The choice of kinetic terms $R(p,w)$ describe the saturation in the production of the external signal (see [95]).

Othmer and Stevens [95] numerically show that a variety of dynamics of system (4.1.1)-(4.1.4) are possible, which include aggregation, blowup or collapse depending on whether the dynamics admit stable bounded peaks, whether solutions blow up in finite time, or whether a suitable spatial norm of the density function is asymptotically less than its initial value. In [75], Levine and Sleeman present the analytical results that support the numerical observations presented by Othmer and Stevens [95]. Furthermore some additional numerical computations are made in [75]. Local and global existence of solutions of the Othmer-Stevens model (4.1.1)-(4.1.4) has been studied in [126] and in a recent paper [127]. In [127] the authors apply the existence theory of Ladyzhenskaya *et al* [71] to obtain a very general result on local and global existence of solutions. In [113] asymptotic expansions are used to prove the existence and stability of spike solutions for the case of saturation in the signal production term.

It should be pointed out that since the first equation of (4.1.1) is parabolic in p, it is easy to observe that $p(x,t) \geq 0$ provided that the initial value is nonnegative. To simplify model (4.1.1) and gain some insight into the Othmer-Stevens model, it is worthwhile to consider special cases which were considered in [75]. The results we obtain in this paper are for a simplified version of the Othmer-Steven model. To simplify equations (4.1.1), we first apply the representation of $\phi(w)$ in (4.1.4) to deduce that from the first equation of (4.1.1)

$$\frac{\partial p}{\partial t} = D\left[\frac{\partial^2 p}{\partial x^2} - \frac{\partial}{\partial x}\left(\frac{\alpha(\gamma-\beta)p}{(w+\gamma)(w+\beta)}\frac{\partial w}{\partial x}\right)\right].$$

From this expression, we observe that if $\gamma >> w >> \beta$, the coefficient of w_x is nearly α/w, whereas if $\beta >> w >> \gamma$, the coefficient is $-\alpha/w$. These two extreme cases can be modelled by taking $\phi(w) = w^{-\alpha}$ where α can be positive or negative. Throughout this paper, we consider $\gamma_r = 0$, $\phi(w) = w^{-\alpha}$ and $R(p,w) = \lambda pw - \mu w$.

Substituting these choices into system (4.1.1)-(4.1.4), we end up with the following simplified system

$$\begin{cases} p_t = D\left(p_{xx} + \alpha\left(p\dfrac{w_x}{w}\right)_x\right), 0 < x < l,\ t > 0, \\ w_t = \lambda p w - \mu w, \end{cases} \tag{4.1.5}$$

with boundary condition

$$\alpha\frac{w_x}{w} + \frac{p_x}{p} = 0 \ \text{ for } \ x = 0, l,\ t > 0, \tag{4.1.6}$$

and initial data

$$p(x,0) = p_0(x) \geq 0, w(x,0) = w_0(x) > 0 \ \text{ for } \ 0 \leq x \leq l. \tag{4.1.7}$$

Here the first equation of (4.1.5) becomes a classical Patlak-Keller-Segel type. The substance w is generally refereed to as attractant for $\alpha < 0$ and repellent for $\alpha > 0$.

Furthermore, with these simplifications, using scaling theory by writing $t = \frac{l^2\tau}{\pi^2 D}, x = \frac{x'l}{\pi}$ and setting $\mu' = \frac{l^2\mu}{\pi^2 D}, \lambda' = \frac{l^2\lambda}{\pi^2 D}$, we find we may take $D = 1$ in (4.1.5). If we multiply the first equation of (4.1.5) by λ we observe that we may replace p by $p' = \lambda p$. Moreover, if we define $w' = w\exp(\mu t)$, we see that we may take $\mu = 0$ in (4.1.5) if replacing w by w'. After these rescalings, we can recast the system (4.1.5)-(4.1.7) to the following initial-boundary problem by dropping the prime for convenience

$$\begin{cases} p_t = p_{xx} + \alpha\left(p\dfrac{w_x}{w}\right)_x, \ (x,t) \in (0,l) \times (0,\infty), \\ w_t = pw, \end{cases} \tag{4.1.8}$$

with boundary condition

$$\alpha\frac{w_x}{w} + \frac{p_x}{p} = 0 \ \text{ for } \ x = 0, l, t > 0, \tag{4.1.9}$$

and initial data

$$p(x,0) = p_0(x) \geq 0, w(x,0) = w_0(x) > 0 \ \text{ for } \ 0 \leq x \leq l. \tag{4.1.10}$$

From the second equation of (4.1.8), it follows that $w(x,t) > 0$ since $w_0(x) > 0$ as long as the solution (p,w) exists in time. So it makes sense to let $\psi(x,t) = \ln w(x,t)$ and consequently $\psi_x = \dfrac{w_x}{w}$. Moreover it follows from the second equation of (4.1.8)

that $\psi_t = \dfrac{w_t}{w} = p$. We therefore obtain the following form from (4.1.8)-(4.1.10)

$$\begin{cases} \pounds\psi = \psi_{tt} - \alpha\psi_x\psi_{xt} - \alpha\psi_t\psi_{xx} = \psi_{xxt}, \ (x,t) \in (0,l) \times (0,\infty), \\ \alpha\psi_x\psi_t + \psi_{xt} = 0, \ \text{for } x = 0, l, t > 0, \\ \psi(x,0) = \psi_0(x) = \ln w_0(x), \ \text{ for } 0 \le x \le l \\ \psi_t(x,0) = p_0(x), \ \text{for } 0 \le x \le l. \end{cases} \tag{4.1.11}$$

The operator $\pounds$ defined by the first equation of (4.1.11) is a quasilinear second-order differential operator. The damping term ψ_{xxt} here does not really affect the overall structure of the solution. So we can specify the type of the operator $\pounds$ by determining the sign of the discriminant

$$\triangle = \alpha^2\psi_x^2(x,t) + 4\alpha\psi_t(x,t),$$

at a point (x,t). The operator $\pounds$ will be hyperbolic at the point (x,t) on a function ψ if $\triangle > 0$, while elliptic if $\triangle < 0$. When $\triangle = 0$, we say $\pounds$ is parabolic. Since we have that $p(x,t) = \psi_t(x,t) > 0$, it follows that $\triangle > 0$ if $\alpha = 1$ (or $\alpha > 0$) and we refer to this case as hyperbolic. When $\alpha = -1$ (or $\alpha < 0$), the sign of the discriminant can change and we refer to this case as mixed-type case.

When $\alpha = 1$, Levine and Sleeman [75] construct solution pairs (p, w) for which $p > 0$ and p collapses to a constant in finite time exponentially. When $\alpha = -1$, they show that there are solution pairs (p, w) for which $p > 0$ but for which p blows up on the parabolic boundary in finite time and the power spectrum converges to that of delta function in finite time. Furthermore, they construct an explicit family of such solutions (see section 3 of [75]). Moreover, Levine and Sleeman argued that the system (4.1.5) contains the seeds of shock formation which can be obtained in the "zero diffusion" limits if $D \to 0$, $\alpha \to \infty$ in such a way that $\alpha D =$ constant. But they did not provide the rigorous justification for this contention. One of the purposes of this paper is to present the analytical justification for their assertion. Beyond this, we study the shock structure by examining the traveling wave and prove that the shock speed is identical to traveling speed. Furthermore, we find the entropy inequality for attractive case ($\alpha > 0$) and then the uniqueness of weak shock solution of attractive case is obtained.

The organization of the rest of this chapter is as follows. In Section 2, we show that for both attractive case ($\alpha < 0$) and repulsive case ($\alpha > 0$), there exist shock solutions for the chemotaxis model (4.1.5), (4.1.6) and (4.1.7) without diffusion in the sense of $\alpha D =$ constant. We start with the Rankine-Hugonoit condition to

explicitly find the shock curves in parameterized forms that connect left and right states through a shock solution. Furthermore we observe the difference between the attractive case and the repulsive case and plot the Hugoniot locus for both cases. In addition, we briefly discuss the general Riemann problem for system (4.1.5)-(4.1.7) with zero diffusion. The shock structures will be examined in Section 3 by studying the traveling waves to system (4.1.5)-(4.1.7) for small $D > 0$. We show the existence of nondecreasing traveling waves for the attractive case and nonincreasing traveling waves for the repulsive case. Essentially, we prove the traveling speed is identical to the shock speed. Numerically we confirm the existence of the traveling wave solutions. In Section 4, an entropy condition for the repulsive case ($\alpha > 0$) is identified and the uniqueness of the shock solutions follows. In the final Section 5, we provide some discussion for further research.

4.1.1 Hyperbolic Systems

To make the paper self-contained and for the convenience to read, in this subsection, we would like to introduce some basic definitions and associated notations related to the theory of hyperbolic conservation laws (see [15, 73, 74]).

Let $\Omega \subseteq \mathbb{R}^n$ be an open set and $f : \Omega \to \mathbb{R}^n$ a smooth vector field. The Riemman problem for the system of conservation laws in one-space dimension

$$u_t + f(u)_x = 0, \quad x \in \mathbb{R}, \ t > 0, \tag{4.1.12}$$

consists in finding a weak solution $u(x,t) \in \Omega$ of (4.1.12) with piecewise constant initial data of the form

$$u(x,0) = \begin{cases} u^-, & \text{if } x < 0, \\ u^+, & \text{if } x > 0, \end{cases} \tag{4.1.13}$$

where $u^-, u^+ \in \Omega, u^- \neq u^+$. Then we have the following notions for (4.1.12) and (4.1.13).

Definition 4.1.1. *We say that (4.1.12) is a* ***hyperbolic system*** *of partial differential equations if for each $u \in \Omega$ the Jacobian matrix $A(u) = Df(u)$ has n real eigenvalues $\lambda_1(u) \leq \lambda_2(u) \leq \cdots \leq \lambda_n(u)$ together with a basis of right eigenvectors $r_i(u)_{1 \leq i \leq n}$. The eigenvalues are also called the* ***wave speeds*** *or* ***characteristic speeds*** *associated with (4.1.12). The pair (λ_i, r_i) is referred as the* ***i-th characteristic field.*** *Furthermore, the system is said to be* ***strictly hyperbolic*** *if its eigenvalues are distinct: $\lambda_1(u) < \lambda_2(u) < \cdots < \lambda_n(u)$.*

Definition 4.1.2. *For $i \in 1, \cdots, n$, we say that the i-th characteristic field is* ***genuinely nonlinear*** *if*

$$r_i \bullet \lambda_i(u) \neq 0 \quad \text{for all} \quad u \in \Omega$$

and ***linearly degenerate*** *if*

$$r_i \bullet \lambda_i(u) = 0 \quad \text{for all} \quad u \in \Omega,$$

where $r_i \bullet \lambda_i(u)$ means the directional derivative of the function $\lambda_i(u)$ in the direction of the vector $r_i(u)$ defined by

$$r_i \bullet \lambda_i(u) = \nabla \lambda_i(u) \cdot r_i(u) = \lim_{\varepsilon \to 0} \frac{\lambda_i(u + \varepsilon r_i(u)) - \lambda_i(u)}{\varepsilon}.$$

Definition 4.1.3. *Fix the point $u^- \in \mathbb{R}^n$. The set of the points u^+ which can be connected to u^- by a discontinuity satisfying the* ***Rankine-Hugoniot jump condition***

$$f(u^+) - f(u^-) = s(u^+ - u^-)$$

for some s is often collectively called the ***Hugoniot locus*** *for the point u^-, where s is called the shock speed, the speed at which the discontinuity travels. If u_i^+ lies on the Hugoniot locus through u_i^-, we say that u_i^- and u_i^+ are connected by an i-shock.*

Definition 4.1.4. *A smooth function $(\eta, \rho) : \mathbb{R}^n \to \mathbb{R}^2$ is called an* ***entropy pair*** *if any smooth solution u of (4.1.12) and (4.1.13) satisfies the additional conservation law*

$$\eta(u)_t + \rho(u)_x = 0,$$

where the functions η and ρ are called ***entropy*** *and* ***entropy flux*** *respectively.*

Definition 4.1.5 ([114]). *We say that the shock wave of system (4.1.12) with (4.1.13) "****admits structure****" if the viscous equation*

$$u_t + f(u)_x = \varepsilon u_{xx}, \ \varepsilon > 0, \quad x \in \mathbb{R}, \ t > 0,$$

admits a traveling wave solution of the form

$$u = u\left(\frac{x - st}{\varepsilon}\right),$$

which tends to the given shock wave solution $(u^-, u^+; s)$ as $\varepsilon \to 0$.

The following theorem established in [15] will be useful in the present paper.

Theorem 4.1.6. (Theorem 5.1[15]). *Let the system (4.1.12) be strictly hyperbolic. Then, for every $u_0 \in \Omega$, there exist $\sigma_0 > 0$ and n smooth curves $S_i : [-\sigma_0, \sigma_0] \to \Omega$, together with scalar functions $\lambda_i : [-\sigma_0, \sigma_0] \to \mathbb{R}$ $(i = 1, \cdots, n)$, such that*

$$f(S_i(\sigma)) - f(u_0) = \lambda_i(\sigma)(S_i(\sigma) - u_0), \ \sigma \in [-\sigma_0, \sigma_0]. \tag{4.1.14}$$

Moreover, the parametrization can be chosen so that $|dS_i/d\sigma| \equiv 1$ and

$$S_i(0) = u_0, \lambda_i(0) = \lambda_i(u_0), \tag{4.1.15}$$

$$\left.\frac{S_i(\sigma)}{d\sigma}\right|_{\sigma=0} = r_i(u_0). \tag{4.1.16}$$

4.1.2 LaSalle's Invariant Principle

Asymptotic or global stability of a dynamic system is often an important property to be determined. It is well know that the Lyapunov stability theorem is a powerful approach to determine the stability or instability of a system. However, the Lyapunov stability theorem is often difficulty to establish the asymptotic properties, as the derivative of the Lyapunov function candidate $\dot{V}$ is only negative semi-definite, namely, $\dot{V} \leq 0$. But this does not mean that the equilibrium of the dynamic system is not asymptotically stable. In this kind of situation, it is still possible to draw conclusions on asymptotic stability by *invariant set* theorems, which are due to the pioneering work of LaSalle [72]. In this subsection, we introduce LaSalle's invariant principles as stated in [8, 45].

Definition 4.1.7 (Invariant set). *Consider an autonomous dynamic system*

$$\dot{x} = f(x). \tag{4.1.17}$$

*Then a set S is called an **invariant set** for the above system (4.1.17) if every trajectory $x(t)$ starting from a point in S remains in S for all time.*

Theorem 4.1.8 (LaSall's invariant principle). *Consider an autonomous system of the form (4.1.17) with f locally Lipschitz. If there exists a continuous differentiable function $V(x) : \mathbb{R}^n \to \mathbb{R}$ for which*

(i) for some $l > 0$, the set $\Omega_l = \{x \in \mathbb{R}^n : V(x) \leq l\}$ is bounded.

(ii) $\dot{V}(x) \leq 0$ for all x in Ω_l.

Define $R = \{x \in \mathbb{R}^n : \dot{V}(x) = 0\}$ and let M be the largest invariant set contained in R. Then for each $x_0 \in \Omega_l$, the ω-limit set $w(x_0)$ is contained in M.

4.2 Shock Solutions

4.2.1 The Hugoniot Locus and Existence of Shocks

Following the argument by Levine and Slemann [75], we assume first $\alpha D = \mathcal{C}$ in the Othmer and Stevens model (4.1.5)-(4.1.7), where $\mathcal{C}$ is a constant. In this situation, the negative constant ($\mathcal{C} < 0$) corresponds to attractive chemotaxis and positive one ($\mathcal{C} > 0$) to repulsive chemotaxis. Without loss of generality we may assume that $\mathcal{C} = \pm 1$. The spatial domain is extended to be $I = \mathbb{R}$. There are two cases to follow regarding the sign of the constant $\mathcal{C}$.

Case 1: Attractive case ($\alpha = -\frac{1}{D} < 0$). Following this condition, applying the same scaling technique used in the introduction, we reformulate system (4.1.5) to the following equivalent equations

$$\begin{cases} p_t = Dp_{xx} - \left(p\dfrac{w_x}{w}\right)_x, \ (x,t) \in I \times (0,\infty), \\ w_t = pw. \end{cases} \tag{4.2.1}$$

We define $q = (\ln w)_x$ and reformulate system (4.2.1) to obtain the following form

$$\begin{cases} p_t + pq_x + qp_x = Dp_{xx}, \\ q_t = p_x. \end{cases} \tag{4.2.2}$$

Let $u = (p,q)^T$ and $A(u) = \begin{pmatrix} q & p \\ -1 & 0 \end{pmatrix}$, $\bar{D} = \begin{pmatrix} D & 0 \\ 0 & 0 \end{pmatrix}$. Then the system (4.2.2) becomes

$$u_t + f(u)_x = u_t + A(u)u_x = \bar{D}u_{xx}, \tag{4.2.3}$$

where $f(u) = f(p,q) = (pq, -p)^T$. To study the shock formation of system (4.2.3), we let $D = 0$ such that system (4.2.3) becomes the following conservation law

$$u_t + A(u)u_x = 0, \quad (x,t) \in I \times (0,\infty). \tag{4.2.4}$$

The characteristic equation of $A(u)$ is easily computed as $\lambda^2 - q\lambda + p = 0$. Thus when $q^2 - 4p > 0$, the matrix $A(u)$ has two real distinct eigenvalues $\lambda_1(u) < \lambda_2(u)$ given by

$$\lambda_1(u) = \frac{q}{2} - \frac{\sqrt{q^2-4p}}{2} \ \text{ and } \ \lambda_2(u) = \frac{q}{2} + \frac{\sqrt{q^2-4p}}{2},$$

with corresponding eigenvectors which are

$$r_1(u) = (-\lambda_1(u), 1)^T \ \text{ and } \ r_2(u) = (\lambda_2(u), -1)^T,$$

respectively. This means the conservational law (4.2.4) is strictly hyperbolic for $q^2 - 4p > 0$. Furthermore it is straightforward to obtain that $\nabla\lambda_1(u) \cdot r_1(u) =$

$-\frac{q}{\sqrt{q^2-4p}}+1 \neq 0$ as well as $\nabla\lambda_2(u)\cdot r_2(u) = \frac{q}{\sqrt{q^2-4p}}+1 \neq 0$ and $\lambda_1(u) < \lambda_2(u)$ due to $p > 0$. Hence the characteristic fields $(\lambda_1(u), r_1(u))$ and $(\lambda_2(u), r_2(u))$ are genuinely nonlinear which motivates us to look for shock solutions for system (4.2.4). To investigate the shock solution, we augment the system (4.2.4) with Riemann initial value

$$u(x,0) = u_0(x) = (p_0(x), q_0(x)) = \begin{cases} u^-, & x < 0, \\ u^+, & x > 0, \end{cases} \tag{4.2.5}$$

where $u^- = (p^-, q^-), u^+ = (p^+, q^+)$.

We suppose here that $u^+ \neq u^-$. Otherwise the characteristic speeds are constant $\lambda_i(u) = \lambda_i(u^-) = \lambda_i(u^+)$ and therefore $\nabla\lambda_i(u) = 0$. This is the case of linear degeneracy in which the shock wave and rarefaction wave coincide with each other and we refer to this situation as a contact discontinuity (see [15]). In this work, we restrict our attention to the case of $u^+ \neq u^-$.

Recall that if a discontinuity propagating with speed s has constant u^- and u^+ on either side of the discontinuity, then the Rankine-Hugoniot jump condition must hold

$$f(u^+) - f(u^-) = s(u^+ - u^-). \tag{4.2.6}$$

Now let us fix a state u^- and attempt to determine the set of states u^+ that can be connected to u^- by a discontinuity satisfying (4.2.6) for some s. To this end, we rewrite the Rankine-Hugoniot condition (4.2.6) as

$$\begin{cases} s(p^+ - p^-) = p^+q^+ - p^-q^-, \\ s(q^+ - q^-) = -p^+ + p^-. \end{cases} \tag{4.2.7}$$

Observe that system (4.2.7) gives a system of two equations in three unknowns: p^+, q^+ and s. This enables us to expect a one parameter family of solutions. Here we take q^+ as the free parameter. Then it follows from the second equation of (4.2.7) that

$$p^+ = p^- - s(q^+ - q^-). \tag{4.2.8}$$

Substituting (4.2.8) into the first equation of (4.2.7) yields

$$-s^2(q^+ - q^-) = p^+q^+ - p^-q^-. \tag{4.2.9}$$

Applying (4.2.8) into (4.2.9) gives that

$$(q^- - q^+)(s^2 - q^+s + p^-) = 0. \tag{4.2.10}$$

It is worthwhile to note here that $q^+ \neq q^-$. Otherwise it follows from the second equation of (4.2.7) that $p^+ = p^-$ which implies that $u^+ = u^-$ and violates our assumption. Therefore we end up with

$$s^2 - q^+ s + p^- = 0.$$

and get the shock speed

$$s = \frac{q^+}{2} \pm \frac{\sqrt{q^{+2} - 4p^-}}{2}, \tag{4.2.11}$$

here we have assumed that $(q^+)^2 - 4p^- > 0$. As a consequence we obtain p^+ from (4.2.8)

$$p^+ = p^- - \frac{1}{2}\left(q^+ \pm \sqrt{q^{+2} - 4p^-}\right)(q^+ - q^-), \tag{4.2.12}$$

where $\pm$ signs in these equations give two solutions, one for each family. Since p^+ and s can be expressed in terms of q^+, we can parameterize these curves by taking

$$q^+ = (1+\sigma)q^-, \tag{4.2.13}$$

where σ is a parameter.

Therefore given $u^- \in \Omega$, we obtain the shock curves for the first characteristic fields which are parameterized by

$$S_1(\sigma, u^-) = u^- + \sigma \begin{pmatrix} -\frac{q^-}{2}\left[(1+\sigma)q^- - \sqrt{(1+\sigma)^2 q^{-2} - 4p^-}\right] \\ q^- \end{pmatrix},$$

with shock speed

$$s_1(\sigma, u^-) = \frac{1+\sigma}{2}q^- - \frac{1}{2}\sqrt{(1+\sigma)^2 q^{-2} - 4p^-}.$$

The shock curves for the second characteristic field is

$$S_2(\sigma, u^-) = u^- + \sigma \begin{pmatrix} -\frac{q^-}{2}\left[(1+\sigma)q^- + \sqrt{(1+\sigma)^2 q^{-2} - 4p^-}\right] \\ q^- \end{pmatrix},$$

with shock speed

$$s_2(\sigma, u^-) = \frac{1+\sigma}{2}q^- + \frac{1}{2}\sqrt{(1+\sigma)^2 q^{-2} - 4p^-}.$$

Here we write $S_i(\sigma, u^-) = u_i^+(\sigma, u^-), i = 1, 2$ and $u_i^+(\sigma, u^-)$ denote the solutions corresponding to the shock speed s_i. We thus obtain two shock curves through any

point u^-, one for each characteristic family. By denoting the corresponding shock speed by $s_i(\sigma, u^-)$ we parameterize these curves by $S_i(\sigma, u^-)$ with $S_i(0, u^-) = u^-$. To make notations simpler, we will frequently substitute $S_i(\sigma)$ for $S_i(\sigma, u^-)$ and $s_i(\sigma)$ for $s_i(\sigma, u^-)$ when the point u^- is clearly understood. Replacing u^+, s by $S_i(\sigma), s_i(\sigma)$ respectively in the Rankine-Hugoniot condition (4.2.6), we find that

$$f(S_i(\sigma)) - f(u^-) = s_i(\sigma)(S_i(\sigma) - u^-). \tag{4.2.14}$$

Differentiating the expression (4.2.14) with respect to σ and evaluating at $\sigma = 0$ yields

$$f'(u^-)S_i'(0) = s_i(0)S_i'(0) \tag{4.2.15}$$

so that $S_i'(0)$ must be a scalar multiple of the eigenvector $r_i(u^-)$ of $f'(u^-)$ since here the speed $s_i(0)$ coincides with the corresponding characteristic speed, i.e., $s_i(0) = \lambda_i(u^-)$. However, with the above notations, it is evident to check that

$$\frac{\partial}{\partial \sigma} S_i(0, u^-) = q^- r_i(u^-) \propto r_i(u^-),\ s_i(0, u^-) = \lambda_i(u^-), i = 1, 2. \tag{4.2.16}$$

as required.

Now let us examine the conditions which the parameter σ needs to satisfy. For the shock curves $S_i(\sigma, u^-)(i = 1, 2)$ to be well defined, it is required that $(1 + \sigma)^2 q^{-2} - 4p^- \geq 0$. But it has been required that $q^{-2} - 4p^- > 0$ to get a strictly hyperbolic conservation law which was discussed at the beginning of this section. Hence we require that $|1 + \sigma| > 1$ which implies two situations: either $\sigma > 0$ or $\sigma < -2$. For $-2 < \sigma < 0$, the system (4.1.5)-(4.1.7) is not strictly hyperbolic and the Hugoniot locus has a gap (see Figure 4.1(a)). Therefore, when $-2 < \sigma < 0$, the shock curves are not well defined and hence we only consider the domain $\sigma > 0$.

From the preceding construction, we obtain, by standard arguments (see [15, 114]), the existence of shock solutions of the Riemann problem (4.2.4) and (4.2.5) with left and right states u^- and u^+ for the attractive case. The existence theorem is summarized in the following and the Hugonoit locus of the attractive case is plotted in Figure 4.1(a).

Theorem 4.2.1. *Let $\alpha = -\frac{1}{D}$ and Ω be an open set of $\mathbb{R}^2$. For each $u^- \in \Omega$ with $q^{-2} - 4p^- > 0$, there exists a parameter σ such that for each σ with $\sigma \geq 0$, the pair $(u^-, S_i(\sigma))(i = 1, 2)$ satisfies the Rankine-Hugoniot conditions (4.2.14) and the function*

$$u(x,t) = \begin{cases} u^-, & if\ x < s_i(\sigma)t, \\ S_i(\sigma), & if\ x > s_i(\sigma)t, \end{cases} \tag{4.2.17}$$

is a weak solution of the system (4.2.4) which satisfies the Riemann condition (4.2.5) with $u^+ = S_i(\sigma)$.

Case 2: Repulsive case ($\alpha = \frac{1}{D} > 0$). Substituting $1/D$ for α in system (4.1.5) and rescaling the resulting system, we end up with

$$\begin{cases} p_t = Dp_{xx} + \left(p\dfrac{w_x}{w}\right)_x, \ (x,t) \in I \times (0,\infty), \\ w_t = pw. \end{cases} \tag{4.2.18}$$

Similarly by defining $q = (\ln w)_x$, the system (4.2.18) can be reduced to

$$\begin{cases} p_t - (pq)_x = Dp_{xx}, \\ q_t - p_x = 0. \end{cases} \tag{4.2.19}$$

or written by

$$u_t + \tilde{A}(u)u_x = \bar{D}u_{xx}, \tag{4.2.20}$$

where $u = (p,q)^T$ and $\tilde{A}(u) = \begin{pmatrix} -q & -p \\ -1 & 0 \end{pmatrix}$, $\bar{D} = \begin{pmatrix} D & 0 \\ 0 & 0 \end{pmatrix}$. Then system (4.2.20) for $D = 0$ becomes a conservation law

$$u_t + \tilde{f}(u)_x = u_t + \tilde{A}(u)u_x = 0, \quad (x,t) \in I \times (0,\infty), \tag{4.2.21}$$

where $\tilde{f}(u) = \tilde{f}(p,q) = (-pq, -p)^T$ and $\tilde{f}'(u) = \tilde{A}(u)$. The characteristic equation of $\tilde{A}(u)$ is $\lambda^2 + q\lambda - p = 0$. Noticing $p > 0$, it is clear that the discriminant $q^2 + 4p$ of the characteristic equation is always positive. Therefore the matrix $A(u)$ has two real distinct eigenvalues $\tilde{\lambda}_1(u)$ and $\tilde{\lambda}_2(u)$ which are given by

$$\tilde{\lambda}_1(u) = -\frac{q}{2} - \frac{\sqrt{q^2+4p}}{2} \ \text{ and } \ \tilde{\lambda}_2(u) = -\frac{q}{2} + \frac{\sqrt{q^2+4p}}{2}.$$

The corresponding eigenvectors are determined by

$$\tilde{r}_1(u) = (-\tilde{\lambda}_1(u), 1)^T \ \text{ and } \ \tilde{r}_2(u) = (\tilde{\lambda}_2(u), -1)^T$$

respectively. It is obvious that $\tilde{\lambda}_1(u) < 0 < \tilde{\lambda}_2(u)$ which implies that the conservational law is strictly hyperbolic. Furthermore, we easily verify that $\nabla\tilde{\lambda}_1(u) \cdot \tilde{r}_1(u) = -\dfrac{q}{\sqrt{q^2+4p}} - 1 < 0$ and $\nabla\tilde{\lambda}_2(u) \cdot \tilde{r}_2(u) = \dfrac{q}{\sqrt{q^2+4p}} - 1 < 0$ because of $p > 0$. Hence the characteristic fields $(\tilde{\lambda}_i(u), \tilde{r}_1(u))$ and $(\tilde{\lambda}_2(u), \tilde{r}_2(u))$ are genuinely nonlinear. Then the Rankine-Hugoniot jump condition

$$\tilde{f}(u^+) - \tilde{f}(u^-) = \tilde{s}(u^+ - u^-)$$

takes the form

$$\begin{cases} \tilde{s}(p^+ - p^-) = -p^+q^+ + p^-q^-, \\ \tilde{s}(q^+ - q^-) = -p^+ + p^-. \end{cases} \tag{4.2.22}$$

System (4.2.22) consists of two equations in three unknowns: p^+, q^+ and $\tilde{s}$. We thus can regard one unknown, say q^+, as a parameter to get from the second equation of (4.2.22) that

$$p^+ = p^- - \tilde{s}(q^+ - q^-). \tag{4.2.23}$$

We substitute (4.2.23) into the first equation of (4.2.22) and obtain the following equation

$$-\tilde{s}^2(q^+ - q^-) = -p^+q^+ + p^-q^-. \tag{4.2.24}$$

Applying (4.2.23) into (4.2.24), we have

$$(q^+ - q^-)(\tilde{s}^2 + q^+\tilde{s} - p^-) = 0. \tag{4.2.25}$$

Note that $q^+ \neq q^-$. We obtain an equivalent equation to (4.2.25)

$$\tilde{s}^2 + q^+\tilde{s} - p^- = 0.$$

and therefore the shock speed can be found

$$\tilde{s} = -\frac{q^+}{2} \pm \frac{\sqrt{q^{+2} + 4p^-}}{2}. \tag{4.2.26}$$

Then we substitute (4.2.26) into (4.2.23) and get

$$p^+ = p^- - \frac{1}{2}\left(-q^+ \pm \sqrt{q^{+2} + 4p^-}\right)(q^+ - q^-), \tag{4.2.27}$$

where the $\pm$ signs in these equations give two solutions, one for each family. Since p^+ and s can be expressed in terms of q^+, we can assume σ to be parameter and let

$$q^+ = (1 + \sigma)q^-. \tag{4.2.28}$$

Then we substitute (4.2.28) into (4.2.26) and (4.2.27) to get the shock curves. For the first characteristic field, we find the shock curves

$$\widetilde{S}_1(\sigma, u^-) = u^- + \sigma \begin{pmatrix} \frac{q^-}{2}\left[(1+\sigma)q^- + \sqrt{(1+\sigma)^2 q^{-2} + 4p^-}\right] \\ q^- \end{pmatrix},$$

with shock speed

$$\tilde{s}_1(\sigma, u^-) = -\frac{1+\sigma}{2}q^- - \frac{1}{2}\sqrt{(1+\sigma)^2 q^{-2} + 4p^-}.$$

For the second characteristic field we find the shock curve

$$\widetilde{S}_2(\sigma, u^-) = u^- + \sigma \begin{pmatrix} \frac{q^-}{2}\left[(1+\sigma)q^- - \sqrt{(1+\sigma)^2 q^{-2} + 4p^-}\right] \\ q^- \end{pmatrix},$$

with shock speed

$$\tilde{s}_2(\sigma, u^-) = -\frac{1+\sigma}{2}q^- + \frac{1}{2}\sqrt{(1+\sigma)^2 q^{-2} + 4p^-}.$$

where we denote $\widetilde{S}_i(\sigma, u^-) = u_i^+(\sigma, u^-), i = 1, 2$

Performing the same analysis as we did for case 1, we obtain the following theorem similar to Theorem 4.2.1.

Theorem 4.2.2. *Assume $\alpha = \frac{1}{D}$. For each $u^- \in \Omega$, there exists a parameter σ and $\sigma_0 > 0$ such that for each $\sigma \in [-\sigma_0, \sigma_0]$, the pair $(u^-, \widetilde{S}_i(\sigma))(i = 1, 2)$ satisfies the Rankine-Hugoniot jump conditions and the function*

$$u(t,x) = \begin{cases} u^-, & if\ x < \tilde{s}_i(\sigma)t, \\ \widetilde{S}_i(\sigma), & if\ x > \tilde{s}_i(\sigma)t, \end{cases} \tag{4.2.29}$$

is a weak solution of the system (4.2.21) satisfying the Riemann condition (4.2.5) with $u^+ = \widetilde{S}_i(\sigma)$.

Remark 4.1. *We observe from the above analysis that there are shock solutions in both attractive and repulsive cases. In the first case, we need the additional assumptions $q^2 - 4p > 0$ and $q^{+2} - 4p^- > 0$ and hence $\sigma \geq 0$. However, in the second case, there was no such restriction on p, q and hence on σ to ensure the formation of the shock. Indeed, from the definition of S_i and $\widetilde{S}_i$ given above, it is evident that the real-valued solution $S_i(\sigma)$ $(i = 1, 2)$ exists only for $|1+\sigma| \geq 2\sqrt{p^-}/q^-$ while $\widetilde{S}_i(\sigma)$ takes real values for any σ.*

Remark 4.2. *From (4.2.16), it is clear that the Hugoniot locus $S_i(\sigma)$ is tangent to the eigenvector $r_i(u^-)$ at the point u^-. In a similar manner, the Hugoniot locus $\widetilde{S}_i(\sigma)$ is tangent to the eigenvector $\tilde{r}_i(u^-)$ at the point u^-. Then the Hugoniot locus of the state u^- for both attractive and repulsive cases can be sketched in Figure 4.1.*

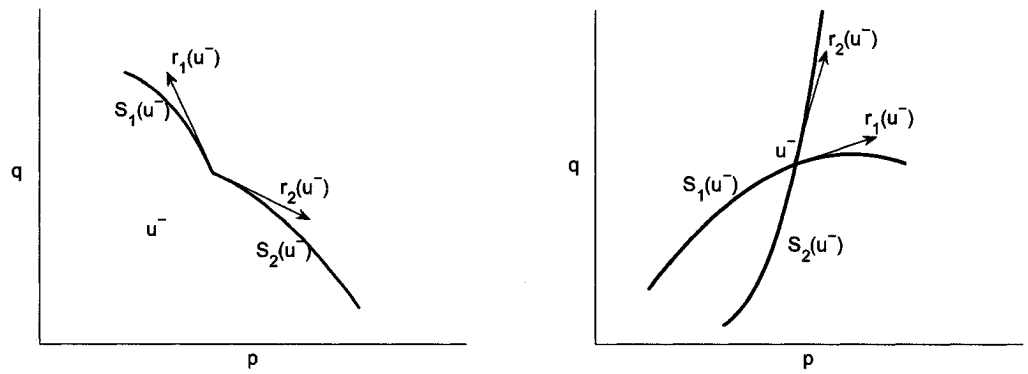

(a) (b)

Figure 4.1: (a) Hugoniot locus for the left state $u^- = (2,3)$ for attractive case where $r_1(u^-) = (-1,1), r_2(u^-) = (2,-1)$; (b) Hugoniot locus for the left state $u^- = (2,3)$ for repulsive case where $r_1(u^-) = \tilde{r}_1(u^-) = (3.56,1), r_2(u^-) = \tilde{r}_2(u^-) = (0.56,1), S_1(u^-) = \tilde{S}_1(u^-)$ and $S_2(u^-) = \tilde{S}_2(u^-)$.

4.2.2 General Riemann Problem

Next, we attempt to solve the Riemann problem graphically by drawing the Hugoniot locus for each states u^- and u^+ and looking for intersections. As illustrated in [74], we can accomplish this by finding an intermediate state u_m such that u^- and u_m are connected by a discontinuity satisfying the Rankine-Hugoniot condition and so for u_m and u^+.

Let us first examine the attractive case, i.e., the Riemann problem (4.2.4) and (4.2.5). Note that $\lambda_1(u) < \lambda_2(u)$ which requires the jump from u^- to u_m to travel more slowly than the jump from u_m to u^+. Precisely speaking, the u_m must be connected to u^- by a 1-shock S_1 while u^+ connected to u_m by a 2-shock S_2. We replace u^+ by u_m in (4.2.6) and go through the same calculation as we did in Case 1 to derive that the 1-shock connected to u_m has speed

$$s_1(\sigma, u_m) = \frac{1+\sigma}{2} q_m - \frac{1}{2}\sqrt{(1+\sigma)^2 q_m^2 - 4p_m} < \frac{1+\sigma}{2} q_m$$

while 2-shock has speed

$$s_2(\sigma, u_m) = \frac{1+\sigma}{2} q_m + \frac{1}{2}\sqrt{(1+\sigma)^2 q_m^2 - 4p_m} > \frac{1+\sigma}{2} q_m$$

and consequently $s_1(\sigma, u_m) < s_2(\sigma, u_m)$ for all σ. In a similar fashion, it is straightforward to deduce that $\tilde{s}_1(\sigma, u_m) < \tilde{s}_2(\sigma, u_m)$ for the repulsive case. Figure 4.2 gives

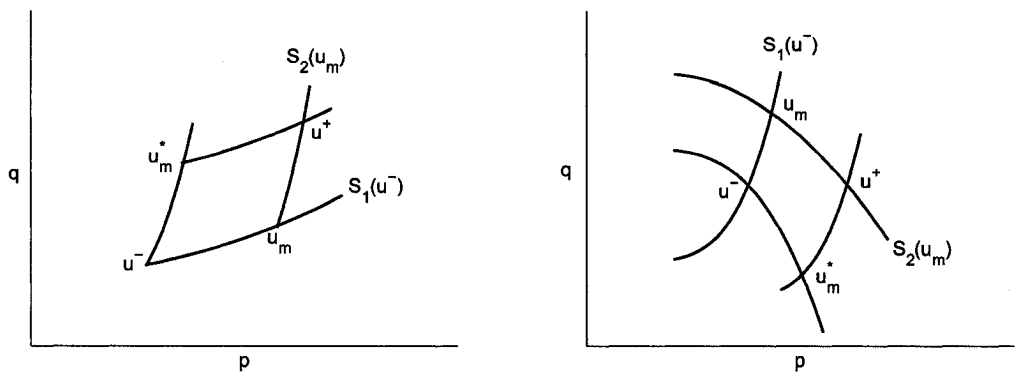

(a) $\alpha = -\frac{1}{D}$ (b) $\alpha = \frac{1}{D}$

Figure 4.2: Construction of a shock wave for the general Riemann problem with left state u^- and right state u^+. (a) is for attractive case and (b) is for repulsive case. Both (a) and (b) give two points of intersection, labeled u_m and u_m^*, but only u_m gives a single-valued solution to the Riemann problem since the requirement that the jump from u^- to u_m moves more slowly than the jump from u_m to u^+ due to $\lambda_1(u) < \lambda_2(u)$ and $\tilde{\lambda}_1(u) < \tilde{\lambda}_2(u)$.

two points of intersection for each case, labeled u_m and u_m^*, but only u_m gives a single-valued solution to the general Riemann problem since we require the jump from u^- to u_m to travel more slowly than the jump from u_m to u^+ due to the convention $\lambda_1(u) < \lambda_2(u)$ and $\tilde{\lambda}_1(u) < \tilde{\lambda}_2(u)$.

4.3 Traveling Wave with Shock Profile

In this section we will investigate the structure of the shock solution by considering the traveling wave for the problem

$$u_t + B(u)u_x = \tilde{D}u_{xx}, \tag{4.3.1}$$

where $B(u) = A(u)$ in the attractive case and $B(u) = \tilde{A}(u)$ in the repulsive case discussed in Section 2.

We define the traveling wave ansatz $u(x - ct) := u(z)$ with traveling speed c. In this paper, we restrict ourself to $c \geq 0$ since the shock speed s is nonnegative and we shall prove that c is identical to s later to show the existence of a traveling wave with shock profile. But it turns out from our analysis that c can be negative and hence a standing wave ($c = 0$) is admitted if we ignore the biological relevance.

Substituting the ansatz into equation (4.3.1), one has that

$$(B(u) - cI_2)u' = \bar{D}u'', \tag{4.3.2}$$

where the prime means the differentiation with respect to variable z and the I_2 is the 2×2 identity matrix. Assume now that the left state u^- and the right state u^+ are given and satisfy

$$\lim_{z\to-\infty} u = u^-, \lim_{z\to+\infty} u = u^+, \lim_{z\to\pm\infty} u' = 0.$$

Later we shall prove the traveling speed c coincides with the shock speed s, i.e., the traveling wave carries the shock profile $u(z) = u(x - st)$. Hence, if we define

$$\lim_{\bar{D}\to 0} u^{\bar{D}}(t,x) = \begin{cases} u^-, & \text{if } x < st, \\ u^+, & \text{if } x > st, \end{cases}$$

the limit as $\bar{D} \to 0$ of solution to (4.3.2) then gives us a shock wave connecting the left state u^- and the right state u^+. The purpose of this section is to carefully study the form of s and traveling wave $u(z)$ to gain more detailed insight into the structure of the shock for positive but small D. Again, we consider two cases corresponding to the sign of α.

4.3.1 Traveling Wave for Aggregative Case ($\alpha < 0$)

In this subsection, we will study the traveling solution of system (4.3.1) for $\alpha < 0$. As we point out before, when $\alpha < 0$, $B(u) = A(u)$, where $A(u)$ is as defined in Case 1 in Section 2. We take up $A(u)$ and expand (4.3.2) to get

$$\begin{cases} qp' + pq' - cp' = Dp'', \\ -p' - cq' = 0. \end{cases} \tag{4.3.3}$$

Introducing $v = p'$ and deducing from the second equation of (4.3.3) that $q' = -\dfrac{v}{c}$, we obtain equation $v' = \dfrac{v}{D}\left(q - \dfrac{p}{c} - c\right)$ from the first equation of (4.3.3). Coupling these equations gives rise to the following system

$$\begin{cases} p' = v, \\ q' = -\dfrac{v}{c}, \\ v' = \dfrac{v}{D}\left(q - \dfrac{p}{c} - c\right). \end{cases} \tag{4.3.4}$$

Observe that p and q have an invariant of motion: $p' + cq' = 0$. Then $p + cq = \varrho_1$, where ϱ_1 is a constant determined by the left state $u^- = (p^-, q^-)$ and the right state $u^+ = (p^+, q^+)$, i.e.,

$$\varrho_1 = p^- + cq^- = p^+ + cq^+, \tag{4.3.5}$$

which is an agreement with the identity (4.2.8) if $c = s$. Using the invariant of motion, the system (4.3.4) is reduced to

$$\begin{cases} p' = v, \\ v' = -\sigma v(p - \beta), \end{cases} \tag{4.3.6}$$

where $\sigma = \dfrac{2}{Dc}, \beta = \dfrac{\varrho_1}{2} - \dfrac{c^2}{2}$.

It is clear that system (4.3.6) has a continuum of steady states $(\theta, 0)$, where $\theta > 0$ due to the particle density $p > 0$. The corresponding community matrix about the steady state $(\theta, 0)$ is

$$J = \begin{bmatrix} 0 & 1 \\ 0 & \sigma(\beta - \theta) \end{bmatrix}$$

and hence the eigenvalues of J are

$$\lambda_1 = 0, \ \lambda_2 = \sigma(\beta - \theta),$$

with corresponding eigenfunctions, respectively,

$$r_1 = \begin{bmatrix} 1 \\ 0 \end{bmatrix}, \ r_2 = \begin{bmatrix} 1 \\ \lambda_2 \end{bmatrix} = \begin{bmatrix} 1 \\ -\sigma(\theta - \beta) \end{bmatrix}.$$

In the following, we shall study the existence of a traveling solution to nonlinear system (4.3.6) for fixed traveling speed. We give a class of equilibria in which two equilibria can be appropriately chosen to generate a nonnegative heteroclinic orbit connecting the two equilibria. To this end, we first investigate the stability of the linearized system of (4.3.6).

Note that the eigenvector r_1 corresponding to zero eigenvalue λ_1 is in the direction of the p axis $v = 0$ and every point $(\theta, 0)$ on the p axis is a steady state. To determine the stability of the linearized system, we only need to determine the sign of the second eigenvalue. Since $\sigma > 0$, we have the following relation

$$\begin{aligned} &\theta < \beta \Rightarrow \lambda_2 > 0, \\ &\theta = \beta \Rightarrow \lambda_2 = 0, \\ &\theta > \beta \Rightarrow \lambda_2 < 0. \end{aligned} \tag{4.3.7}$$

Therefore $\theta = \beta$ is a critical point which separates the steady states into stable parts and unstable parts. So a heteroclinic connection is possible for the linearized system. Note that it has been mentioned in the Introduction that p, as the particle density, preserves the positivity. So $p > 0$ and hence $p^-, p^+ > 0$. To have the biological relevance, we require that $\beta > 0$ to obtain a real unstable manifold corresponding to λ_2. This requires that

$$c^2 < \varrho_1 = p^- + cq^-. \tag{4.3.8}$$

In (4.3.8), we tacitly admit that $p^- + cq^- > 0$. Indeed from the definition of q, we know q can be negative and hence q^- and q^+ can be negative as the limits of q. Therefore it gives an additional requirement

$$p^- + cq^- > 0. \tag{4.3.9}$$

Observe that inequality (4.3.9) holds true for all $q^- \geq 0$. We only worry about the case of $q^- < 0$ which yields that from (4.3.9)

$$c < -\frac{p^-}{q^-}. \tag{4.3.10}$$

Then using (4.3.10) and solving (4.3.8) gives a maximum shock speed c^* such that

$$0 \leq c < c^*, \tag{4.3.11}$$

where

$$c^* = \begin{cases} \frac{q^- + \sqrt{(q^-)^2 + 4p^-}}{2}, & \text{for } q^- > 0, \\ \max\left\{-\frac{p^-}{q^-}, \frac{q^- + \sqrt{(q^-)^2 + 4p^-}}{2}\right\}, & \text{for } q^- < 0. \end{cases} \tag{4.3.12}$$

Then we can obtain a local stability theorem of linearization of system (4.3.6).

Lemma 4.3.1. *Let the traveling wave speed c satisfy (4.3.11) and (4.3.12). Then $\beta > 0$ and the steady state $(\theta, 0)$ of the linearized system of (4.3.6) is stable for $\theta > \beta$ whereas unstable for $\theta < \beta$.*

So far, we have obtained the stability of the lineariazation of the nonlinear system (4.3.6). But it is still not clear about the stability even local stability of the original nonlinear system (4.3.6) since there is a zero eigenvalue. To find an orbit connecting a stable manifold and an unstable manifold, we need to proceed to study the stability of system (4.3.6). We shall apply LaSall's invariant principle introduced in section 4.1.2 to prove the existence of a heteroclinic connection.

Since the p axis $v = 0$ $(p > 0)$ is a continuum of steady states, it splits the $p - v$ plane into two parts: $v > 0$ and $v < 0$. When $v > 0$, $p' > 0$ and hence p grows which requires that $p^- < p^+$. Analogously, $p^- > p^+$ when $v < 0$. We shall show that the monotonically decreasing traveling front wave does not exist. Whereas an increasing traveling front wave exists for $v > 0$ and $p^- < p^+$ using a constructive approach. We first give the following result.

Lemma 4.3.2. *Let (4.3.11) and (4.3.12) be satisfied. Assume that $v \leq 0$ and $p^- > p^+$. Then all solutions of the system (4.3.6), have an ω-limit set that is contained in the following set*

$$\mathbb{L} = \{(p, v)|\ v = 0, p > \beta\},$$

and the α-limit set is contained in

$$\mathbb{M} = \{(p, v)|\ v = 0, 0 < p < \beta\}.$$

Proof. Define a function $V(p, v)$ by $V(p, v) = p$. Since $p(z) > 0$ for all z, then $V(p(z), v(z)) > 0$ and $\frac{dV}{dz} = p' = v \leq 0$ thanks to the first equation of (4.3.6). For any $L > 0$, we now define $\Omega_L = \{(p, v) : p > 0, V(p, v) \leq L\} = \{(p, v) : 0 < p \leq L\}$. From the system (4.3.6), we can solve for v in terms of p such that

$$v(p) = -\frac{\sigma}{2}p^2 + \sigma\beta p + C,$$

where C is a constant of integration. It then follows from the above equation that v is bounded for any $0 < p \leq L$. Hence for any $L > 0$, the set Ω_L defined above is bounded. Moreover, it has that $\frac{dV}{dz} = v \leq 0$ due to the assumption $v \leq 0$.

Now we define another set

$$\mathbb{L}_1 = \left\{(p, v)\middle|\ \frac{dV}{dz} = 0,\ p > 0, v \leq 0\right\}. \tag{4.3.13}$$

From the first equation of (4.3.6), we have that

$$\frac{dV}{dz} = 0 \Longleftrightarrow v = 0. \tag{4.3.14}$$

Therefore $\mathbb{L}_1 = \{(p, v)|p > 0, v = 0\}$. Then $\mathbb{L}_1$ is invariant since it is comprised of steady states only. With the help of LaSall's invariant principle (Theorem 4.1.8), every solution of the system (4.3.6) starting in Ω_l for any $L > 0$ converges to $\mathbb{L}_1$ as $z \to +\infty$. Indeed, we can describe the asymptotic behavior of the solution more precisely. We know that $\lambda_2 > 0$ for all $0 < p < \beta$. Hence the manifold of system

(4.3.6) corresponding to eigenvalue $\lambda_2 > 0$ is unstable and all orbits will leave the neighborhood of the set $\mathbb{L}_2$ defined by.

$$\mathbb{L}_2 = \{(p, v)|\ v \leq 0, 0 < p < \beta\}.$$

Therefore, every solution of the system (4.3.6) converges to the set as $z \to +\infty$

$$\mathbb{L} = \mathbb{L}_1 \setminus \mathbb{L}_2 = \{(p, v)|\ v = 0, p > \beta\}.$$

Similarly, if we study the problem backward on variable z, we can show that all solutions of the system (4.3.6) converge to the set $\mathbb{M}$ as $z \to -\infty$, which completes the proof.

□

Now we are in a position to state the non-existence theorem of decreasing traveling solutions for system (4.3.6).

Theorem 4.3.1. *Let (4.3.11) and (4.3.12) be satisfied. Assume that $v \leq 0$. Then there is no traveling wave solution for system (4.3.6).*

Proof. (By contraction). Assume that there exists a traveling wave solution (p, v) for system (4.3.6). Since $p' = v \leq 0$, the traveling wave p is non-increasing. So $p(-\infty) = p^- \geq p^+ = p(+\infty)$. By Lemma 4.3.2, it follows that $(p^+, 0) \in \mathbb{L}$ and $(p^-, 0) \in \mathbb{M}$. Thus $p^+ > \beta$ and $0 < p^- < \beta$ and hence $p^- < p^+$. This is contradictive. So the system (4.3.6) has no traveling solutions.

□

Below we shall investigate the existence of traveling wave solutions of system (4.3.6) for $v > 0$. We provide a constructive proof to show the existence of a traveling solution and sketch the phase portrait and numerically plot the traveling solution of system (4.3.6). To this end, we first write (4.3.6) as

$$\frac{dv}{dp} = -\sigma(p - \beta).$$

Integrating the equation gives rise to

$$v(p) = -\frac{\sigma}{2}p^2 + \sigma\beta p + \varrho_2 = -\frac{1}{Dc}p^2 + \frac{1}{Dc}(\varrho_1 - c^2)p + \varrho_2, \tag{4.3.15}$$

where ϱ_2 is constant of integration to be determined.

Noting that $p' = v$. Then

$$p' = -\frac{\sigma}{2}p^2 + \sigma\beta p + \varrho_2. \tag{4.3.16}$$

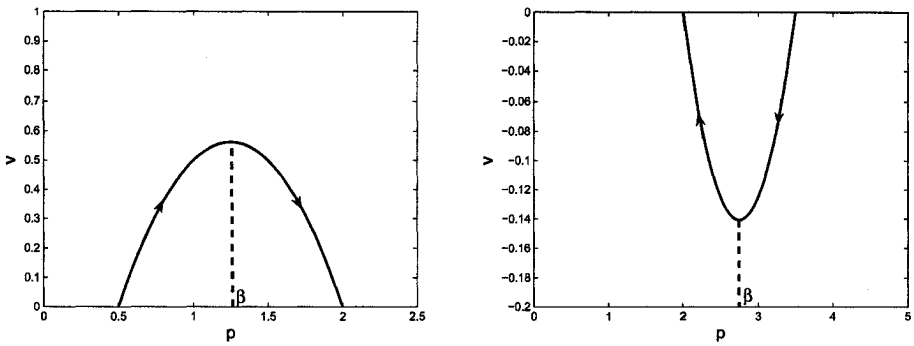

(a) (b)

Figure 4.3: (a) A plot of phase portrait for system (4.3.6), where $c = 1, D = 1$ and hence $\sigma = 2$. The value of $\beta = \frac{\varrho_1}{2} - \frac{c^2}{2}$ depends on the choice of ϱ_1, here we choose $\rho_1 = 3.5$ and then $\beta = 1.25$. (b) A plot of phase portrait for system (4.3.28) with $\tilde{c} = 4, D = 1$ and $\tilde{\sigma} = 0.5$. The value of $\tilde{\beta} = \frac{\tilde{\varrho}_1}{2} + \frac{\tilde{c}^2}{2}$ depends on the choice of $\tilde{\varrho}_1$, here we choose $\tilde{\varrho}_1 = -10.5$ and hence $\tilde{\beta} = 2.75$.

Solving equation (4.3.16), one obtains the solution

$$p = a_2 + \frac{a_2 - a_1}{C_0 \exp\left(\frac{\sigma}{2}(a_2 - a_1)z\right) - 1}, \tag{4.3.17}$$

where $a_1 = \beta - \sqrt{\beta^2 + \frac{2\varrho_2}{\sigma}}$, $a_2 = \beta + \sqrt{\beta^2 + \frac{2\varrho_2}{\sigma}}$.

Note that $a_2 - a_1 > 0$. Then the limits of (4.3.17) are

$$p(-\infty) = a_1, \ p(+\infty) = a_2. \tag{4.3.18}$$

By the boundary condition $p(-\infty) = p^-, p(+\infty) = p^+$, it follows that

$$a_1 = p^-, \ a_2 = p^+. \tag{4.3.19}$$

Then $p^- < p^+$ which is consistent with the fact $p' = v > 0$. Moreover, from the first equation of system (4.3.6), it follows that

$$v(\pm\infty) = \lim_{z \to \pm\infty} p' = 0,$$

which implies that system (4.3.6) has a pulse wave in v. Therefore, applying (4.3.15), we have that

$$v(p^-) = v(p^+) = 0. \tag{4.3.20}$$

Recovering σ and β and applying (4.3.20) into (4.3.15) gives that

$$\varrho_2 = \frac{1}{Dc}(p^-)^2 - \frac{1}{Dc}(\varrho_1 - c^2)p^- \tag{4.3.21}$$

as well as

$$-\frac{1}{Dc}(p^-)^2 + \frac{1}{Dc}(\varrho_1 - c^2)p^- = -\frac{1}{Dc}(p^+)^2 + \frac{1}{Dc}(\varrho_1 - c^2)p^+. \tag{4.3.22}$$

Since we have $p^- < p < p^+$, then v as a quadratic of p (see (4.3.15)), is uniformly bounded. From (4.3.18), (4.3.19) and (4.3.20), we know there exists a nonnegative heteroclinic orbit to system (4.3.6) connecting the left state $(p^-, 0)$ and right state $(p^+, 0)$. Given any one of end states, the other one can be determined by identity (4.3.22). The phase portrait of system (4.3.6) can be sketched by using (4.3.15) which gives rise to a parabola (see Figure 4.3 (a)). The traveling solution of system (4.3.6) is numerically given in Figure 4.4, where we employed the ODE solver of Matlab to solve the equations.

By above analysis, we obtain a traveling wave (p, v) for system (4.3.6). Utilizing the relation between v and q, we can connect the results to system (4.3.1) and obtain the following existence theorem for shock wave solutions to system (4.3.1).

Theorem 4.3.2. *Let $\alpha = -\frac{1}{D} < 0$, then there exists a nondecreasing traveling wave solution $u(z) = u(x - ct)$ for system (4.3.1) , such that $c = s$, where s is the shock speed. The traveling wave $u(x - st)$ connects left state u^- and right state u^+ if and only if $u^+ \in S_i(u^-)$, where $S_i(u^-)$ denotes the Hugoniot locus for left state u^-. Furthermore, the shock structure near $z = 0$, i.e., $x = st$, is given by*

$$\begin{cases} sq = \varrho_1 - p, \\ p' = -\frac{1}{Ds}p^2 + \frac{1}{Ds}(\varrho_1 - s^2)p + \frac{1}{Ds}(p^-)^2 - \frac{1}{Ds}(\varrho_1 - s^2)p^-, \end{cases} \tag{4.3.23}$$

where $\varrho_1 = p^- + sq^- = p^+ + cq^+$.

Proof. From the above analysis, it only remains to prove that the traveling wave speed c is identical to the shock speed s. Note that $\varrho_1 = p^- + cq^-$. Feeding this expression into (4.3.22) yields that

$$c^2q^- - c^2q^+ - q^+q^- - q^{+2} + q^-p^- - q^+p^- = 0, \tag{4.3.24}$$

which is an agreement with the reformulated Rankine-Hugonoit jump condition (4.2.10). This implies that the traveling speed c and the left state $u^- = (p^-, q^-)$ as well as the right state $u^+ = (p^+, q^+)$ agree with the Rankine-Hugoniot jump condition (4.2.6). Hence $c = s$ and (4.3.23) is obtained directly from (4.3.6), (4.3.15) and (4.3.21). □

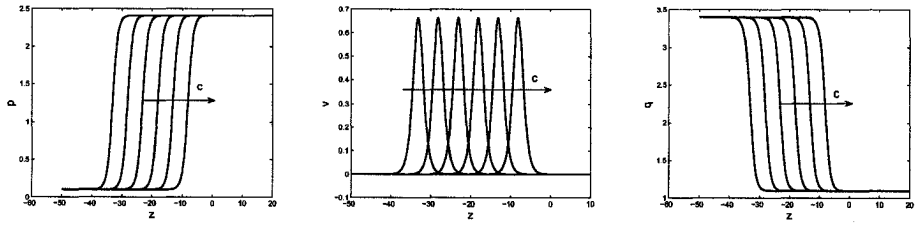

Figure 4.4: The traveling wave (p, q) determined by (4.3.23) for the case $\alpha = -\frac{1}{D} < 0$, where we choose $s = 1, D = 2, p^- = 0.5, q^- = 3$ and time $t = 0, 5, 10, 15, 20, 25$. The wave moves from left to right.

4.3.2 Traveling Wave for Repulsive Case ($\alpha > 0$)

In this section, we shall consider the traveling wave solutions of system (4.3.1) for the repulsive case, which is an opposite case compared to the preceding subsection. Here we have $B(u) = \tilde{A}(u)$, where $\tilde{A}(u)$ is as defined in Section 2 for the repulsive case. In this subsection, many details will be omitted since they are analogous to the analysis of the preceding subsection. We denote the traveling speed by $\tilde{c}$ to distinguish it with the traveling speed c used for the case $\alpha < 0$. Then we use the relation (4.3.2) to derive that

$$\begin{cases} -qp' - pq' - \tilde{c}p' = Dp'', \\ -p' - \tilde{c}q' = 0. \end{cases} \tag{4.3.25}$$

By the second equation of (4.3.25), we get that $p + \tilde{c}q = \tilde{\varrho}_1$ with a constant $\tilde{\varrho}_1$ determined by the two end states (p^-, q^-) and (p^+, q^+)

$$\tilde{\varrho}_1 = p^- + \tilde{c}q^- = p^+ + \tilde{c}q^+. \tag{4.3.26}$$

Then using the invariant of motion, we obtain from (4.3.25) that

$$Dp'' = \frac{2}{\tilde{c}}\left[p - \left(\frac{\tilde{\varrho}_1}{2} + \frac{\tilde{c}}{2}\right)\right]p'. \tag{4.3.27}$$

Denoting $v = p'$, $\tilde{\sigma} = \dfrac{2}{D\tilde{c}}$ and $\tilde{\beta} = \dfrac{\tilde{\varrho}_1}{2} + \dfrac{\tilde{c}^2}{2}$, we convert (4.3.27) into a system

$$\begin{cases} p' = v, \\ v' = \tilde{\sigma}v(p - \tilde{\beta}), \end{cases} \tag{4.3.28}$$

Clearly system (4.3.28) has a continuum of steady states $(\tilde{\theta}, 0)$ with $\tilde{\theta} > 0$ and the eigenvalues of the linearized system about equilibria $(\tilde{\theta}, 0)$ are

$$\tilde{\lambda}_1 = 0, \ \tilde{\lambda}_2 = \sigma(\tilde{\theta} - \tilde{\beta}).$$

We have the following observation due to $\tilde{\sigma} > 0$

$$\begin{aligned} &\tilde{\theta} < \tilde{\beta} \Rightarrow \tilde{\lambda}_2 < 0, \\ &\tilde{\theta} = \tilde{\beta} \Rightarrow \tilde{\lambda}_2 = 0, \\ &\tilde{\theta} > \tilde{\beta} \Rightarrow \tilde{\lambda}_2 > 0. \end{aligned} \tag{4.3.29}$$

Due to the biological relevance, it is required that $\tilde{\beta} > 0$ to obtain a heteroclinic connection. Then we have

$$\tilde{c}^2 + \tilde{\varrho}_1 = \tilde{c}^2 + \tilde{c}q^+ + p^+ > 0. \tag{4.3.30}$$

Note that $p^+ > 0$. Hence (4.3.30) holds for all $\tilde{c} \geq 0$ if $q^+ > 0$. For $q^+ < 0$, by solving (4.3.30), we find a sufficient condition $(q^+)^2 - 4p^+ < 0$ to obtain a nonnegative traveling speed $\tilde{c}$ satisfying (4.3.30). So we assume that

$$q^+ < 0, \ (q^+)^2 - 4p^+ < 0 \tag{4.3.31}$$

and solve (4.3.30), to obtain that

$$\underline{c} \leq \tilde{c} \leq \overline{c}, \tag{4.3.32}$$

where

$$\underline{c} = \frac{-q^+ - \sqrt{(q^+)^2 - 4p^+}}{2}, \ \overline{c} = \frac{-q^+ + \sqrt{(q^+)^2 - 4p^+}}{2}. \tag{4.3.33}$$

Then by the very routine argument as we used in Section 3.1, we easily obtain the following results for the corresponding linearized system of (4.3.28).

Lemma 4.3.3. *Let either $q^+ > 0, \tilde{c} \geq 0$ or (4.3.31), (4.3.32) and (4.3.33) hold. Then the linearized system of (4.3.28) is locally stable for $\tilde{\theta} < \tilde{\beta}$ and unstable $\tilde{\theta} > \tilde{\beta}$.*

Next, we study the stability of the nonlinear system (4.3.28). As before, we separate $p - v$ space into two regions: $v > 0$ and $v \leq 0$. We first look at the case $v \leq 0$ and give the following theorem.

Lemma 4.3.4. *Let either $q^+ > 0, \tilde{c} \geq 0$ or (4.3.31), (4.3.32) and (4.3.33) hold. Assume that $v \leq 0$ and $p^- > p^+$. Then the ω-limit set of all solutions of the system (4.3.28), is contained in the set*

$$\mathbb{V} = \{(p, v) |\ v = 0, 0 < p < \tilde{\beta}\},$$

and converge, as $z \to -\infty$, to the set

$$\mathbb{W} = \{(p, v) |\ v = 0, p > \tilde{\beta}\}.$$

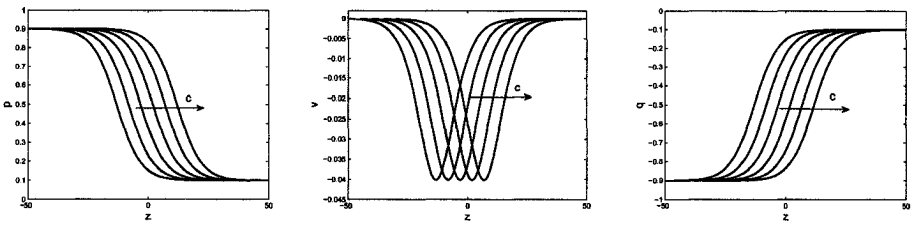

Figure 4.5: The traveling wave (p, q) determined by (4.3.36) for the case $\alpha = \frac{1}{D} > 0$, where we choose $s = 1, D = 4, p^+ = 2, q^+ = -2$ and time $t = 0, 5, 10, 15, 20, 25$. The wave moves from left to right.

Proof. By defing a function $\widetilde{V}(p, v)$ by $\widetilde{V}(p, v) = p$, we can use the same approach as in the proof of Theorem 4.3.2 by using the LaSall's invariant principle to get the results. The details are omitted.

□

With Lemma 4.3.4 in hand, we shall show the existence of a non-increasing traveling solution for system (4.3.28).

Lemma 4.3.5. *Let the assumptions in Lemma 3.6 hold. Then there exists a uniformly bounded, negative heteroclinic orbit (for v) connecting equilibria* $(e_1, 0)$ *and equilibria* $(e_2, 0)$ *for system (4.3.28), where* $e_1 < \tilde{\beta}, e_2 > \tilde{\beta}$. *As a consequence, there exists a traveling pulse in v and a non-increasing traveling front in p.*

Proof. According to Lemma 4.3.4, we only need to prove that the solution v as a function of p is bounded. To this end, we first write (4.3.28) as

$$\frac{dv}{dp} = \tilde{\sigma}(p - \tilde{\beta}).$$

Integrating the equation gives rise to

$$v(p) = \frac{1}{D\tilde{c}}p^2 - \frac{1}{D\tilde{c}}(\tilde{\varrho}_1 + \tilde{c}^2)p + \tilde{\varrho}_2, \tag{4.3.34}$$

where $\tilde{\sigma}$ and $\tilde{\beta}$ has been recovered and $\tilde{\varrho}_2$ is a constant of integration which can be determined by the boundary conditions of p and q,

$$\tilde{\varrho}_2 = -\frac{1}{D\tilde{c}}(p^+)^2 + \frac{1}{D\tilde{c}}(\tilde{\varrho}_1 + \tilde{c}^2)p^+. \tag{4.3.35}$$

Since $p' = v \leq 0$, p is decreasing. By the boundary condition $p(-\infty) = p^-$, $p(+\infty) = p^+$, if follows that $p^+ \leq p \leq p^-$ and hence p is uniformly bounded. Therefore v, as a quadratic form of p, is uniformly bounded as well. This finishes the proof.

□

Connecting the traveling wave solutions obtained above with the shock solution obtained in Section 2, we have the following existence theorem for a traveling wave with shock profile $u(x-\tilde{c}t)$, i.e., $\tilde{c}=\tilde{s}$, where $\tilde{s}$ is the shock speed discussed in Section 2 for case $\alpha>0$.

Theorem 4.3.3. *Let $\alpha=\frac{1}{D}>0$ and the assumptions in Lemma 3.7 hold, then there exists a non-increasing traveling wave solution $u(z)=u(x-\tilde{c}t)$ for system (4.3.1) such that $c=s$, where $\tilde{s}$ is the shock speed. The conditions that p^- and p^+ lie on the same parabola $v(p)$ given by (4.3.34) is identical to the Rankine-Hugoniot condition. The traveling wave connects left state u^- and right state u^+ if and only if $u^+\in\tilde{S}_i(u^-)$, where $u^+\in\tilde{S}_i(u^-)$ denotes the Hugoniot locus for left state u^- obtained in Section 2. Furthermore, the shock structure near $z=0$, i.e., $x=\tilde{s}t$, is given by*

$$\begin{cases} \tilde{s}q=\tilde{\varrho}_1-p, \\ p'=\frac{1}{D\tilde{s}}p^2-\frac{1}{D\tilde{s}}(\tilde{\varrho}_1+\tilde{s}^2)p-\frac{1}{D\tilde{s}}(p^+)^2+\frac{1}{D\tilde{s}}(\tilde{\varrho}_1+\tilde{s}^2)p^+, \end{cases} \tag{4.3.36}$$

where $\tilde{\varrho}_1=p^-+\tilde{s}q^-=p^++\tilde{s}q^+$.

Proof. System (4.3.36) is obtained from (4.3.28), (4.3.34) and (4.3.35) directly if we replace $\tilde{c}$ by $\tilde{s}$. So by Lemma 3.7, it only remains to prove that the traveling speed $\tilde{c}$ is identical to the shock speed $\tilde{s}$. Since $v(p^-)=v(p^+)=0$, we have from (4.3.34) that

$$-\frac{1}{D\tilde{c}}(p^-)^2+\frac{1}{D\tilde{c}}(\tilde{\varrho}_1+\tilde{c}^2)p^-=-\frac{1}{D\tilde{c}}(p^+)^2+\frac{1}{D\tilde{c}}(\tilde{\varrho}_1+\tilde{c}^2)p^+. \tag{4.3.37}$$

Hence substituting $\tilde{\varrho}_1=p^-+\tilde{c}q^-$ into (4.3.37) and canceling D out yields that

$$\tilde{c}(q^+)^2-p^-q^+-\tilde{c}q^-q^++\tilde{c}^2q^++p^-q^--\tilde{c}^2q^-=0, \tag{4.3.38}$$

which is the same as the reformulated Ranking-Hugoniot jump condition (4.2.25). Hence $\tilde{c}=\tilde{s}$, as required. □

A phase portrait of system (4.3.28) is given in Figure 4.3 (b) and a numerical traveling solution is plotted in Figure 4.5. In the remainder of this section, we will investigate the traveling solutions for the other case $v>0$. It turns out that traveling wave solutions do not exist for $v>0$. To prove this, we first derive from (4.3.28) that

$$p'=\frac{1}{2}\tilde{\sigma}p^2-\tilde{\sigma}\tilde{\beta}p+\tilde{\varrho}_2. \tag{4.3.39}$$

Note that

$$\tilde{\beta}^2 - \frac{2\tilde{\varrho}_2}{\tilde{\sigma}} = \frac{1}{4}(\tilde{\varrho}_1 + \tilde{c}^2 - 2p^-)^2 \geq 0.$$

Then we solve equation (4.3.39) to get that

$$p = \tilde{a}_2 + \frac{\tilde{a}_2 - \tilde{a}_1}{\tilde{C}_0 \exp\left(\frac{\tilde{\sigma}}{2}(\tilde{a}_1 - \tilde{a}_2)z\right) - 1}, \tag{4.3.40}$$

where $\tilde{a}_1 = \tilde{\beta} - \sqrt{\tilde{\beta}^2 - \frac{2\tilde{\varrho}_2}{\tilde{\sigma}}}$, $\tilde{a}_2 = \tilde{\beta} + \sqrt{\tilde{\beta}^2 - \frac{2\tilde{\varrho}_2}{\tilde{\sigma}}}$.

It is clear that $\tilde{a}_1 - \tilde{a}_2 \leq 0$. Taking the limits for (4.3.40), we have that

$$\begin{aligned} p(z) &\to \tilde{a}_2 \text{ as } z \to -\infty, \\ p(z) &\to \tilde{a}_1 \text{ as } z \to +\infty. \end{aligned} \tag{4.3.41}$$

Using (4.3.41), we can show the nonexistence of traveling solutions of system (4.3.28) for $v > 0$.

Theorem 4.3.4. *Assume that either $p^+ > 0, \tilde{c} \geq 0$ or (4.3.31), (4.3.32) and (4.3.33) hold. Then there is no traveling wave solution to system (4.3.28) for $v > 0$.*

4.4 Entropy Solution

As is well known, weak solutions of the Cauchy problem of a system of conservation laws are generally non-unique and a so-called " entropy condition" is required to pick out the physical relevant viscosity solution [15]. One condition which picks a physical solution is that it should be the limiting solution of the viscous equation as the viscosity coefficient tends to zero [34]. Another approach to the "entropy condition" is to define an entropy pair for which an additional conservation law holds for smooth solutions that becomes an inequality for discontinuous solutions. In this section, we are devoted to developing a convex entropy and an entropy flux pair (η, ρ) for the case of $\alpha = \frac{1}{D} > 0$. Toward this end, we first rewrite the conservation law (4.2.21) in the form

$$\begin{cases} p_t - (pq)_x = 0, \\ q_t - p_x = 0, \end{cases} \tag{4.4.1}$$

or

$$u_t + \tilde{f}(u)_x = 0, \tag{4.4.2}$$

where $u = (p, q)$ and $\tilde{f}(u) = (-pq, -p)$.

From the Definition 4.1.4 given in the Introduction, we know that the entropy pair (η, ρ) satisfies an additional conservation law for any smooth solution $u = (p, q)$ to system (4.4.1)

$$\eta(u)_t + \rho(u)_x = 0. \tag{4.4.3}$$

Substituting (4.4.2) into (4.4.3), we end up with

$$\eta'(u) \cdot f'(u) = \rho'(u), \tag{4.4.4}$$

where $'$ denotes the derivative with respect to vector $u = (p, q)$. Expanding (4.4.4) gives the following relation

$$\begin{cases} \rho_p = -\eta_q - q\eta_p, \\ \rho_q = -p\eta_p. \end{cases} \tag{4.4.5}$$

Eliminating η from (4.4.5) gives that

$$\eta_{qq} + q\eta_{pq} - p\eta_{pp} = 0. \tag{4.4.6}$$

We assume that the entropy $\eta(u)$ of the conservation law (4.4.2) has the following form

$$\eta(p, q) = \frac{1}{2}q^2 + g(p), \tag{4.4.7}$$

where $g(p)$ is expected to be a convex function.

Substituting (4.4.7) into (4.4.6) yields that

$$1 - pg''(p) = 0. \tag{4.4.8}$$

Solving (4.4.8) gives

$$g(p) = p\ln p - p + k_1 p + k_2, \tag{4.4.9}$$

where k_1, k_2 are arbitrary constants.

Then Substituting (4.4.7) and (4.4.9) into the first equation of (4.4.5) enables us to find $\rho(p, q)$ as

$$\rho(p, q) = -pq\ln p - k_1 pq + k_3, \tag{4.4.10}$$

where k_3 is an arbitrary constant.

If we particularly choose $k_1 = k_2 = k_3 = 0$, we obtain an entropy-entropy flux pair (η, ρ) which reads

$$\begin{cases} \eta(p, q) = \frac{1}{2}q^2 + p\ln p - p, \\ \rho(p, q) = -pq\ln p. \end{cases} \tag{4.4.11}$$

Accordingly, $g(p) = p\ln p - p$ and it is easy to verify that $g''(p) = 1/p > 0$ due to $p > 0$. As a consequence, the second derivative of $\eta(u)$ is a positive definite quadratic form. That is $\eta(u)$ is a convex function.

The entropy $\eta(u)$ is conserved for smooth solutions of (4.4.2) by its definition. For discontinuous solutions (shock solutions), however, the manipulations performed above in general are not valid, i.e., $\eta(u)$ is not conserved. Since we are particularly interested in how the entropy behaves for the vanishing viscosity weak solution, we look at the related viscous problem

$$u_t + \tilde{f}(u)_x = \bar{D}u_{xx}, \tag{4.4.12}$$

and let the viscosity coefficient $\bar{D}$ tend to zero.

Since the solutions of equation (4.4.12) are always smooth, we can derive the corresponding evolution equation for the entropy following the same procedure applied for smooth solutions for the inviscid equation (4.4.2). Therefore we multiply (4.4.12) by $\eta'(u)$ to obtain from (4.4.4) that

$$\eta(u)_t + \rho(u)_x = \bar{D}\eta'(u)u_{xx}. \tag{4.4.13}$$

That is

$$\eta(u)_t + \rho(u)_x = \bar{D}\eta(u)_{xx} - \bar{D}\eta''(u)u_x^2. \tag{4.4.14}$$

Applying a standard argument (e.g. p.604-606 in [34]), we end up with the following inequality

$$\int_0^T \int_0^l \eta(u)_t + \rho(u)_x dxdt \leq 0. \tag{4.4.15}$$

The fact that inequality (4.4.15) holds for any l and T is summarized by saying that $\eta(u)_t + \rho(u)_x \leq 0$ almost everywhere. We are led to the following theorem.

Theorem 4.4.1. (Entropy solution). *Any solution (p, q) of (4.4.2) which is the limit of the viscosity equation (4.4.12) satisfies*

$$\eta(p, q)_t + \rho(p, q)_x \leq 0, \tag{4.4.16}$$

in the weak sense, where $\eta(p, q)$ and $\rho(p, q)$ are given by (4.4.11).

4.5 Discussion

In this chapter, we establish the shock structure for a simplified version of a chemotaxis model (4.1.1), (4.1.2), (4.1.3) and (4.1.4) for both attractive ($\alpha > 0$) and

repulsive ($\alpha < 0$) cases. The shock curves are given in parameterized forms. The requirements on the choice of the parameter σ are different for the cases of $\alpha > 0$ and $\alpha < 0$. Moreover, we discuss the general Riemann problem. We show that, for the attractive case, there exists only nondecreasing traveling waves, and for the repulsive case there exists only nonincreasing traveling waves. Furthermore we prove that the traveling wave speed is identical to the shock speed and the traveling waves converge to the given shock waves as the viscosity constant $D \to 0$, which means the sharp transition of cell movements (movement disturbance) from one state to the other as viscosity vanishes. This is indeed expected. When viscosity turns to zero, the chemotactic movement becomes dominant and cell aggregation or dispersal is more pronounced, which might lead to a sharp transition corresponding to the occurrence of shocks.

For the uniqueness of the weak solutions (shock solutions), we also find an entropy-entropy pair for the repulsive case. For the attractive case, the question of uniqueness of weak solutions is still open.

When $\alpha = -1$ (or < 0), it has been proven by Levine and Sleeman [75] that there are solutions (p, w) for which $p > 0$ blows up in finite time and an explicit family of such blow-up solutions has been constructed in the section 3 of [75]. But there are no results available about the global existence or non-existence of solutions for $\alpha > 0$. To show the global existence for model (4.1.5)-(4.1.7) is not an easy problem. Below we give a reformulation of the problem that leads to Dirichlet boundary conditions. We hope it can provide some useful clues for the global existence for the solution.

The boundary condition (4.1.2) or (4.1.6) seems like a Neumann boundary condition. But it is not the standard form of a Neumann boundary condition. We will first reformulate the form of boundary conditions. A direct calculation shows that the boundary condition (4.1.2) is weaker than the non-flux boundary condition $p_x(0,t) = p_x(l,t) = 0$. However, for those solutions of the simplified problem (4.1.5)-(4.1.7) for which this stronger condition holds, one might be able to apply the argument in [105] to obtain the local-in-time existence and the uniqueness of solution as well. Furthermore, from the second equation of (4.1.5), it follows that $(\ln w)_t = \lambda p - \mu$. Hence at the domain boundaries $x = 0, l$, we have that $(\ln w)_{tx} = \lambda p_x = -\lambda\alpha p\frac{w_x}{w} = -\lambda\alpha(\ln w)_x$, i.e., $(\ln w)_{tx} + \lambda\alpha(\ln w)_x = 0$. Solving this equation gives the solution

$$(\ln w)_x = \frac{w_x}{w} = \frac{w_x(x,0)}{w(x,0)} \exp\left(-\lambda\alpha \int_0^t p(x,\tau)d\tau \right), \text{ at } x = 0, l.$$

From this point, we know that if $w_x = 0$ initially at the domain boundaries, both p and w have zero flux on the boundary in the entire existence time interval. We

therefore always have the local existence and uniqueness for problem (4.1.5)-(4.1.7) such that either p or w initially satisfies the zero flux boundary condition. And consequently we get the zero flux boundary condition for either p or w. Therefore it is plausible to suppose that $w_x(0,t) = w_x(l,t) = 0$ for all $t > 0$.

In addition, we can simplify system (4.1.8)-(4.1.10) as well. As usual we let $q = (\ln w)_x$. Then from the second equation of (4.1.8) it follows that $q_t = (\ln w)_{xt} = \left(\frac{w_t}{w}\right)_x = p_x$. Together with the boundary condition discussed above, we translate system (4.1.8), (4.1.9) and (4.1.10) into the following nicer form

$$\begin{cases} p_t = p_{xx} + \alpha(pq)_x, \ (x,t) \in (0,l) \times (0,\infty), \\ q_t = p_x, \end{cases} \tag{4.5.1}$$

with boundary condition

$$p(0,t) = M, \ q(0,t) = q(l,t) = 0, \tag{4.5.2}$$

and initial data

$$p(x,0) = p_0(x) > 0, q(x,0) = q_0(x) \ \text{ for } \ 0 \le x \le l, \tag{4.5.3}$$

where M is a positive constant.

If $\alpha > 0$, we introduce the new variables by $\bar{t} = \frac{t}{1/\alpha M}, \bar{x} = \frac{x}{l\sqrt{\frac{1}{\alpha M}}}, \bar{p} = \frac{p}{M}, \bar{q} = \frac{q}{\sqrt{\frac{\alpha}{M}}}$ and redefine initial data by $\bar{p}_0(x) = \frac{p_0(x)}{M}, \bar{q}_0(x) = \frac{q_0(x)}{\sqrt{\frac{\alpha}{M}}}$. Substituting these transformations into (5.1)-(5.3) and dropping the bar for clarity, we obtain the following non-dimensional form

$$\begin{cases} p_t - (pq)_x = p_{xx}, \ (x,t) \in (0,1) \times (0,\infty), \\ q_t - p_x = 0, \end{cases} \tag{4.5.4}$$

with boundary condition

$$p(0,t) = 1, \ q(0,t) = q(1,t) = 0, \quad \text{for } \ t \ge 0, \tag{4.5.5}$$

and initial data

$$p(x,0) = p_0(x) > 0, \ q(x,0) = q_0(x) \ \text{ for } \ 0 \le x \le 1. \tag{4.5.6}$$

It is worthwhile to point out that the spatial domain has been rescaled to $[0,1]$. By ignoring the diffusion term in (4.5.4), we obtain

$$\begin{cases} p_t - (pq)_x = 0, \ (x,t) \in (0,1) \times (0,\infty), \\ q_t - p_x = 0, \end{cases} \tag{4.5.7}$$

It is easy to get the characteristic equation of system (4.5.7) which reads $\lambda^2 - \lambda q - p = 0$ where λ denotes the eigenvalues. So the discriminant $\triangle = q^2 + 4p$ is positive due to $p > 0$. Hence, system (4.5.7) is a hyperbolic system which is consistent with the discussion in section 1.1.

The problem (4.1.8)-(4.1.10) now is reduced to nondimensional system (4.5.4)-(4.5.6). One of the difficulties to consider the global existence of the solution to (4.1.5)-(4.1.7) is that the second equation of (4.5.4) missed the diffusion component. Novel ideas need to be developed to deal with such an issue.

Chapter 5

MESENCHYMAL MOTION MODELS IN ONE DIMENSION [1]

5.1 Introduction

Mesenchymal motion is a form of cellular movement through tissues which are formed from fibre networks. An example is the invasion of tumor metastases through collagen networks. The cell movement is guided by directionality of the networks and in addition, the networks is degraded by matrix-degrading enzymes (protease) which are released by cells.

One of the examples of mesenchymal motion is reported in a review article by Friedl and Bröcker [38]. They find that the movement of amoeboid cells on a surface is significantly different from their movement in a tissue matrix. On a two dimensional surface, cells are free to move in any direction. However, in three dimensional tissues, cells are embedded inside the tissue and their movement is constrained. For example, some tumor cells appear elongated and spindle shaped and send out thin pseudopods for directional guidance from the ambient matrix. Moreover, cells can excrete some tissue degrading enzyme (for example, protease) to degrade tissues by cutting for moving through. Such a movement is called mesenchymal motion in [38].

Mesoscopic and macroscopic models for mesenchymal motion were derived by Hillen [47] in a timely varying network tissue. The mesoscopic models are based on a transport equation for correlated random walk and consist of a transport equation for the cell movement coupled to an ordinary differential equation for the tissue fibres. The macroscopic models have the form of a drift-diffusion equation where the mean drift velocity is given by the mean orientation of the tissue, and the diffusion tensor is given by the variance-covariance matrix of the tissue orientation. The tissue matrix is divided into the undirected and the directed tissues according to the distribution of fibre orientation. In undirected tissues, the fibres are symmetrical along their axis and both fibre directions are identical. For example, collagen fibres are undirected and they form the basis for many human and animal tissues. For directed tissues, the fibres are unsymmetrical and the two ends can be distinguished

[1] This is a collaboration with Thomas Hillen and Michael Li.

(positive/negative, forward/backward, north/south). Directed components do not play a major role for cell movement in tissues, however, directed fibres occur inside cells (such as microtubules and actin filaments). Branching collagen fibre networks can also be considered directional if the branching points are of significance for the movement of cells.

In this chapter, I will present a detailed analysis of the one-dimensional model for mesenchymal motion, including existence of solutions, macroscopic limits, traveling waves as well as results on pattern formation. First, of course, we present the original model derived by Hillen [47].

5.1.1 Models for Mesenchymal Motion

As in [47], we let S^{n-1} denote the unit sphere in $\mathbb{R}^n$ and θ the fibre orientation in S^{n-1}. Let Ω be n-dimensional spatial domain. We denote the distribution of fibre orientations at time $t \geq 0$ and at location $x \in \Omega$ by the probability density $q(t, x, \theta)$, which naturally satisfies the normalization condition for all $t \geq 0, x \in \Omega$

$$\int_{S^{n-1}} q(t, x, \theta) d\theta = 1. \tag{5.1.1}$$

The function $q(t, x, \theta)$ can be understood as the probability density that cells decide to choose a new direction $\theta \in S^{n-1}$ if it occurs. Let V denote the set of all possible velocities of moving cells and $p(t, x, v)$ the population density of cells that have velocity v at time t at location x. V is assumed to be radially symmetric and can be written as

$$V = [s_1, s_2] \times S^{n-1}, \quad 0 < s_1 \leq s_2 < \infty,$$

where $[s_1, s_2]$ is the range of possible speeds. We define $\hat{v}$ as the unit vector in direction of a vector $v \in V$. That is

$$\hat{v} := \frac{v}{\|v\|}.$$

In addition we define a weight parameter ω such that

$$\omega = \int_V q(t, x, \hat{v}) dv = \begin{cases} \frac{s_2^n - s_1^n}{n}, & \text{for } s_1 < s_2, \\ s^{n-1}, & \text{for } s_1 = s_2 = s. \end{cases} \tag{5.1.2}$$

Let a constant $\mu \geq 0$ denote the turning rate and a constant $\kappa \geq 0$ the cutting efficiency (rate of fibre degradation). Then the model for mesenchymal motion of cells for undirected tissues consists of a transport equation for cell motion and an

equation for the fibre distribution, which reads (see [47])

$$p_t(t,x,v) + v \cdot \nabla p(t,x,v) = -\mu p(t,x,v) + \mu \int_V \frac{q(t,x,\hat{v})}{\omega} p(t,x,v')dv', \quad (5.1.3)$$

$$q_t(t,x,\theta) = \kappa(\Pi_u(t,x,\theta) - A_u(t,x))\rho(t,x)q(t,x,\theta), \quad (5.1.4)$$

where $\rho(t,x)$ denotes the macroscopic density of cells

$$\rho(t,x) = \int_V p(t,x,v)dv,$$

$\Pi_u(t,x,\theta)$ denotes the mean projection of the cell movement direction onto a given fibre orientation θ

$$\Pi_u(t,x,\theta) = \frac{1}{\rho(t,x)} \int_V |\theta \cdot \hat{v}| p(t,x,v)dv,$$

and $A_u(t,x)$ is the mean value of these mean projections over all fibre directions

$$A_u(t,x) = \int_{S^{n-1}} \Pi_u(t,x,\theta)q(t,x,\theta)d\theta.$$

The mesenchymal motion model for directed tissues is similar to the undirected case, which is (see also [47])

$$p_t(t,x,v) + v \cdot \nabla p(t,x,v) = -\mu p(t,x,v) + \mu \int_V \frac{q(t,x,\hat{v})}{\omega} p(t,x,v')dv', \quad (5.1.5)$$

$$q_t(t,x,\theta) = \kappa(\Pi_d(t,x,\theta) - A_d(t,x))\rho(t,x)q(t,x,\theta), \quad (5.1.6)$$

where the projection operator $\Pi_d(t,x,\theta)$ for directed tissue is defined by

$$\Pi_d(t,x,\theta) = \frac{1}{\rho(t,x)} \int_V \theta \cdot \hat{v}\ p(t,x,v)dv,$$

and the corresponding mean value $A_d(t,x,\theta)$ of all mean projections is determined by

$$A_d(t,x) = \int_{S^{n-1}} \Pi_d(t,x,\theta)q(t,x,\theta)d\theta.$$

In the paper by Hillen [47], three scaling arguments are used to study the macroscopic limits of system (5.1.3) and (5.1.4) for undirected tissues and (5.1.5) and (5.1.6) for directed tissues. These are the moment closure, the parabolic scaling and the hydrodynamic scaling. The resulting macroscopic models have the form of drift-diffusion equations where the mean drift velocity is given by the mean orientation of the tissue and the diffusion tensor is given by the variance-covariance matrix of the tissue orientations. Some examples and applications are also discussed in [47]. The

numerical schemes and pattern formation in n-dimension are obtained by Painter [97]. The steady state analysis is investigated by Hillen (2007). However, the global existence of solutions and rigorous derivation of macroscopic limits are not known so far.

In case of chemotaxis, a system of a transport equation for the cell motion and a parabolic equation for the chemical signal was studied by Alt [2], Chalub *et al.* [17] and Hwang *et al.* [63, 62]. However, their arguments are based on L^∞ estimates of the turning kernel. In case of mesenchymal motion models, the turning kernel is given by the fibre distribution $q(t,x,\theta)$ which is a delta distribution $q(\theta) = \delta_b(\theta)$ for a totally aligned tissue in direction of $b \in \mathbb{R}^n$. As a result, the fibre distribution is not necessarily bounded in L^∞. In particular, assumption (A0) in paper [17] does not apply and hence their results can not be applied directly for the case discussed here. The global existence analysis is quite technically involved.

In this chapter, the one dimensional models are fully analyzed. We study the global existence of solutions, macroscopic limits, traveling waves and pattern formation. We can gain some fundamental and instructive insight into the mechanisms involved in the model. For example, we find the existence of traveling pulse solutions for the cell population and no pattern formation is observed.

This chapter is organized as follows. In the rest of this section, we will present the one dimensional mesenchymal motion models derived in [47] and discuss the telegraph process in more detail. In section 5.2, we will classify the system (5.1.8) and (5.1.9) as degenerated hyperbolic system and verify that there are no shock solutions. In section 5.3, the global existence of classical solutions are obtained along characteristics using a fix point theorem. In section 5.4, we non-dimensionalize system (5.1.3), (5.1.4) and find appropriate time and space scales which lead to parabolic and hyperbolic scalings. Furthermore, we prove the existence of weak limits of solutions to rescaled equations. In section 5.5, we study the traveling wave solutions and find the traveling pulse solution for the cell population. In section 5.6, we perform the stability analysis and conclude that there is no pattern formation for the one dimensional model. In the final section 5.7, we summarize and compare our results with the results obtained in [47].

5.1.2 One Dimensional Models for Mesenchymal Motion

The one-dimensional mesenchymal motion models correspond to the case where the fibre orientations are totaly aligned in the tissue. Although the higher dimensional models have significant difference than in the one-dimensional models, the one-

dimensional models are still very instructive and provide many basic insight into the mechanism involved. For example, the existence of travelling pulse solutions and macroscopic limits and so on that we will demonstrate in the following sections.

We first treat the directed case and the undirected case follows easily. Following the argument in [47], we fix speed to $|v| = s$, i.e., $v = \pm s$. In a one-dimensional domain, cells can only move to the right or the left. For notational convenience, we denote

$$p^+(t,x) = p(t,x,+s),\ p^-(t,x) = p(t,x,-s),$$

respectively. The distribution $q(t,x,\theta)$ describes a bias of choosing right over left and vice versa. In one dimension, $S^0 = \{+1,-1\}$ and $\theta = \pm 1$, and we define

$$q^+(t,x) = q(t,x,+1),\ q^-(t,x) = q(t,x,-1).$$

Then it follows from (5.1.1) that

$$q^+(x,t) + q^-(x,t) = 1. \tag{5.1.7}$$

The projection operator $\Pi_d(t,x,\theta)$ can be explicitly obtained in one dimension

$$\Pi_d(t,x,\theta) = \frac{1}{p^+ + p^-}(\theta p^+ - \theta p^-),$$

which gives the following projection for right and left direction, respectively,

$$\Pi_d^{\pm} = \Pi_d(t,x,\pm 1) = \frac{p^{\pm} - p^{\mp}}{p^+ + p^-}$$

Then the mean projection A_d is obtained as

$$A_d(t,x) = \Pi_d^+ q^+ + \Pi_d^- q^- = \frac{p^+ - p^-}{p^+ + p^-}(q^+ - q^-).$$

Substituting all these results into the model (5.1.5) and (5.1.6), we obtain the one-dimensional mesenchymal transport model for the directed case (see [47])

$$\begin{aligned} p_t^+ + sp_x^+ &= -\mu p^+ + \mu q^+(p^+ + p^-), \\ p_t^- - sp_x^- &= -\mu p^- + \mu q^-(p^+ + p^-), \\ q_t^+ &= \kappa(p^+ - p^-)(q^- - q^+ + 1)q^+, \\ q_t^- &= \kappa(p^+ - p^-)(q^- - q^+ - 1)q^-. \end{aligned} \tag{5.1.8}$$

For the undirected case, it is easy to calculate the projection and the mean projection as

$$\Pi_u^{\pm} = A_u = 1.$$

Consequently the one-dimensional mesenchymal transport model in undirected tissue has the form (see [47])

$$\begin{aligned} p_t^+ + sp_x^+ &= -\mu p^+ + \mu q^+(p^+ + p^-), \\ p_t^- - sp_x^- &= -\mu p^- + \mu q^-(p^+ + p^-), \\ q_t^+ &= 0, \\ q_t^- &= 0, \end{aligned} \tag{5.1.9}$$

where $(t, x) \in [0, \infty) \times \Omega$ and Ω is an interval in $\mathbb{R}$. All above results are from paper [47] and we recommend readers to see details in it.

Now we investigate the connections between the one dimensional mesenchymal motion models and well known Goldstein-Kac model [40, 66] which describes the correlated random walk in one space dimension. We use condition (5.1.7) to substitute $q^- = 1 - q^+$ into the first two equations of (5.1.8) or (5.1.9) and obtain that

$$\begin{aligned} p_t^+ + sp_x^+ &= -\mu(1 - q^+)p^+ + \mu q^+ p^-, \\ p_t^- - sp_x^- &= \mu(1 - q^+)p^+ - \mu q^+ p^-. \end{aligned} \tag{5.1.10}$$

The model (5.1.9) for the undirected case is simpler than the directed case. But it possesses some very interesting phenomena. We know that, in undirected tissues, the fibres are symmetrical along their axis and both fibre directions are identical. Hence $q^+ = q^- = \frac{1}{2}$. Then the model (5.1.10) becomes the Goldstein-Kac model [40, 66]

$$\begin{aligned} p_t^+ + sp_x^+ &= \frac{\mu}{2}(p^- - p^+), \\ p_t^- - sp_x^- &= -\frac{\mu}{2}(p^- - p^+). \end{aligned} \tag{5.1.11}$$

The parabolic scaling for the Goldstein-Kac model, which leads to a parabolic equation, has been discussed in [41] and references therein.

For directed tissues, we define $\lambda^+ = \mu(1 - q^+), \lambda^- = \mu q^+$, then (5.1.10) is converted into

$$\begin{aligned} p_t^+ + sp_x^+ &= -\lambda^+ p^+ + \lambda^- p^-, \\ p_t^- - sp_x^- &= \lambda^+ p^+ - \lambda^- p^-, \end{aligned} \tag{5.1.12}$$

which is a modification of the Goldstein-Kac model. The extension of Goldstein-Kac model and the local and global existence of the solution to the extended model has been extensively investigated in reference [56, 57, 64]. The results obtained in [56, 57, 64] can be applied to system (5.1.12). The telegraph process of (5.1.12) has

been briefly discussed by Erban and Othmer [32] recently. In the next subsection, we will discuss the telegraph process of mesenchymal motion models for the directed case.

We supply the system (5.1.8) and (5.1.9) with initial condition

$$p^{\pm}(0,x) = p_I^{\pm}(x),\ q^{\pm}(0,x) = q_I^{\pm}(x),\ x \in \Omega. \tag{5.1.13}$$

Due to the biological interest and condition (5.1.7), we make the following assumptions for the above initial data.

(ic) $p_I^{\pm} \geq 0$, $0 \leq q_I^{+}, q_I^{-} \leq 1$ and $q_I^{+} + q_I^{-} = 1$. For undirected tissues, we assume the initial data is symmetrical, i.e., $q_I^{+} = q_I^{-} = \frac{1}{2}$.

In this chapter, Here we consider two types of boundary conditions.

(bc1) $\Omega = \mathbb{R}$ and $p_I^{\pm}(x), q_I^{\pm}(x)$ have compact support in Ω.

(bc2) $\Omega = [-l, l]$ and zero flux boundary condition

$$j(t, \pm l) = 0, \quad \text{i.e.,} \quad p^{+}(t, \pm l) = p^{-}(t, \pm l).$$

5.1.3 Nonhomogeneous Steady State

In this section we first review some associated results from [47] and give some further discussion. We first present a second-order telegraph equation which is derived from system (5.1.8) or (5.1.9). To this end, we add and subtract the first two equations of (5.1.8) or (5.1.9) and obtain equations for the total population $p = p^{+} + p^{-}$ and the population flux $j = s(p^{+} - p^{-})$

$$\begin{aligned} p_t + j_x &= 0, \\ j_t + s^2 p_x &= -\mu j + \mu(q^{+} - q^{-}) sp. \end{aligned} \tag{5.1.14}$$

with initial conditions $p(0,x) = p_0(x)$ and $j(0,x) = j_0(x)$, where p_0 and j_0 are determined from the initial distribution of p^{+} and p^{-}. We differentiate the first equation of (5.1.14) with respect to t and the second equation with respect to x. After that, we subtract the resulting equations and end up with a damped wave equation with drift term (see [47])

$$p_{tt} + \mu p_t + \mu(s\mathbb{E}_q p)_x = s^2 p_{xx}, \tag{5.1.15}$$

where the drift velocity is given by the expectation of q denoted by $\mathbb{E}_q = q^{+} - q^{-}$. The equation (5.1.15) is a form of telegraph equation which describes electrical transmission in a telegraph cable when current leak to the ground. A drift-diffusion equation can be approximated by taking the limit $\mu \to \infty, s \to \infty$ with diffusion

constant $D \equiv s^2/\mu$ and drift velocity $s\mathbb{E}_q$. The same drift-diffusion equation also can be obtained by rescaling space and time variables appropriately as done in [47].

Suppose that the equations (5.1.14) are defined in the interval $\Omega = [-l, l]$ and satisfies the boundary condition (bc2). In terms of cell population density, the zero flux boundary condition is equivalent to $p^+(\pm l) = p^-(\pm l) = \frac{1}{2}p(\pm l)$. We want to know under what conditions, if any, these equations have time-independent, nonconstant solutions for $p^\pm$. The steady state condition $j_x = 0$ of the first equation of (5.1.14) implies that j is a constant and zero flux boundary condition $j(\pm l) = 0$ furthermore gives that $j = 0$. Consequently the second equation of (5.1.14) becomes

$$p_x = \frac{\mu}{s}(q^+ - q^-)p.$$

This is a first order equation for p whose solution can be easily found

$$p(x) = p(-l)\exp\left(\frac{\mu}{s}\int_{-l}^{x}(q^+(\xi) - q^-(\xi))d\xi\right). \tag{5.1.16}$$

The vanishing flux $j = 0$ gives that $p^+ = p^-$ and hence

$$p^\pm(x) = \frac{p(-l)}{2}\exp\left(\frac{\mu}{s}\int_{-l}^{x}(q^+(\xi) - q^-(\xi))d\xi\right). \tag{5.1.17}$$

Here the above integrals are bounded since q^+ and q^- are bounded by 1 which will be proven in section 5.3. From the above equations, one can see how the distribution of fiber orientations $q^\pm$ affect the distribution of cell population p and $p^\pm$. In particular, if $\mu \neq 0$ and $q^+ \neq q^-$, then p and $p^\pm$ are nonconstants which correspond to the nonhomogeneous steady states of the system (5.1.14).

Particulary in undirected tissues, $q^+ = q^- = \frac{1}{2}$ due to symmetry, then p and $p^\pm$ are constants and $p^+ = p^- = \frac{p(-l)}{2}$, which means that there is no aggregation of cells.

If $q^+ = 1, q^- = 0$, then

$$p^\pm(x) = \frac{p(-l)}{2}\exp\left(\frac{\mu}{s}(x + l)\right).$$

The cells accumulate at the end $x = l$. This is not unexpected since all cells bias to move to the right and eventually accumulate at the right end due to zero-flux boundary condition.

Similarly, if $q^+ = 0, q^- = 1$, then

$$p^\pm(x) = \frac{p(-l)}{2}\exp\left(-\frac{\mu}{s}(x + l)\right),$$

and $p^\pm$ attains the maximum at $x = -l$ since all cells bias to move to the left.

Therefore here we identify a mechanism which can lead to aggregation, namely, $\mu \neq 0$ and the tissue orientation of the right and the left are different.

5.2 Classification as Hyperbolic System

We show that both systems (5.1.8) and (5.1.9) are hyperbolic and we discuss shock solutions. To this end, we rewrite (5.1.8) in a matrix form

$$u_t + \Theta u_x = H(u), \tag{5.2.1}$$

where Θ and $H(u)$ is defined as follows

$$u = \begin{bmatrix} p^+ \\ p^- \\ q^+ \\ q^- \end{bmatrix}, \Theta = \begin{bmatrix} s & 0 & 0 & 0 \\ 0 & -s & 0 & 0 \\ 0 & 0 & 0 & 0 \\ 0 & 0 & 0 & 0 \end{bmatrix}, H(u) = \begin{bmatrix} -\mu p^+ + \mu q^+(p^+ + p^-) \\ -\mu p^- + \mu q^-(p^+ + p^-) \\ \kappa(p^+ - p^-)(q^- - q^+ + 1)q^+ \\ \kappa(p^+ - p^-)(q^- - q^+ - 1)q^- \end{bmatrix}.$$

The drift term is linear and hence the system (5.2.1) cannot create shock solutions. The 4×4 matrix Θ in this equation has eigenvalues $\lambda_1 = -s < 0, \lambda_2 = \lambda_3 = 0, \lambda_4 = s$, which satisfy $\lambda_1 < \lambda_2 = \lambda_3 < \lambda_4$ provided that $s > 0$. This implies system (5.2.1) and hence (5.1.8) is hyperbolic but not strictly hyperbolic. The same argument applied to system (5.1.9) shows that (5.1.9) is hyperbolic as well. The eigenvectors r_i corresponding to eigenvalues λ_i, $i = 1, 2, 3, 4$ are

$$r_1 = \begin{bmatrix} 0 \\ 1 \\ 0 \\ 0 \end{bmatrix}, r_2 = \begin{bmatrix} 0 \\ 0 \\ 1 \\ 0 \end{bmatrix}, r_3 = \begin{bmatrix} 0 \\ 0 \\ 0 \\ 1 \end{bmatrix}, r_4 = \begin{bmatrix} 1 \\ 0 \\ 0 \\ 0 \end{bmatrix}.$$

It can be verified that $\nabla\lambda_i(u) \cdot r_i(u) = 0$ for $i = 1, 2, 3, 4$, where $\nabla\lambda_i(u) \cdot r_i(u)$ means the directional derivative of the eigenvalues λ_i in the direction of the eigenfunction r_i as defined in chapter 4. Hence all characteristic field (λ_i, r_i) are linearly degenerated [15, 73]. Thus a shock which separates intersecting characteristics defining a discontinuity does not exist and however the solution might contain a contact discontinuity if data are discontinuous (see [15]).

The characteristic slopes are determined from the eigenvalues of the 4×4 matrix Θ in the equation (5.2.1) by $\frac{dx}{dt} = \lambda_i$, which is never infinite, so the line $t = 0$ is nowhere tangent to a characteristics. Therefore if initial data for p^+, p^-, q^+, q^- is given along the line $t = 0$, the resulting Cauchy problem should be well-posed for boundary condition (bc1). This is verified in the next section.

5.3 Global Existence

In this section, we will prove the global existence of solutions to initial-boundary problem for the system (5.1.8) subject to the initial condition (ic) and boundary

condition (bc1). The global existence of solutions to system (5.1.9) thus is proven as a special case of (5.1.8) for $\kappa = 0$. For bounded domain, the analysis for global existence will be much more complicated than unbounded domain and is left open to be further explored in the future. In the rest of this chapter, we will focus on unbounded domain and denote $\Omega = \mathbb{R}$ for the convenience of presentation.

The system (5.1.8) is a coupled system of two partial differential equations and two ordinary differential equations. To prove the global existence of solutions to the system (5.1.8), we first prove the nonnegativity property of solutions.

Lemma 5.3.1. *Let $p_I^{\pm} \geq 0$ and $q_I^{\pm} \geq 0$ with $q_I^+ + q_I^- = 1$. Assume that $p^{\pm}, q^{\pm} \in L^\infty(0,T;L^\infty(\Omega))$ is a solution to system (5.1.8) for some $T > 0$, then $p^{\pm} \geq 0$ and $0 \leq q^{\pm}(t,x) \leq 1$ with $q^+ + q^- = 1$.*

Proof. We first show that $q^+ + q^- = 1$. Toward this end, We first define two new quantities: $q = q^+ + q^-$, $\xi = q^+ - q^-$. Then we add and subtract the third and fourth equations of (5.1.8) to obtain equations for q and ξ as follows:

$$\begin{aligned} q_t &= -\kappa(p^+ - p^-)(q-1)\xi, \\ \xi_t &= \kappa(p^+ - p^-)(q - \xi^2), \end{aligned} \tag{5.3.1}$$

which can be rewritten as a matrix form

$$Q_t = -\kappa(p^+ - p^-)F(Q), \tag{5.3.2}$$

where

$$Q = \begin{pmatrix} q \\ \xi \end{pmatrix}, \; F(Q) = \begin{pmatrix} (q-1)\xi \\ \xi^2 - q \end{pmatrix}$$

Then the initial data of the system (5.3.1) is given by

$$q_I = q_I^+ + q_I^- = 1, \xi_I = q_I^+ - q_I^-. \tag{5.3.3}$$

It is straightforward to verify that the vector field $F(Q) \in C^1(\mathbb{R}^2)$ and hence is locally Lipschitz continuous with respect to Q for given $p^{\pm} \in L^\infty(0,T;L^\infty(\Omega))$. Then the Cauchy problem (5.3.1), (5.3.3) has a unique solution by the fundamental existence-uniqueness theorem. On the other hand, $q = 1$ is a solution of the first equation (5.3.1). Hence the system (5.3.1) and (5.3.3) has a unique solution ($q = 1, \xi$) where ξ can be determined by the equation

$$\xi_t = \kappa(q^+ - q^-)(1 - \xi^2), \; \xi_I = q_I^+ - q_I^-.$$

It is worthwhile to point out that we here provide an idea to prove that $q = 1$ and the existence (local) of q and ξ for the given $p^{\pm} \in L^{\infty}(0, T; L^{\infty}(\Omega))$ only, which will be used later in the proof for the Theorem 5.2.

We proceed to show that solutions $q^{\pm}$ preserve the positivity. Substituting $q^{-} = 1 - q^{+}$ into the third equation of (5.1.8), we have

$$q_t^+ = 2\kappa(p^+ - p^-)(1 - q^+)q^+. \tag{5.3.4}$$

There are three cases to proceed.

Case 1: $q_I^+ = 1$. Then we have that $q^+ = 1$ is a solution to equation (5.3.4) with initial condition $q_I^+ = 1$. Since the right hand side of equation (5.3.4) is locally Lipschitz continuous with respect to q^+, the solution of the equation (5.3.4) is unique. Hence $q^+(t, x) = 1$ for all t, x.

Case 2: $q_I^+ = 0$. Using the similar argument as in Case 1 we can show that $q^+(t, x) = 0$ to the equation (5.3.4).

Case 3: $0 < q_I^+ < 1$. Then integrating the above equation (5.3.4) with respect to t from 0 to t, one has

$$\frac{q^+}{1 - q^+} = \frac{q_I^+}{1 - q_I^+} \exp\left(\int_0^t 2\kappa(p^+(\tau, \cdot) - p^-(\tau, \cdot))d\tau \right).$$

Note that $0 < q_I^+ < 1$. Then one has that

$$\frac{q^+}{1 - q^+} \geq 0$$

It follows immediately from the above equality that $0 \leq q^+ \leq 1$. Combining Case 1, Case 2 and Case 3, we have that $0 \leq q^+ \leq 1$ provided that $0 \leq q_I^+ \leq 1$. Applying $q^+ = 1 - q^-$ into the fourth equation of (5.1.8) and using the same approach we can show that $0 \leq q^- \leq 1$.

Finally we come to the proof for the positivity of cell density $p^{\pm}(t, x)$. We use a theory of invariant principle in paper [46] for the hyperbolic random walk system to achieve this goal. To this end, we first write the first two equations of the system (5.1.8) in a matrix form

$$\phi_t = G\phi + B\phi + \mathcal{F}(\phi), \tag{5.3.5}$$

where

$$\phi = \begin{pmatrix} p^+ \\ p^- \end{pmatrix}, \; G := \begin{pmatrix} -s\dfrac{\partial}{\partial x} & 0 \\ 0 & s\dfrac{\partial}{\partial x} \end{pmatrix}, B = \begin{pmatrix} -\mu & \mu \\ \mu & -\mu \end{pmatrix},$$

and

$$\mathcal{F}(\phi) = \begin{pmatrix} \mu q^+(p^+ + p^-) - \mu p^- \\ \mu q^-(p^+ + p^-) - \mu p^+ \end{pmatrix}.$$

Let $\Lambda = [0, \infty) \subset \mathbb{R}$. Then Λ is closed and convex and for each $z \in \partial\Lambda$, Λ has on out normal vector. Moreover, define $\Sigma = \Lambda \times \Lambda$. Let $\phi \in \partial\Sigma$ and without loss of generality we assume that $\phi = (\vartheta, 0)$ with $\vartheta \geq 0$. Then for the out normal vector $\eta(\phi) = (0, -1)$ of ϕ, we have

$$\eta(\phi) \cdot (B\phi + \mathcal{F}(\phi)) = -\mu q^- \vartheta \leq 0,$$

where we have used the positivity of q^-. Then by the theory in [46] (Theorem 2), the set Σ is positively invariant for the system (5.3.5), which shows the positivity of $p^\pm$. The proof is completed.

□

By the Lemma 5.3.1, we obtain the following theorem.

Theorem 5.1. *The set* $\{ (p^+, p^-, q^+, q^-) \mid p^\pm \geq 0, q^\pm \geq 0, q^+ + q^- = 1\}$ *is invariant to the system* (5.1.8) *provided that* $p^\pm, q^\pm \in L^\infty(0, \infty; L^\infty(\Omega))$.

Remark 5.1. *For* $p^+ > p^-$, *the term* $p^+ - p^- > 0$ *and* q^+ *will increase while* q^- *decreases. Hence directionality is enhanced by equations* $(5.1.8)_3$ *and* $(5.1.8)_4$.

Next, we are devoted to proving the global existence of solutions to system (5.1.8). Due to the Theorem 5.1, we can reformulate the system (5.1.8) as a three dimensional system

$$\begin{aligned} p_t^+ + sp_x^+ &= -\mu p^+ + \mu q^+(p^+ + p^-), \\ p_t^- - sp_x^- &= -\mu p^- + \mu q^-(p^+ + p^-), \\ \xi_t &= \kappa(p^+ - p^-)(1 - \xi^2), \end{aligned} \tag{5.3.6}$$

where q^+ and q^- are given by

$$q^+ = \frac{1+\xi}{2}, \; q^- = \frac{1-\xi}{2}. \tag{5.3.7}$$

It is worthwhile to note that here ξ represents the expectation of fibre orientation in one dimension. We seek the global solutions of the system (5.3.6) in the following space

$$\mathbb{X}(0,T) := \{(p^+, p^-, \xi) |\; p^+, p^- \in L^\infty(\Omega_T), \xi \in C(0,T; L^\infty(\Omega))\}$$

where $\Omega_T = [0,T) \times \Omega$, $L^\infty(\Omega_T) = L^\infty(0,T; L^\infty(\Omega))$. In the following, we denote the norm $\|u(t)\|_\infty := \|u(t,\cdot)\|_{L^\infty(\Omega)}$ for $u(t,\cdot) \in L^\infty(\Omega)$ for the sake of convenience.

One of our main results is given as follows.

Theorem 5.2. *Let $p_I^{\pm}, q_I^{\pm} \geq 0$ and $q_I = q_I^+ + q_I^- = 1$. If $p_I^{\pm}, q_I^{\pm} \in L^\infty(\Omega)$, then the system (5.3.6) subject to boundary condition (bc1) admits a unique solution $(p^+, p^-, \xi) \in \mathbb{X}(0, \infty)$ such that $-1 \leq \xi(t, x) \leq 1$.*

Proof. The proof consists of five steps. In Step 1, we show for any $p^+, p^- \in L^\infty(\Omega_T)$, the solution ξ of the third equation of (5.3.6) is uniformly bounded. The existence of ξ follows the idea in the proof for the Lemma 5.3.1. In Step 2, we show that if $\xi \in L^\infty(\Omega_T)$, then the functions on the right hand side of the first and second equation of (5.3.6) are Lipschitz continuous. In Step 3, we use the ξ obtained in Step 1 and results proved in Step 2 to show that the solution of the first two equations of (5.3.6) satisfies $p^+, p^- \in L^\infty(\Omega_T)$. In Step 4, we prove the existence of local solutions with the help of contraction mapping principle. The global solutions will follow in Step 5.

Step 1. We define a vector $\varrho = (p^+, p^-)$ and denote

$$\|\varrho\|_{L^\infty(\Omega_T)} = \max\{\|p^+\|_{L^\infty(\Omega_T)}, \|p^-\|_{L^\infty(\Omega_T)}\},$$

where

$$\|p^+\|_{L^\infty(\Omega_T)} = \sup_{0\leq t\leq T} \|p^+(t)\|_\infty, \ \|p^-\|_{L^\infty(\Omega_T)} = \sup_{0\leq t\leq T} \|p^-(t)\|_\infty.$$

For a given $w = (w^+, w^-) \in L^\infty(\Omega_T) \times L^\infty(\Omega_T)$, we consider the equation for ξ

$$\xi_t = \kappa(w^+ - w^-)(1 - \xi^2). \tag{5.3.8}$$

Under the assumptions for initial data, we can use the same argument as in the proof for Lemma 5.3.1 to easily derive that $-1 \leq \xi \leq 1$. We omit details here.

Step 2. With the ξ obtained in Step 1, we consider equations

$$p_t^+ + sp_x^+ = -\mu p^+ + \frac{\mu}{2}(1+\xi)(p^+ + p^-), \tag{5.3.9}$$

$$p_t^- - sp_x^- = -\mu p^- + \frac{\mu}{2}(1-\xi)q^-(p^+ + p^-), \tag{5.3.10}$$

For the sake of presentation, we define $\eta = (p^+, p^-)$ and

$$f_1(\eta, \xi) = f_1(p^+, p^-, \xi) = -\mu p^+ + \frac{\mu}{2}(1+\xi)(p^+ + p^-),$$
$$f_2(\eta, \xi) = f_2(p^+, p^-, \xi) = -\mu p^- + \frac{\mu}{2}(1-\xi)(p^+ + p^-).$$

Then for given $\eta_1 = (p_1^+, p_1^-), \eta_2 = (p_2^+, p_2^-)$, we have that

$$f_1(\eta_1, \rho) - f_1(\eta_2, \rho) = -\frac{\mu}{2}(1-\xi)(p_1^+ - p_2^+) + \frac{\mu}{2}(1+\xi)(p_1^- - p_2^-).$$

Note that $-1 \leq \xi \leq 1$. Then it is easy to deduce that

$$\begin{aligned} |f_1(\eta_1,\rho) - f_1(\eta_2,\rho)| &\leq 2\mu \cdot \max\{|p_1^+ - p_2^+|, |p_1^- - p_2^-|\} \\ &\leq 2\mu \cdot \max|\eta_1 - \eta_2|. \end{aligned} \tag{5.3.11}$$

This implies that f_1 is Lipschitz continuous for p^+, p^- with Lipschitz constant 2μ. In a similar way, we can easily prove that f_2 is Lipschitz continuous for p^+, p^- with the same Lipschitz constant 2μ. The Lipschitz continuity of f_1 and f_2 will be used in the following step.

Step 3. It is straightforward to show that system (5.3.9) and (5.3.10) is strictly hyperbolic with two distinct uniform bounded eigenvalues λ_1, λ_2 satisfying $-s = \lambda_1 < \lambda_2 = s$. Then for each $i = 1, 2$ and each point (τ, ξ) in the $t - x$ plane, the characteristic equation of (5.3.9) and (5.3.10) defined by

$$\frac{dx}{dt} = \lambda_i, \ x(\tau) = \sigma,$$

has a unique solution defined for all $t > 0$, describing the $i - th$ characteristic through point (τ, σ). We denote such a solution by $t \mapsto \mathbf{x}_i(t;\tau,\sigma)$, where $\mathbf{x}_i(t;\tau,\sigma) = \sigma + \lambda_i(t - \tau)$. Following the argument in [15], we define

$$\mathcal{D} = \{ (t,x) \mid 0 \leq t < l/s, -l + st \leq x \leq l - st \}.$$

Note that l can be arbitrarily large since the domain is unbounded. Then for every $(\tau, \xi) \in \mathcal{D}$ and every $i \in \{1, 2\}$, the characteristic curve $\{(t, x_i(t;\tau,\sigma))| \ 0 \leq t \leq \tau\}$ is entirely contained inside $\mathcal{D}$ with $x_i(0;\tau,\sigma) \in [-l, l]$. Such a set $\mathcal{D}$ is called a domain of determinacy (see [15]).

The system (5.3.9), (5.3.10) has two independent characteristics. We integrate (5.3.9) along the second characteristic curve $\mathbf{x}_2(t;\tau,\sigma)$ and (5.3.10) along the first characteristic $\mathbf{x}_1(t;\tau,\sigma)$, (5.3.9) and (5.3.10) can be rewritten as an ODE system

$$\frac{dp^+}{dt} = -\mu p^+(t, \mathbf{x}_2(t;\tau,\sigma)) + \mu q^+(t, \mathbf{x}_2(t;\tau,\sigma))(p^+(t, \mathbf{x}_2(t;\tau,\sigma)) + p^-(t, \mathbf{x}_2(t;\tau,\sigma))) \tag{5.3.12}$$

$$\frac{dp^-}{dt} = -\mu p^+(t, \mathbf{x}_1(t;\tau,\sigma)) + \mu q^-(t, \mathbf{x}_1(t;\tau,\sigma))(p^+(t, \mathbf{x}_1(t;\tau,\sigma)) + p^-(t, \mathbf{x}_1(t;\tau,\sigma))) \tag{5.3.13}$$

For each $(\tau, \sigma) \in \mathcal{D}$ and $x_i(0;\tau,\sigma) \in [-l, l]$, we integrate (5.3.12) and (5.3.13) with respect to t over $[0, t]$ to obtain that

$$\begin{aligned} p^+(\tau,\sigma\ \ ) = \ & p^+(\mathbf{x}_2(0;\tau,\sigma)) + \\ & \int_0^\tau f_1\big(p^+(t, \mathbf{x}_2(t;\tau,\sigma)), p^-(t, \mathbf{x}_2(t;\tau,\sigma)), \xi(t, \mathbf{x}_2(t;\tau,\sigma))\big)dt. \end{aligned} \tag{5.3.14}$$

and

$$p^-(\tau,\sigma) = p^-(\mathbf{x}_1(0;\tau,\sigma))+ \int_0^\tau f_2\big(p^+(t,\mathbf{x}_1(t;\tau,\sigma)),p^-(t,\mathbf{x}_1(t;\tau,\sigma)),\xi(t,\mathbf{x}_1(t;\tau,\sigma))\big)dt. \quad (5.3.15)$$

Note that in the following, we call (p^+,p^-) a broad solution (see [15]) from the domain of determinacy $\mathcal{D}$ into $\mathbb{R}^2$ for Cauchy problem (5.3.9) and (5.3.10) if p^+ and p^- satisfy (5.3.14) and (5.3.15), respectively, at almost every point $(\tau,\xi) \in \mathcal{D}$. Taking L^∞-norm on both sides of (5.3.14) and (5.3.15), using the fact that f_i is Lipschitz continuous with Lipschitz constant 2μ proven in Step 2, and using $f_i(0,0,\xi) = 0$ for $i = 1,2$ and $\eta_2 = (0,0)$ in (5.3.11), we have that

$$\|p^+(\tau)\|_\infty \le C + 2\mu \int_0^\tau \|\eta(t)\|_\infty dt,$$

and

$$\|p^-(\tau)\|_\infty \le C + 2\mu \int_0^\tau \|\eta(t)\|_\infty dt,$$

where C is a constant such that $\|p_I^\pm\|_\infty \le C$.

Hence

$$\|p^+(\tau)\|_\infty + \|p^-(\tau)\|_\infty \le 2C + 4\mu \int_0^\tau (\|p^+(t)\|_\infty + \|p^-(t)\|_\infty)dt.$$

The application of Gronwall's inequality to the above inequality gives us that

$$\|p^+(\tau)\|_\infty + \|p^-(\tau)\|_\infty \le 2Ce^{4\mu\tau},$$

which implies for any τ with $0 \le \tau \le T$, $p^\pm$ is bounded.

Step 4. In step 1, for every $w = (w^+,w^-) \in L^\infty(\Omega_T) \times L^\infty(\Omega_T)$, we obtain a solution ξ of equation (5.3.8) satisfying $-1 \le \xi \le 1$. Then we can define a mapping $H_1 : L^\infty(\Omega_T) \to L^\infty(\Omega_T)$ by $H_1 w = \xi$. Let $m > 1$, then H_1 maps from $\mathbb{B}_m(0)$ to $\mathbb{B}_1(0)$

$$H_1 : \mathbb{B}_m(0) \to \mathbb{B}_1(0),$$

where

$$\mathbb{B}_m(0) = \{\phi = (\phi_1,\phi_2) \in L^\infty(\Omega_T) \times L^\infty(\Omega_T) |\ \|\phi\|_{L^\infty} < m, \phi(0) = (p_I^+,p_I^-)\}.$$

In step 3, we prove that for every ξ with $-1 \le \xi \le 1$ obtained in Step 1, the solution $\eta = (p^+,p^-)$ of (5.3.9) and (5.3.10) satisfies $\|\eta(t)\|_\infty \le 2Ce^{\mu t}$. So for any $0 \le t \le T$, the solution η is bounded. Then we can define another mapping $H_2 : L^\infty(\Omega_T) \to L^\infty(\Omega_T)$ by $H_2\xi = \eta$. Hence for same m as above, it holds that

$$H_2 : \mathbb{B}_1(0) \to \mathbb{B}_m(0).$$

We now define a composite mapping: $H = H_2 \circ H_1 : \mathbb{B}_m(0) \to \mathbb{B}_m(0)$. Then we have $H(w) = \eta$. We want to show that $w = \eta$. To this end, we only need to show that H is a contraction on $\mathbb{B}_m(0)$ for some $T \geq 0$. We consider two functions $w_1, w_2 \in \mathbb{B}_m(0)$ and denote the images by $Hw_1 = u, Hw_2 = U$, respectively, where $w_1 = (w_1^+, w_1^-)$ and $w_2 = (w_2^+, w_2^-)$. The corresponding solutions of equation (5.3.8) are denoted by ξ_1 and ξ_2, i.e., $\xi_1 = H_1 w_1, \xi_2 = H_1 w_2$. We denote

$$u - U = \begin{pmatrix} u_1 - U_1 \\ u_2 - U_2, \end{pmatrix}$$

where $u_1 = H(w_1^+), u_2 = H(w_1^-), U_1 = H(w_2^+)$ and $U_2 = H(w_2^-)$. Then from the analysis in Step 3, along the characteristic curves, we have that

$$\begin{aligned} u_1 - U_1 &= \int_0^\tau f_1(w_1^+(t,\mathbf{x}_2), w_1^-(t,\mathbf{x}_2), \xi_1) - f_1(w_2^+(t,\mathbf{x}_2), w_2^-(t,\mathbf{x}_2), \xi_2) dt \\ &= \int_0^\tau \Big(-\frac{\mu}{2}(1-\xi)(w_1^+(t,\mathbf{x}_2) - w_2^+(t,\mathbf{x}_2)) \\ &\qquad + \frac{\mu}{2}(1+\xi)(w_1^-(t,\mathbf{x}_2) - w_2^-(t,\mathbf{x}_2)) \Big) dt, \end{aligned}$$

as well as

$$\begin{aligned} u_2 - U_2 &= \int_0^\tau f_2(w_1^+(t,\mathbf{x}_1), w_1^-(t,\mathbf{x}_1), \xi_1) - f_2(w_2^+(t,\mathbf{x}_1), w_2^-(t,\mathbf{x}_1), \xi_2) dt \\ &= \int_0^\tau \Big(-\frac{\mu}{2}(1+\xi)(w_1^+(t,\mathbf{x}_1) - w_2^+(t,\mathbf{x}_1)) \\ &\qquad + \frac{\mu}{2}(1-\xi)(w_1^-(t,\mathbf{x}_1) - w_2^-(t,\mathbf{x}_1)) \Big) dt, \end{aligned}$$

where $\mathbf{x}_i = \mathbf{x}_i(t;\tau,\sigma)$, $i = 1, 2$.

Using the result $-1 \leq \xi_i \leq 1$ for $i = 1, 2$, we derive from the above two inequalities for any $0 < \tau \leq T$ that

$$\begin{aligned} \|u - U\|_\infty = \|Hw_1 - Hw_2\|_\infty &\leq \mu \int_0^\tau (\|w_1^+ - w_2^+\|_\infty + \|w_1^- - w_2^-\|_\infty dt \\ &\leq 2\mu T \sup_{0 \leq t \leq T} \|w_1 - w_2\|_\infty. \end{aligned}$$

Let T be small, then H is a contraction mapping on $\mathbb{B}_m(0)$. Due to the contraction mapping principle, there exists a unique fixed point of H which corresponds a unique solution $(p^+, p^-, \xi) \in \mathbb{X}(0,T)$ such that $p^\pm, \xi \in L^\infty(\Omega_T)$. From the third equation of (5.3.8), it is easy to see that $\xi_t \in L^\infty(\Omega_T)$. Due to the standard regularity results (see [107]), it follows that $\xi \in C(0, T_{\max}; L^\infty(\Omega))$.

Step 5. We have shown that system (5.3.6) has a unique local solution $(p^+, p^-, \xi) \in \mathbb{X}(0,T)$. Now we suppose that the maximal time of existence for solution of (5.3.6) is $T_{\max}$ and $T_{\max} < \infty$. From the step 1, we know that $-1 \le \xi \le 1$ for any t with $0 \le t < T_{\max}$. Hence according to the well known alternative results (for example, see [79, 107]), one has that

$$\lim_{t \to T_{\max}} \|p^+(t)\|_\infty = \infty \quad \text{or} \quad \lim_{t \to T_{\max}} \|p^-(t)\|_\infty = \infty. \tag{5.3.16}$$

On the other hand, when $-1 \le \xi \le 1$, we have proven in Step 2 and Step 3, that for any $T \ge 0$, it holds that

$$\|p^+(t)\|_\infty + \|p^-(t)\|_\infty \le 2Ce^{4\mu T}, \quad 0 \le t \le T,$$

which is obviously contradictive to (5.3.16). This contradiction, in turn confirms that $T_{\max} = \infty$ and hence a global solution follows.

□

Next, we additionally assume that $p_I^\pm \in L^1(\Omega)$, and show the global existence of solutions in the following space

$$\mathbb{M}(0,T) := \{(p^+, p^-, \xi) |\ p^+, p^- \in L^\infty(0,T; L^1 \cap L^\infty(\Omega)), \xi \in C(0,T; L^\infty(\Omega))\}$$

The result is given in the following theorem.

Theorem 5.3. *Let $p_I^\pm \in L^1 \cap L^\infty(\Omega)$ and assumptions in Theorem 5.2 hold. Then the system (5.3.6) has a unique global solution $(p^+, p^-, \xi) \in \mathbb{M}(0,\infty)$.*

Proof. By Theorem 5.2, we only need to show that $(p^+, p^-, \xi) \in L^\infty(0,\infty; L^1(\Omega))$. The local well-posedness result can ba obtained by using a similar as above and we skip the details. It only remains to derive a L^1 global bound for $p^\pm$. From Theorem 5.2, it is known that $(p^+, p^-, \xi) \in L^\infty(0,\infty; L^\infty(\Omega))$ and $-1 \le \xi \le 1$. Then we take L^1-norm of $(5.3.6)_1$ and $(5.3.6)_2$ along the characteristic curves to deduce that

$$\|p^+(\tau,\cdot)\|_{L^1} \le \|p_0^+(\cdot)\|_{L^1} + 2\mu \int_0^\tau \big(\|p^+(t,\cdot)\|_{L^1} + \|p^-(t,\cdot)\|_{L^1}\big) dt \tag{5.3.17}$$

and

$$\|p^-(\tau,\cdot)\|_{L^1} \le \|p_0^-(\cdot)\|_{L^1} + 2\mu \int_0^\tau \big(\|p^+(t,\cdot)\|_{L^1} + \|p^-(t,\cdot)\|_{L^1}\big) dt. \tag{5.3.18}$$

The addition of (5.3.17) and (5.3.18) gives us that

$$\|p^+(\tau,\cdot)\|_{L^1} + \|p^-(\tau,\cdot)\|_{L^1} \le 2M + 4\mu \int_0^\tau \big(\|p^+(t,\cdot)\|_{L^1} + \|p^-(t,\cdot)\|_{L^1}\big) dt, \tag{5.3.19}$$

where M is a constant such that $\|p_I^{\pm}\|_{L^1} \leq M$.

Applying Grownwall's inequality to (5.3.19), we obtain for each $t \geq 0$

$$|p^+(\tau,\cdot)\|_{L^1} + \|p^-(\tau,\cdot)\|_{L^1} \leq 2Me^{4\mu t}, \tag{5.3.20}$$

which gives the existence of global solutions in $L^\infty(0,\infty;L^1(\Omega))$ for $p^{\pm}$. The proof is finished.

□

Coming back to the original system (5.1.8), we thus have the following global existence result for the system (5.1.8).

Theorem 5.4. *Let $q_I^{\pm}(x) \geq 0$ and $q_I^+ + q_I^- = 1$. Assume $p_I^{\pm} \in L^1 \cap L^\infty(\Omega)$. Then there exists a unique solution to the system (5.1.8) such that $q^{\pm} \geq 0$, $q^+ + q^- = 1$ and $p^{\pm} \in L^\infty(0,\infty;L^1 \cap L^\infty(\Omega))$.*

When cutting efficiency $\kappa = 0$, the system (5.1.8) becomes system (5.1.9). Hence the global existence of solutions to (5.1.9) automatically is obtained. Due to the assumption $q^+(t,x) = q^-(t,x)$ for undirected tissues, we obtain the following global theorem for system (5.1.9).

Theorem 5.5. *Let $q_I^{\pm}(x) \geq 0$ and $q_I^+ = q_I^- = 1/2$. Assume $p_I^{\pm} \in L^1 \cap L^\infty(\Omega)$. Then there exists a unique solution to system (5.1.9) such that $p^{\pm} \in L^\infty(0,\infty;L^1 \cap L^\infty(\Omega))$ and $q^+ = q^- = \frac{1}{2}$.*

Since the functions on the right hand side of (5.1.8) are continuously differentiable with respect to p^+, p^-, q^+ and q^-, by a theory for semilinear hyperbolic system in [15] (see Theorem 3.6 in [15]), the broad solution of Cauchy problem (5.1.8) obtained in Theorem 5.4 is indeed a classical solution provided that the initial data (5.1.13) is continuously differentiable. This result is precisely given in the following theorem.

Theorem 5.6. *Let the assumptions in Theorem 5.4 or 5.5 hold. In addition, we assume that the initial data in (5.1.13) are continuously differentiable. Then the broad solution $u : \mathcal{D} \to \mathbb{R}^2$ obtained in Theorem 5.4 or 5.5 provides a classical solution. Moreover, if initial data in (5.1.13) are nonnegative, the solution is nonnegative. Its partial derivatives u_t, u_x are broad solutions of the following semilinear system, respectively,*

$$(u_t)_t = H_u u_t - \Theta \cdot (u_t)_x,$$
$$(u_x)_t = H_u u_x - \Theta \cdot (u_x)_x,$$

where H_u denotes the derivative of H with respect to u.

Proof. The proof is similar to the argument in [15]. We omit the details.

□

5.4 *Macroscopic Limits*

For the given fibre distribution $q^{\pm}(t,x)$, formal parabolic and hydrodynamic limits were derived in [47] for the mesenchymal motion models (5.1.8) and (5.1.9) for $n(n \geq 1)$ dimensions. Here we carry out the macroscopic limits for system (5.1.8) and (5.1.9) coupled to equations for fibre distribution $q^{\pm}(t,x)$ using the argument similar as in paper [64] and prove the existence of weak limits of solutions to rescaled equations. As before, we consider the system (5.1.8) only and the corresponding results can be taken over to (5.1.9) equally.

To see which scales should be chosen to give rise to appropriate macroscopic limits, we depart with non-dimensionalization of system (5.1.3) and (5.1.4) by choosing a reference time t_*, length x_*. Dimensionless quantities are determined according to

$$x = x_*\bar{x},\ t = t_*\bar{t},\ v = v_*\bar{v},\ \omega = \omega_*\bar{\omega},$$

$$p(t,x,v) = p_*\bar{p}\left(\frac{t}{t_*},\frac{x}{x_*},\frac{v}{v_*}\right),\ q(t,x,\theta) = \bar{q}\left(\frac{t}{t_*},\frac{x}{x_*},\theta,\right),$$

$$\Pi(t,x,\theta) = \Pi_*\overline{\Pi}\left(\frac{t}{t_*},\frac{x}{x_*},\theta\right),\ A_u(t,x) = A_*\bar{A}_u\left(\frac{t}{t_*},\frac{x}{x_*}\right),\ \rho(t,x) = \rho_*\bar{\rho}\left(\frac{t}{t_*},\frac{x}{x_*}\right),$$

where v_* is a typical speed for velocities in V. Both quantities are assumed to be bounded.

We now choose other reference quantities such that

$$\Pi_* = v_*,\ \rho_* = \frac{1}{t_*\Pi_*},\ p_* = \frac{\rho_*}{v_*^n},\ \omega_* = v_*^n,$$

where n is the dimension of set V.

Define a parameter $\varepsilon = \frac{v_*}{x_*}$. If we fix the length scale such that $t_* = (\frac{v_*}{x_*})^2$, then we obtain a parabolic scaling and can rewrite the system (5.1.3), (5.1.4) as follows after substituting above transformation into (5.1.3), (5.1.4) and dropping the bar

$$\begin{aligned} \varepsilon^2\frac{\partial p}{\partial t} + \varepsilon v\frac{\partial p}{\partial x} &= -\mu p + \mu\rho\frac{q}{\omega}, \\ \frac{\partial q}{\partial t} &= \kappa(\Pi_u - A_u)\rho q. \end{aligned} \tag{5.4.1}$$

However, if we fix the length scale such that $t_* = \frac{x_*}{v_*}$, we obtain a hyperbolic scaling and derive the following nondimensional version of (5.1.3), (5.1.4)

$$\begin{aligned} \varepsilon\frac{\partial p}{\partial t} + \varepsilon v\frac{\partial p}{\partial x} &= -\mu p + \mu\rho\frac{q}{\omega}, \\ \frac{\partial q}{\partial t} &= \kappa(\Pi_u - A_u)\rho q. \end{aligned} \tag{5.4.2}$$

Our main scaling assumption in this section is the smallness of the dimensionless parameter ε. In the following, we will present a derivation of parabolic and hyperbolic limits for one dimensional version of the above systems (5.4.1) and (5.4.2) by the regular perturbation methods.

5.4.1 Parabolic Limit

From the system (5.4.1), we know that the parabolic scaling leads to the following one dimensional model with initial data

$$\begin{aligned}
\varepsilon^2\frac{\partial p_\varepsilon^+}{\partial t}+\varepsilon s\frac{\partial p_\varepsilon^+}{\partial x} &= -\mu p_\varepsilon^+ + \mu q_\varepsilon^+(p_\varepsilon^+ + p_\varepsilon^-), && (5.4.3)\\
\varepsilon^2\frac{\partial p_\varepsilon^-}{\partial t}-\varepsilon s\frac{\partial p_\varepsilon^+}{\partial x} &= -\mu p_\varepsilon^- + \mu q_\varepsilon^-(p_\varepsilon^+ + p_\varepsilon^-), && (5.4.4)\\
\frac{\partial \xi_\varepsilon}{\partial t} &= \kappa(p_\varepsilon^+ - p_\varepsilon^-)(1-\xi_\varepsilon^2), && (5.4.5)\\
q_\varepsilon(0,\cdot) &= q_I(\cdot) = 1, \xi_\varepsilon(0,\cdot) = q_I^+ - q_I^-, && (5.4.6)
\end{aligned}$$

where

$$q_\varepsilon^+ = \frac{1+\xi_\varepsilon}{2},\ q_\varepsilon^- = \frac{1-\xi_\varepsilon}{2}.$$

Note that the global existence of solutions to the above system has been established in section 5.3 for each $\varepsilon > 0$ and furthermore it holds that

$$0 \le q_\varepsilon^+, q_\varepsilon^- \le 1, -1 \le \xi_\varepsilon \le 1. \tag{5.4.7}$$

Using (5.4.7) and denoting $J_\varepsilon = p_\varepsilon^+ - p_\varepsilon^-$, we obtain by adding and subtracting (5.4.4) from (5.4.3)

$$\begin{aligned}
\varepsilon^2\frac{\partial p_\varepsilon}{\partial t}+\varepsilon s\frac{\partial J_\varepsilon}{\partial x} &= 0, && (5.4.8)\\
\varepsilon^2\frac{\partial J_\varepsilon}{\partial t}+\varepsilon s\frac{\partial p_\varepsilon}{\partial x} &= \mu\xi_\varepsilon p_\varepsilon - \mu J_\varepsilon, && (5.4.9)
\end{aligned}$$

where $\xi_\varepsilon = q_\varepsilon^+ - q_\varepsilon^-$. We define the following expansions

$$\begin{aligned}
p_\varepsilon &= p_0 + \varepsilon p_1 + O(\varepsilon^2),\\
J_\varepsilon &= J_0 + \varepsilon J_1 + \varepsilon^2 J_2 + O(\varepsilon^3),\\
q_\varepsilon^+ &= q_0^+ + \varepsilon q_1^+ + \varepsilon^2 q_2^+ + O(\varepsilon^3),\\
q_\varepsilon^- &= q_0^- + \varepsilon q_1^- + \varepsilon^2 q_2^- + O(\varepsilon^3),\\
\xi_\varepsilon &= \xi_0 + \varepsilon\xi_1 + \varepsilon^2\xi_2 + O(\varepsilon^3),
\end{aligned} \tag{5.4.10}$$

where $\xi_0 = q_0^+ - q_0^-, \xi_1 = q_1^+ - q_1^-, \xi_2 = q_2^+ - q_2^-$. Our aim is to derive equations for the leading order terms of expansion (5.4.10). To proceed, we make an assumptions on the fibre networks distribution $q^\pm(t,x)$.

Assumption 5.1. *The leading order terms $q_0^{\pm}$ are balanced and strictly positive, i.e.,*

$$q_0^+ = q_0^- > C_0 > 0,$$

where C_0 is a positive constant.

Next, we derive the equation for the leading order term p_0. Toward this end, we substitute (5.4.10) into (5.4.8), (5.4.9) and compare terms of equal order in ε to obtain

$$\varepsilon^0 \ : \ \begin{cases} 0 = 0, \\ 0 = \mu\xi_0 p_0 - \mu J_0. \end{cases} \tag{5.4.11}$$

$$\varepsilon^1 \ : \ \begin{cases} 0 = s\frac{\partial J_0}{\partial x}, \\ s\frac{\partial p_0}{\partial x} = \mu\xi_0 p_1 + \mu\xi_1 p_0 - \mu J_1. \end{cases} \tag{5.4.12}$$

$$\varepsilon^2 \ : \ \begin{cases} \frac{\partial p_0}{\partial t} + s\frac{\partial J_1}{\partial x} = 0, \\ \frac{\partial J_0}{\partial t} + s\frac{\partial p_1}{\partial x} = \mu\xi_1 p_1 + \mu\xi_0 p_2 + \mu\xi_2 p_0 - \mu J_2. \end{cases} \tag{5.4.13}$$

By the assumption 5.1, one has $\xi_0 = 0$. Then from the second equation of (5.4.11), we have

$$p_0\xi_0 - J_0 = 0.$$

Hence $J_0 = 0$ due to $\xi_0 = 0$. This is consistent with the first equation of (5.4.12). Furthermore, we have from the second equation of (5.4.12) that

$$J_1 = \xi_1 p_0 - \frac{s}{\mu}\frac{\partial p_0}{\partial x}, \tag{5.4.14}$$

where we again use $\xi_0 = 0$. By the second equation of (5.4.13), it holds that

$$J_2 \ = \ \xi_1 p_1 + \xi_2 p_0 - \frac{s}{\mu}\frac{\partial p_1}{\partial x}. \tag{5.4.15}$$

Now we substitute (5.4.14) into the first equation of (5.4.13) to derive an equation for the leading order term p_0

$$\frac{\partial p_0}{\partial t} + s\frac{\partial(\xi_1 p_0)}{\partial x} = \frac{s^2}{\mu}\frac{\partial^2 p_0}{\partial x^2}. \tag{5.4.16}$$

This equation compares to the formulation given in paper [47] with an equation for ξ_1 obtained from the equation (5.4.5) and (5.4.14)

$$\frac{\partial \xi_1}{\partial t} = \kappa p_0 \xi_1 - \frac{\kappa s}{\mu}\frac{\partial p_0}{\partial x}.$$

The formal limits of (5.4.8) is (5.4.16). Now we are in a position to prove the convergence of the solution p_ε and J_ε as $\varepsilon \to 0$. It suffices to derive a uniform estimates for the solutions of system (5.4.8) and (5.4.9), which is given in the following Lemma.

Lemma 5.4.1. *Assume $p_0 \in L^1 \cap L^2(\Omega)$. Let the assumption 5.1 hold. Assume further that there exists a constant $C_1 > 0$, independent of ε, such that*

$$|\xi_\varepsilon| \le C_1 \varepsilon. \tag{5.4.17}$$

Then the solution $(p_\varepsilon, q_\varepsilon)$ of system (5.4.3)-(5.4.6) satisfies, uniformly in ε, that

$$p_\varepsilon \in L^\infty_{\text{loc}}(0,\infty; L^1 \cap L^2(\Omega)),$$
$$\xi_\varepsilon \in C([0,\infty) \times L^\infty(\Omega)).$$

Proof. We use the energy methods to prove the Lemma. Multiplying the equation (5.4.8) by p_ε and the equation (5.4.9) by J_ε, adding the resultant equations and integrating it over $[0,t) \times \mathbb{R}$, we end up with the following equality

$$\begin{aligned} &\frac{1}{2}\int_\Omega (|p_\varepsilon|^2 + |J_\varepsilon|^2)dx + \int_0^t \int_\Omega \mu\varepsilon^{-2}|J_\varepsilon|^2 dx d\tau \\ &\quad = \frac{1}{2}\int_\Omega (|p_0|^2 + |J_0|^2)dx + \int_0^t \int_\Omega \mu\varepsilon^{-2}\xi_\varepsilon p_\varepsilon J_\varepsilon dx d\tau \\ &\quad \le \frac{1}{2}\int_\Omega (|p_0|^2 + |J_0|^2)dx + \int_0^t \int_\Omega \mu C_1 |\varepsilon^{-1} p_\varepsilon J_\varepsilon| dx d\tau, \end{aligned} \tag{5.4.18}$$

where we have used the assumption (5.4.17). Applying Young's inequality $|C_1\varepsilon^{-1}p_\varepsilon J_\varepsilon| \le \frac{1}{2}(\varepsilon^{-2}|J_\varepsilon|^2 + C_1^2|p_\varepsilon|^2)$ in (5.4.18), we have

$$\begin{aligned} &\int_\Omega (|p_\varepsilon|^2 + |J_\varepsilon|^2)dx + \int_0^t \int_\Omega \mu\varepsilon^{-2}|J_\varepsilon|^2 dx d\tau \\ &\quad \le \int_\Omega (|p_0|^2 + |J_0|^2)dx + \mu C_1^2 \int_0^t \int_\Omega |p_\varepsilon|^2 dx d\tau. \end{aligned} \tag{5.4.19}$$

By Grownwall's inequality, we get a L^2-estimate of p_ε and J_ε independent of ε from the above estimate. Hence we obtain L^2-bounds of $p_\varepsilon^\pm$ also independent of ε since $0 \le p_\varepsilon^\pm \le p_\varepsilon$. Due to the boundary assumptions (bc1) or (bc2), it is easy to see from (5.4.8) that mass of p_ε conserves, i.e., $\|p_\varepsilon(t)\|_{L^1} = \|p_0\|_{L^1}$. Then the first assertion of Lemma 5.4.1 is proved.

The boundedness of ξ_ε is clear since we can use the same argument as in the previous section to show that $-1 \le \xi_\varepsilon \le 1$. Then the proof of Lemma 5.4.1 is finished.

□

The following theorem gives the convergence of solutions of the system (5.4.3)-(5.4.6) as $\varepsilon \to 0$.

Theorem 5.7. *Let the assumptions in Lemma 5.4.1 hold. Then the solution $(p_\varepsilon, q_\varepsilon)$ of system (5.4.3)-(5.4.6) satisfies, after extracting an appropriate subsequences, uniformly in ε,*

$$p_\varepsilon \to P_0, \quad \text{weakly in } L^\infty_{\text{loc}}(0,\infty; L^1 \cap L^2(\Omega)),$$

$$J_\varepsilon \to \tilde{J}_0, \quad \text{weakly in } L^\infty_{\text{loc}}(0,\infty; L^2(\Omega)),$$

$$\left(\xi_\varepsilon, \frac{\partial \Xi_\varepsilon}{\partial t}\right) \to \left(\Xi_0, \frac{\partial \Xi_0}{\partial t}\right), \quad \text{weak}^* \text{ in } C([0,\infty) \times L^\infty(\Omega)).$$

Proof. The mass conservation and uniform boundedness of the L^2-norm of p_ε confirms the weak convergence of p_ε to P_0 by the compactness theorem. The second assertion is confirmed directly by the fact that $-1 \le \xi_\varepsilon \le 1$.

□

Remark 5.2. *The theorem 5.4.1 only gives the weak convergence of the solution of the system (5.4.8) and (5.4.9). We did not show that the limit P_0 satisfies the limit equation (5.4.16). So the rigorous proof of convergence of limit P_0 to the solution of limit equation is still open. The uniform estimates for higher order derivative of p_ε are needed for convergence. We leave this to be done in the future.*

5.4.2 Hyperbolic Limit

The hyperbolic scaled system (5.4.2) in one dimension is as follows

$$\varepsilon \frac{\partial p_\varepsilon^+}{\partial t} + \varepsilon s \frac{\partial p_\varepsilon^+}{\partial x} = -\mu p_\varepsilon^+ + \mu q_\varepsilon^+ (p_\varepsilon^+ + p_\varepsilon^-), \tag{5.4.20}$$

$$\varepsilon \frac{\partial p_\varepsilon^-}{\partial t} - \varepsilon s \frac{\partial p_\varepsilon^+}{\partial x} = -\mu p_\varepsilon^- + \mu q_\varepsilon^- (p_\varepsilon^+ + p_\varepsilon^-), \tag{5.4.21}$$

$$\frac{\partial \xi_\varepsilon}{\partial t} = \kappa (p_\varepsilon^+ - p_\varepsilon^-)(1 - \xi_\varepsilon^2), \tag{5.4.22}$$

$$p_\varepsilon(0,\cdot) = p_I(\cdot),\ \xi_\varepsilon(0,\cdot) = q_I^+ - q_I^- \tag{5.4.23}$$

where $q_\varepsilon^+ = \frac{q_\varepsilon + \xi_\varepsilon}{2}$, $q_\varepsilon^- = \frac{q_\varepsilon - \xi_\varepsilon}{2}$, as usual. Then we get the following equations for $p_\varepsilon = p_\varepsilon^+ + p_\varepsilon^+$, $J_\varepsilon = p_\varepsilon^+ - p_\varepsilon^+$, and $\xi_\varepsilon \doteq q_\varepsilon^+ - q_\varepsilon^+$

$$\varepsilon \frac{\partial p_\varepsilon}{\partial t} + \varepsilon s \frac{\partial J_\varepsilon}{\partial x} = 0, \tag{5.4.24}$$

$$\varepsilon \frac{\partial J_\varepsilon}{\partial t} + \varepsilon s \frac{\partial p_\varepsilon}{\partial x} = \mu \xi_\varepsilon p_\varepsilon - \mu J_\varepsilon, \tag{5.4.25}$$

To derive the macroscopic limits, we define, as before, the asymptotic expansion $p_\varepsilon = p_0 + \varepsilon p_1 + O(\varepsilon^2), J_\varepsilon = J_0 + \varepsilon J_1 + O(\varepsilon^2), q_\varepsilon^+ = q_0^+ + \varepsilon q_1^+, q_\varepsilon^- = q_0^- + \varepsilon q_1^-$. This definition gives that $\xi_\varepsilon = \xi_0 + \varepsilon\xi_1$, where $q_0 = q_0^+ + q_0^-, q_1 = q_1^+ + q_1^-, \xi_0 = q_0^+ - q_0^-, \xi_1 = q_1^+ - q_1^-$. Next we derive the equations for the leading order terms of p_ε and J_ε. For this purpose, we substitute these expansions into (5.4.24) and (5.4.25) and equate coefficients of the terms of equal order in ε , and obtain

$$\varepsilon^0 \ : \ \begin{cases} 0 = 0, \\ 0 = \mu\xi_0 p_0 - \mu J_0. \end{cases} \tag{5.4.26}$$

$$\varepsilon^1 \ : \ \begin{cases} \frac{\partial p_0}{\partial t} + s\frac{\partial J_0}{\partial x} = 0, \\ \frac{\partial J_0}{\partial t} + s\frac{\partial p_0}{\partial x} = \mu\xi_0 p_1 + \mu\xi_1 p_0 - \mu J_1. \end{cases} \tag{5.4.27}$$

From the second equation of (5.4.26), one has that $J_0 = \xi_0 p_0$. Substituting this into the first equation of (5.4.27), we obtain the equation for the leading order term p_0

$$\frac{\partial p_0}{\partial t} + s\frac{\partial(\xi_0 p_0)}{\partial x} = 0, \tag{5.4.28}$$

which is the formal limit equation for q_ε and is comparable to the equation derived in paper [47] with an equation for ξ_0 as follows

$$\frac{\partial \xi_0}{\partial t} = \kappa\xi_0(1 - \xi_0^2)p_0,$$

which can be obtained from the equation (5.4.22).

The following Lemma gives the uniform boundedness of the solutions $p_\varepsilon, J_\varepsilon$ and ξ_ε for the system (5.4.24) and (5.4.25).

Lemma 5.4.2. *Assume that there exists a constant $\overline{C_1} > 0$, independent of ε, such that*

$$|\xi_\varepsilon|^2 \le \overline{C_1}\varepsilon. \tag{5.4.29}$$

If $p_0 \in L^1 \cap L^2(\Omega)$, then the solution $(p_\varepsilon, q_\varepsilon)$ of system (5.4.20)-(5.4.23) satisfies, uniformly in ε, that

$$\begin{aligned} p_\varepsilon &\in L^\infty_{\text{loc}}(0,\infty; L^1 \cap L^2(\Omega)), \\ J_\varepsilon &\in L^\infty_{\text{loc}}(0,\infty; L^2(\Omega)), \\ \xi_\varepsilon &\in C([0,\infty) \times L^\infty(\Omega)). \end{aligned}$$

Proof. The proof is the same as the proof of Lemma 5.4.1 and hence we skip the details. The only difference is that we have different smallness assumptions for ξ_ε. □

Applying the Lemma 5.4.2, we have the following compactness results.

Theorem 5.8. *Let the assumptions in Lemma 5.4.2 hold. Then the solution $(p_\varepsilon, q_\varepsilon)$ of system (5.4.20)-(5.4.23) satisfies, up to an appropriate subsequences*

$$p_\varepsilon \to P_0, \quad \text{weakly in } L^\infty_{\text{loc}}(0,\infty; L^1 \cap L^2(\Omega)),$$

$$J_\varepsilon \to \tilde{J}_0, \quad \text{weakly in } L^\infty_{\text{loc}}(0,\infty; L^2(\Omega)),$$

$$\left(\xi_\varepsilon, \frac{\partial \Xi_\varepsilon}{\partial t}\right) \to \left(\Xi_0, \frac{\partial \Xi_0}{\partial t}\right), \quad \text{weak}^* \text{ in } C([0,\infty) \times L^\infty(\Omega)).$$

Proof. The proof is the same as the proof of Theorem 5.7 and hence the details are omitted.

□

Remark 5.3. *As we mention for parabolic limits in Remark 5.2, here we only get the weak limits for solutions of the system (5.4.24) and (5.4.25). We still need to prove that the limit P_0 satisfies the limit equation (5.4.28), which is left for future research.*

5.5 Traveling Wave

Since the system (5.1.8) models the invasion of cells through tissues, it is of interest to look for the traveling wave solutions for (5.1.8) and see what kinds of movement patterns are used by individual cells for invasion. To this end, we first use the invariant motion $q^+ + q^- = 1$ to rewrite system (5.1.8) as follows

$$\begin{aligned} p_t + j_x &= 0, \\ j_t + s^2 p_x &= -\mu j + \mu s(2q^+ - 1)p, \\ q^+_t &= \frac{2\kappa}{s} j(1-q^+)q^+, \end{aligned} \tag{5.5.1}$$

where $p = p^+ + p^-, j = s(p^+ - p^-)$, as usual.

We introduce the wave variable

$$z = x - ct,$$

where $c \geq 0$ denotes the wave speed. Then we can define the wave profile by

$$\begin{aligned} p(z) &= p(t,x) = p(x-ct), \\ j(z) &= j(t,x) = j(x-ct), \\ q^+(z) &= q^+(t,x) = q^+(x-ct). \end{aligned} \tag{5.5.2}$$

Substituting (5.5.2) into (5.5.1), we convert (5.5.1) into an ODE system

$$\begin{aligned} -cp_z + j_z &= 0, \\ -cj_z + s^2 p_z &= -\mu j + \mu s(2q^+ - 1)p, \\ -cq_z^+ &= \frac{2\kappa}{s} j(1-q^+)q^+. \end{aligned} \tag{5.5.3}$$

We assume the traveling wave ansatz

$$p(-\infty) = p(+\infty) = 0,\ q^+(-\infty) = q_l^+,\ q^+(+\infty) = q_r^+, \tag{5.5.4}$$

where q_l^+ and q_r^+ are constants and satisfy $0 \le q_l^+, q_r^+ \le 1$ and $q_l^- > q_r^+$. That is, we look for the traveling pulse for p and decreasing traveling front for q^+.

Due to (5.5.4) we have

$$j(-\infty) = j(+\infty) = 0. \tag{5.5.5}$$

Applying (5.5.4) and (5.5.5), we obtain an invariant of motion for j and p from the first equation of (5.5.3)

$$j = cp. \tag{5.5.6}$$

Then the system (5.5.3) is reduced to the following two dimensional system by the substitution of (5.5.6)

$$\begin{aligned} (c^2 - s^2)p_z &= \mu p[c - s(2q^+ - 1)], \\ q_z^+ &= -\frac{2\kappa}{s} p(1-q^+)q^+. \end{aligned} \tag{5.5.7}$$

It is obvious that (5.5.7) becomes a singular problem when $c = s$. It is straightforward to show that this singular problem has no solution satisfying the traveling wave ansatz (5.5.4). Hence we assume $c \neq s$ from now on. Then (5.5.7) can be rewritten as

$$\begin{aligned} p_z &= -\alpha p[c - s(2q^+ - 1)], \\ q_z^+ &= -\beta p(1-q^+)q^+. \end{aligned} \tag{5.5.8}$$

where $\alpha = -\dfrac{\mu}{c^2 - s^2}$, $\beta = \dfrac{2\kappa}{s} > 0$. Due to the biological interest, we only consider nonnegative solutions. Hence, we are only interested in those heteroclinic orbits that remains nonnegative, where $p \ge 0$ and $0 \le q^{\pm} \le 1$.

5.5.1 Phase Plane Analysis

It is easy to determine that system (5.5.8) has a continuum of steady state $(0, \theta)$, where $0 \le \theta \le 1$. The Jacobian matrix linearized about the steady state $(0, \theta)$ is

$$J_s = \begin{bmatrix} -\alpha(c - s(2\theta - 1)) & 0 \\ -\beta(1-\theta)\theta & 0 \end{bmatrix}.$$

The eigenvalues of J_s are

$$\lambda_1 = -\alpha\big(c - s(2\theta - 1)\big),\ \lambda_2 = 0. \tag{5.5.9}$$

The corresponding eigenvectors are

$$r_1 = \begin{bmatrix} \lambda_1 \\ -\beta(1-\theta)\theta \end{bmatrix},\ r_2 = \begin{bmatrix} 0 \\ 1 \end{bmatrix}. \tag{5.5.10}$$

When $c \neq s$, we have two cases to consider corresponding to the sign of eigenvalue λ_1.

Case 1. If $c > s > 0$, then $\alpha < 0$. It is easy to determine that $\lambda_1 > 0$ which indicates the steady state $(0, \theta)$ is unstable and there is no nonnegative heteroclinic connection due to the lack of the stable manifold. We thus have that $0 \leq c < s$ is a necessary condition for the existence of a traveling wave and s is then a critical traveling speed. Thus, in the following, we always assume that $c < s$ otherwise stated.

Case 2. If $0 \leq c < s$, then $\alpha > 0$. We first fix traveling speed c and solve $c - s(2\theta^* - 1) = 0$ to get $\theta^* = \frac{c+s}{2s}$. Clearly it follows that $0 < \theta^* < 1$ and we furthermore have the following relation

$$\begin{aligned} &\theta < \theta^* \Rightarrow \lambda_1 < 0, \\ &\theta = \theta^* \Rightarrow \lambda_1 = 0, \\ &\theta > \theta^* \Rightarrow \lambda_1 > 0. \end{aligned} \tag{5.5.11}$$

Next, we are devoted to proving that there exists a pair of equilibria which produce a heteroclinic connection for each fixed c satisfying $0 \leq c < s$. From (5.5.11), it is easy to see that the steady state $(0, \theta)$ with $0 \leq \theta < \theta^*$ has one stable manifold corresponding to eigenvalue $\lambda_1 < 0$ and the steady state $(0, \theta)$ with $\theta^* < \theta < 1$ has one unstable manifold associated with eigenvalue $\lambda_1 > 0$, and the other manifold has a zero eigenvalue and acts in the direction of the q^+ axis $p = 0$. The existence of an unstable manifold as $z \to \infty$ and a stable manifold as $z \to -\infty$ corresponds to the existence of a traveling wave (heteroclinic orbit) connecting the two states.

Note that every steady state $(0, \theta)$ with $0 \leq \theta \leq 1$ has two manifolds one of which is a one dimensional center manifold corresponding to zero eigenvalue λ_2. Since each center manifold is invariant under the flow of the system (5.5.8) and the set $\{(p, q^+) : p = 0, 0 \leq q^+ \leq 1\}$ consists of all steady states and is invariant, hence the center manifold of each steady state is q^+ axis where $0 \leq q^+ \leq 1$. So the heteroclinic connection is only determined by the stable and unstable manifolds corresponding to eigenvalue λ_1 as discussed above.

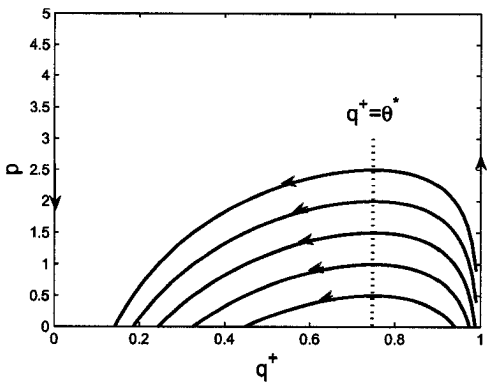

Figure 5.1: The phase portrait for the system (5.5.8), where $c = 1, s = 2, \mu = 2, \kappa = 1$ and consequently $\theta^* = 0.75$. The arrow denotes the orientation of trajectories of the system (5.5.8).

5.5.2 Asymptotics of Solutions

To show that unstable manifold can be connected by stable manifold, we need to investigate the global stability of the original nonlinear system (5.5.8). Below we shall apply LaSall's invariant principle (see Theorem 4.1.8) to study the asymptotics of solutions of the system (5.5.8). We first give the following Lemma which describes the asymptotic behavior of solutions to the system (5.5.8) in the set where $p \geq 0,\ 0 \leq q^+ \leq 1$.

Lemma 5.5.1. *Assume $0 \leq c < s$. Then the ω-limit set of all solutions to the system (5.5.8) is contained in the following set*

$$\mathbb{N} = \{(p, q^+) |\ p = 0,\ 0 \leq q^+ < \theta^*\}, \tag{5.5.12}$$

and α-limit set is contained in the set

$$\mathbb{G} = \{(p, q^+) |\ p = 0,\ \theta^* < q^+ \leq 1\}, \tag{5.5.13}$$

where $\theta^* = \frac{c+s}{2s}$.

Proof. We define a function $V(p, q^+)$ by $V(p, q^+) = q^+$. Then for all z, we can verify from (5.5.8) that $V \geq 0$ and $\frac{dV}{dz} \leq 0$ in the set $\{(p, q^+) |\ p \geq 0, 0 \leq q^+ \leq 1\}$. Moreover, we see that the set $\mathbb{N}_1 = \{(p, q^+) | \frac{dV}{dz} = 0, 0 \leq q^+ \leq 1\}$ consists of the continuum of steady states $(0, \theta)$ only, where $0 \leq \theta \leq 1$. Also $\mathbb{N}_1$ is invariant due to all elements of $\mathbb{N}_1$ are steady states. According to LaSall's invariant principle, all

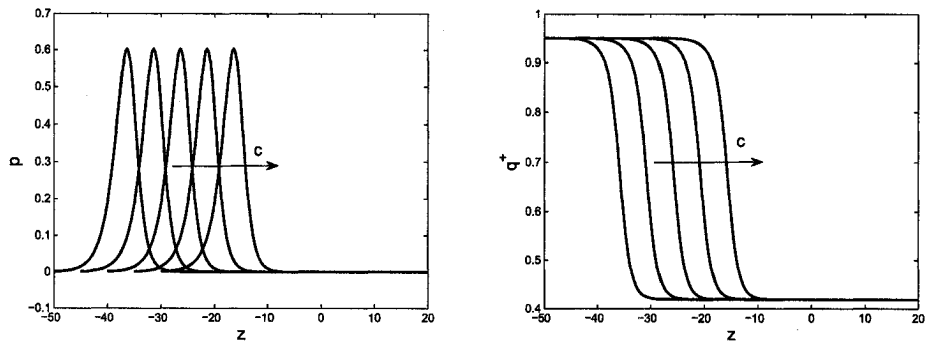

Figure 5.2: The traveling wave for the system (5.5.8), where $c = 1, s = 2, \mu = 2, \kappa = 1$. The waves travel from let to right and c denotes the traveling speed and time $t = 0, 5, 10, 15, 20$.

solutions of system (5.5.8) converge, as $z \to +\infty$, to the set $\mathbb{N}_1$. From the second equation of (5.5.8), we know that

$$\frac{dV}{dz} = 0 \Longleftrightarrow p = 0 \text{ or } q^+ = 0 \text{ or } q^+ = 1.$$

However, from (5.5.11), we know that for all $\theta > \theta^*$ with $\theta^* < 1$, the equilibrium $(0, \theta)$ is unstable and hence all trajectories will emanate out of the equilibrium at $(0, \theta)$ where $\theta > \theta^*$. So the set $\mathbb{N}_1$ excludes the set

$$\mathbb{N}_2 = \left\{ (p, q^+) \middle| \, p = 0, \theta^* \leq q^+ \leq 1 \right\},$$

which implies all solutions of system (5.5.8) converge to the set $\mathbb{N} = \mathbb{N}_1 \setminus \mathbb{N}_2$ as $z \to +\infty$. In a similar fashion, we can prove all solutions of (5.5.8) converge to the set $\mathbb{G}$ as $z \to -\infty$. This completes the proof.

□

Remark 5.4. *It is easy to verify that $q^+ = 0$ or $q^+ = 1$ is a solution of the system (5.5.8) and furthermore it holds that*

(a) If $q^+ = 0$, then $p \to 0$ as $z \to +\infty$.

(b) If $q^+ = 1$, then $p \to +\infty$ as $z \to +\infty$.

Therefore, the orbit neither $q^+ = 0$ nor $q^+ = 1$ can form a heteroclinic connection although $q^+ = 0$ is the unstable manifold of the equilibrium $(0, 1)$ and $q^+ = 0$ is the stable manifold of the equilibrium $(0, 0)$.

5.5.3 *Existence of Traveling Waves*

The Lemma 5.5.1 and the Remark 5.4 show that any trajectory of the system (5.5.8) starting from a neighborhood of an equilibrium $(0,\theta)$ with $\theta^* < \theta < 1$ converges, as $z \to +\infty$, to another equilibrium $(0,\theta)$ with $0 < \theta < \theta^*$, which gives a nonnegative heteroclinic connection (traveling wave) between these two equilibria. We come to our main result of this section.

Theorem 5.9. *Let us consider the system (5.5.8). For each traveling speed c with $0 \le c < s$, there exists a bounded, nonnegative heteroclinic orbit connecting an equilibrium $(0,c_1)$ to the other equilibrium $(0,c_2)$, where $\theta^* < c_1 < 1$ and $0 < c_2 < \theta^*$ with $\theta^* = \frac{c+s}{2s}$. That is, there exists a traveling solution (p,q^+) of system (5.5.8) connecting $(0,c_1)$ and $(0,c_2)$. Particularly, system (5.5.8) admits a standing wave for $c = 0$.*

Proof. The result is a direct consequence of the above analysis. □

Note that the ODE system (5.5.8) has a one dimensional manifold $\{(0,\theta) : 0 \le \theta \le 1\}$ of equilibrium. Therefore, we may expect a family of traveling wave solutions parameterized by the left state q_l^+ of fibre orientation where $\theta^* < q_l^+ < 1$. We need to determine how the right state q_r^+ depends on the left state q_l^+. That is, we need to find the relation between q_l^+ and q_r^+. To this end, we divide the first equation of (5.5.8) by the second equation to obtain that

$$\frac{dp}{dq^+} = -\frac{\alpha(c+s)}{\beta}\frac{1}{(1-q^+)q^+} + \frac{2\alpha s}{\beta}\frac{1}{1-q^+}. \tag{5.5.14}$$

Note that here we assume $q^+ \neq 0$ and $q^+ \neq 1$. Otherwise, there is no traveling wave as discussed in Remark 5.4. Integrating (5.5.14) and recovering α and β yield a first integral

$$p = \frac{\mu s}{2\kappa}\left[\frac{\ln(1-q^+)}{c+s} - \frac{\ln q^+}{c-s}\right] + \sigma_1, \tag{5.5.15}$$

where σ_1 is a constant which can be determined by the initial data of q^+ given in (5.5.4).

The phase portrait can be precisely plotted by using the level curve function defined by (5.5.15) (see Figure 5.1). The plot of traveling solution (p,q^+) of system (5.5.8) is given by Figure 5.2. From the definition of p and the relation (5.5.6) and (5.1.7), it is easy to get

$$p^+ = \frac{s+c}{2s}p,\ p^- = \frac{s-c}{2s}p,\ q^- = 1-q^+,\ j = cp. \tag{5.5.16}$$

which gives the traveling waves in j, p^+, p^- and q^- in terms of p and q^+. The plot of the traveling structures of them are given in Figure 5.3 and Figure 5.4. An example of the standing wave is numerical given in Figure 5.5.

From the equation of (5.5.1), we know that total mass of cells is conserved and so travelling pulse is expected as we found analytically and numerically above. The numerical simulation for p in Figure 5.1 indicates that individual cells can move to left or right, but the whole cell group will move to right continuously. However, when the waves travel through, the fibre orientations are modified by cells and alignment to cell movement direction is enhanced, which is indicated by the numerical simulation for q^+ in Figure 5.1.

Indeed, an explicit heteroclinic connection can be derived from (5.5.15). By the Lemma 5.5.1, it is known that $p(q_l^+) = p(q_r^+) = 0$, which gives rise to

$$\frac{\ln(1-q_l^+)}{c+s} - \frac{\ln q_l^+}{c-s} = \frac{\ln(1-q_r^+)}{c+s} - \frac{\ln q_r^+}{c-s}.$$

Rearranging the above identity yields that

$$\left(\frac{1-q_r^+}{1-q_l^+}\right)^{s-c} = \left(\frac{q_l^+}{q_r^+}\right)^{s+c}, \quad c < s, \tag{5.5.17}$$

which relates the two end states q_l^+ and q_r^+. Given any end state of q^+, the other end state can be determined by (5.5.17).

From the second equation of (5.5.8), we know that the solution q^+ starting from any initial point $q_I^+ (0 < q_I^+ < 1)$ decreases. So q^+ is bounded away from 1 and consequently the term $\frac{\ln(1-q^+)}{c+s}$ is bounded. From Theorem 5.9, we know every trajectory is bounded. Therefore, it is also of interest to find the upper bound for each orbit where $0 < q^+ < 1$. In the following, we will explicitly find the upper bound which depends on the left states q_l^+. Indeed, by (5.5.14), we have a unique critical point $q^+ = \theta^*$ such that $\frac{dp}{dq^+}|_{q^+=\theta^*} = 0$. The second derivative of p with respect to q^+ is

$$\frac{d^2p}{dq^{+2}} = -\frac{\mu s}{2\kappa}\left[\frac{1}{(c+s)(1-q^+)^2} + \frac{1}{(s-c)q^{+2}}\right], \tag{5.5.18}$$

Noting that $0 \leq c < s$. Then it is easy to verify that $\frac{d^2p}{dq^{+2}} < 0$ at $q^+ = \theta^*$. Moreover we know that $p(q_l^+) = p(q_r^+) = 0$. Hence p attains the maximal value at $q^+ = \theta^*$

$$p_{\max} = \frac{\mu s}{2\kappa}\left[\frac{\ln(1-\theta^*)}{c+s} - \frac{\ln\theta^*}{c-s}\right] + \sigma_2, \tag{5.5.19}$$

where

$$\sigma_2 = -\frac{\mu s}{2\kappa}\left[\frac{\ln(1-q_l^+)}{c+s} - \frac{\ln q_l^+}{c-s}\right], \quad \theta^* = \frac{c+s}{2s}. \tag{5.5.20}$$

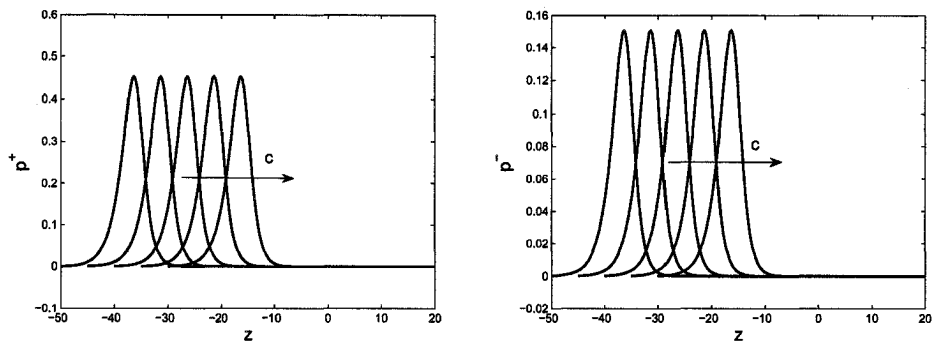

Figure 5.3: The traveling wave of population density p^+ and p^-, where $c = 1, s = 2, \mu = 2, \kappa = 1$. The waves travel from let to right and c denotes the traveling speed and time $t = 0, 5, 10, 15, 20$. Care should taken to the scale used here.

Remark 5.5. *From the above equation, we know that the upper bound* $p_{\max}$ *of* p *depends on the left states* q_l^+ *of* q. *Also, we can easily verify that upper bound* $p_{\max}$ *increases with respect to* $q_l^+ > \theta^* = \frac{c+s}{2s}$ *(see Figure 5.1).*

Remark 5.6. *The results obtained above for traveling waves are only valid for the case of directed tissues. For undirected tissues, there does not exist traveling wave. Indeed, in the undirected case, we know that* $q^+ = q^- = \frac{1}{2}$ *and system (5.5.8) is reduced to a scale equation*

$$p_z = -\alpha c p. \tag{5.5.21}$$

Clearly, there is no solution satisfying boundary conditions (5.5.4) for (5.5.21) and furthermore $p(z) \to +\infty$ *as* $z \to +\infty$.

5.6 No Pattern Formation

In the section 5.3, we prove the global existence of classical solutions to the system (5.1.8). So there is a nature question to system (5.1.8) as a model describing a biological phenomenon: is there pattern formation ? In this section, we will show, with the help of linear stability analysis, that the one-dimensional mesenchymal motion models do not admit pattern formation. Below we briefly discuss the stability of steady state of system (5.1.8).

We first find four homogeneous steady states for system (5.1.8): $S_1 = (0, 0, c_1, 1 - c_1), S_2 = (0, c_2, 0, 1), S_3 = (c_3, 0, 1, 0)$ and $S_4 = (c_4, c_4, \frac{1}{2}, \frac{1}{2})$, where $0 \le c_1 \le 1$ and c_2, c_3, c_4 are positive constants. Let $(p_s^+, p_s^-, q_s^+, q_s^-)$ denote the homogeneous steady

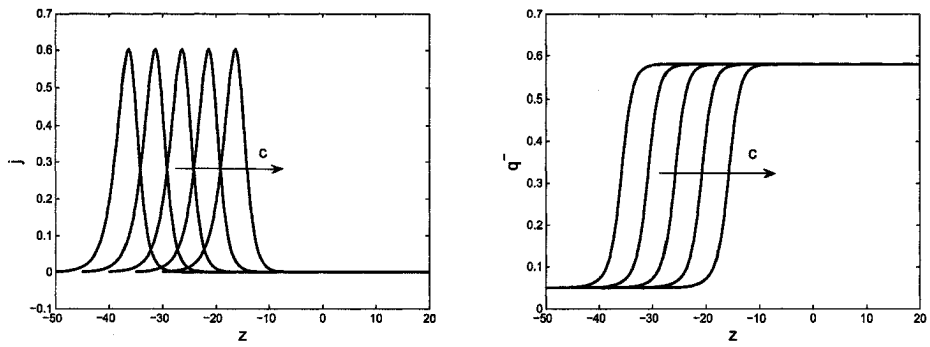

Figure 5.4: The traveling wave of flux j and probability function q^-, where $c = 1, s = 2, \mu = 2, \kappa = 1$. The waves travel from let to right and c denotes the traveling speed and time $t = 0, 5, 10, 15, 20$.

state of (5.1.8). Then the linearization of the system (5.1.8) about the homogeneous steady state is as follows

$$\begin{aligned}
p_t^+ + sp_x^+ &= -\mu p^+ + \mu q_s^+(p^+ + p^-) + \mu q^+(p_s^+ + p_s^-),\\
p_t^- - sp_x^- &= -\mu p^- + \mu q_s^-(p^+ + p^-)\mu q^-(p_s^+ + p_s^-),\\
q_t^+ &= \kappa(p_s^+ - p_s^-)(q_s^- - q_s^+ + 1)q^+ + \kappa(p^+ - p^-)(q_s^- - q_s^+ + 1)q_s^+\\
&\quad +\kappa(p_s^+ - p_s^+)(q^- - q^+)q_s^+,\\
q_t^- &= \kappa(p_s^+ - p_s^-)(q_s^- - q_s^+ - 1)q^- + \kappa(p^+ - p^-)(q_s^- - q_s^+ - 1)q_s^-\\
&\quad +\kappa(p_s^+ - p_s^+)(q^- - q^+)q_s^-.
\end{aligned} \tag{5.6.1}$$

Then the linearization of the above system at the steady state S_1 is

$$\begin{aligned}
p_t^+ + sp_x^+ &= -(1-c_1)\mu p^+ + c_1\mu q^-,\\
p_t^- - sp_x^- &= (1-c_1)\mu p^+ - c_1\mu q^-,\\
q_t^+ &= 2\kappa c_1(1-c_1)(p^+ - p^-),\\
q_t^- &= -2\kappa c_1(1-c_1)(p^+ - p^-).
\end{aligned} \tag{5.6.2}$$

Applying Fourier transform $\hat{}$ to the above system gives rise to

$$\hat{u}_t = A\hat{u},$$

where u and A are given by

$$u = \begin{bmatrix} p^+ \\ p^- \\ q^+ \\ q^- \end{bmatrix}, A = \begin{bmatrix} -isk - (1-c_1) & c_1\mu & 0 & 0 \\ isk + (1-c_1) & -c_1\mu & 0 & 0 \\ 2\kappa c_1(1-c_1) & -2\kappa c_1(1-c_1) & 0 & 0 \\ -2\kappa c_1(1-c_1) & 2\kappa c_1(1-c_1) & 0 & 0 \end{bmatrix}.$$

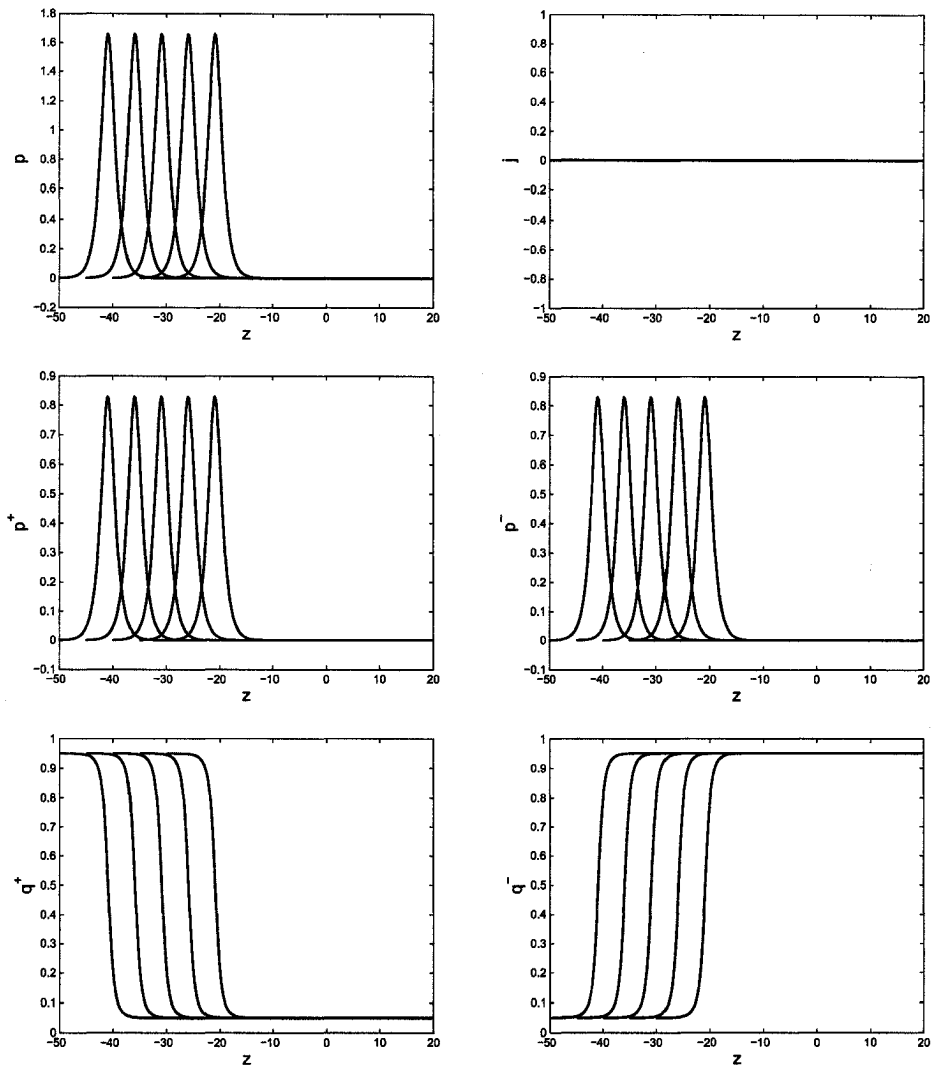

Figure 5.5: An example of a standing wave for system (5.5.8), where $s = 2, \mu = 2, \kappa = 1$ and time $t = 0, 5, 10, 15, 20$.

Here k is the frequency of Fourier transform and i is the imaginary number. It is clear that matrix A has four eigenvalues $\lambda_1 = \lambda_3 = \lambda_4 = 0$ and $\lambda_2 = -c_1\mu < 0$. Hence the steady state S_1 is stable. Using the same argument, we can find eigenvalues for all other three steady states S_2, S_3, S_4 and determine their stability. We summarize the results in the following table.

Steady State	λ_1	λ_2	λ_3	λ_4	Stability
S_1	0	$-c_1\mu$	0	0	Stable
S_2	$-\mu - isk$	isk	$-2c_2\kappa$	$-c_2\kappa$	Stable
S_3	$-isk$	$-\mu + isk$	$-c_3\kappa$	$-2c_3\kappa$	Stable
S_4	$-\mu/2$	0	0	0	Stable

Table 1: Summary of the eigenvalues and stability of steady states for the system (5.1.8), where $\lambda_1, \lambda_2, \lambda_3$ and λ_4 represent the eigenvalues corresponding to steady states S_1, S_2, S_3 and S_4, respectively.

From table 1, we see that all homogeneous steady states are stable to a small spatial perturbation, which implies that there is no pattern formation for the system (5.1.8).

5.7 Conclusions

In this chapter, we establish the global existence of classical solutions to the one dimensional mesenchymal motion models for both directed and undirected tissue. Particularly we show that the model (5.1.9) for undirected tissues in one dimension has a constant solution for fibre orientation distribution such that $q(t, x, +s) = q(t, x, -s) = \frac{1}{2}$, which means cells have no preference in choosing direction to move and have equal probability to move to the right and the left side.

We prove the existence of a weak limit of solutions for parabolic and hyperbolic rescaled equations of the one dimension mesenchymal motion models. Moreover, we study the traveling wave solutions and establish the existence of traveling pulse in total cell population $p(t, x)$ and traveling front waves in fibre orientation distribution $q^{\pm}(t, x)$. The standing wave ($c = 0$) is admitted in our analysis. This is not unexpected since cells can move in two directions (left and right) and two traveling waves with opposite direction can eliminate each other to result in a standing wave. By linear stability analysis, we show that there is no pattern formation for the one dimension mesenchymal motion models.

In paper [47], for a given distribution of fibre orientation $q^{\pm}(t,x)$, the parabolic scaling and hydrodynamic scaling were used to derive the corresponding macroscopic models which describe a population of cells as a whole. These macroscopic models typically take the form of drift-diffusion equations. The parabolic scaling $\xi = \epsilon x, \tau = \epsilon^2 t$ leads to a drift-diffusion equation with diffusion constant s^2/μ and drift velocity $s\mathbb{E}_q$ (see [47])

$$\rho_\tau + (s\mathbb{E}_q(\tau,\xi)\rho)_\xi = \frac{s^2}{\mu}\rho_{\xi\xi}, \tag{5.7.1}$$

which compares to the limit equation (5.4.16) derived in the section 5.4 of this chapter where we consider the coupled system consisting of equations for cell motion and for fibre distribution . Here $\mathbb{E}_q$ represents the mean fibre direction. The hyperbolic scaling $\xi = \epsilon x, \tau = \epsilon t$ gives rise to a pure drift equation drift velocity $s\mathbb{E}_q$

$$\rho_\tau + (s\mathbb{E}_q(\tau,\xi)\rho)_\xi = 0, \tag{5.7.2}$$

which corresponds to the limit equation (5.4.28).

It is worthwhile to point out that one dimensional mesenchymal motion models have significant difference from the higher dimensional models. In one dimension, fibre orientation $q(t,x,\theta)$ only has two direction and hence is bounded due to the normalization condition (5.5.1). However, in higher dimension, fibres have infinite many distributional directions and typically $q(t,x,\theta)$ can be a delta function along unit sphere S^{n-1} by condition (5.5.1). Hence the approaches applied in this chapter does not apply for higher dimensional situation. In a forthcoming paper [58], we will study the existence of solutions for the high dimensional mesenchymal motion models in a measurable Banach space using semigroup theory.

Chapter 6

CONCLUSIONS AND FUTURE WORK

Chemotaxis models and mesenchymal transport equations are studied in this thesis. I establish the global existence of solutions, pattern formation and underlying bifurcation for the volume filling chemotaxis model with a nonlinear squeezing probability which reflects the elastic properties of cells. For a chemotaxis model without transport of chemicals, I fully analyze the shock structures for both the attractive and the repulsive cases. For the one dimensional mesenchymal motion transport model, the qualitative behavior of solutions is analyzed. I show that global classical solutions exist but no pattern formation evolves. In addition, I prove the existence of weak limits of solutions to parabolic and hyperbolic rescaled equations. The existence of traveling wave solutions is established.

In Chapter 2 and Chapter 3, numerical simulations demonstrate a very interesting patterning dynamics: the merging and emerging process. The similar patterning process was also observed in some other chemotaxis models of cancer cell invasion of tissue [18] and a model of turbulence-shear flow interaction [25] as well as the Brusselator model [69]. These models show a complicated interaction of two neighboring maxima that join to form a single maximum (merging). Insertion (emerging) of new maxima arises between two existing maxima. When cell kinetics is zero ($f = 0$), local maxima attract each other and merge into larger and broader maxima (see Figure 2.6(a)). The underlying instability has been investigated by Potapov and Hillen [104], where it is shown that the merging process corresponds to transient dynamics along metastable steady states. In a paper by Dolak and Schmeiser [27], the merging process was analyzed using singular perturbation methods for a small diffusion parameter. Roughly speaking, two local maxima need to be close enough to "feel" each other and come together.

Since the merging and emerging process have appeared in many models which describe different physical or biological phenomena, it would be interesting to provide the underlying mathematical mechanism for these interesting patterns. The mathematical analysis in [27, 104] are very preliminary and a full analysis for the merging and emerging process will be difficult and complicated. Some novel ideas are proposed in [48] to analyze the dynamical behavior, stability of steady states and

periodic orbits as well as asymptotics to these local maxima. Without cell kinetics ($f = 0$), we will prove the critical length l_m for merging will play an important role. When cell kinetics are present ($f \neq 0$), then in addition to the merging we observe the emerging of new local maxima (see Figure 2.7). The emerging of local maxima is driven by a relatively high growth rate in small population density regions. Related to the Lyapunov function given by Wrzosek [124, 125], we expect that the situation is completely different from the case of zero kinetics ($f = 0$). We can not expect these local maxima converge to steady states and the succession of merging and emerging might indicate a chaotic behavior. However, we expect there exists a critical emerging length l_e such that emerging appears only for a distance larger than l_e. The details will be provided in the forthcoming paper [48].

In Chapter 3, I choose another different squeezing probability function $q(u)$ which leads to a singularity in the diffusion component. In spite of open question of global existence, I investigate the pattern formation and the underlying bifurcations. The similar merging and emerging pattern formation as in Chapter 2 are observed. This implies that volume filling chemotaxis model produces a typical patterning process: the merging and emerging process. It is well known that diffusion is a dissipative effect in general and hence global in time solutions should exist. But novel ideas need to be developed to justify this assertion. One possibility is to use a mollifier to smooth the singularity and construct a regularized squeezing probability function q_ϵ. Then I would use standard PDE theory to obtained global existence and uniform boundedness of solutions u_ϵ for the modified system. Eventually I will prove the convergence of the solution u_ϵ as $\epsilon \to 0$.

In Chapter 4, I show that the chemotaxis model of Othmer and Stevens [95] admits a shock structure for both the attractive and the repulsive case, namely, the travelling waves with travelling speed equal to shock speed converge to the shock waves as the viscosity vanishes. This gives the precise information for the limit of travelling waves when viscosity tends to zero. Hence when the viscosity is effectively small, the travelling speed can be approximated by the shock speed that can be easily obtained from Rankine-Hugoniot jump condition, which provide a easier way to estimate the particle travelling speed.

The mesenchymal transport model, introduced by Hillen [47], is analyzed in Chapter 5. The qualitative behavior of the solution to the one dimensional model can be quite well understood. I prove the existence of classical solution and traveling wave solutions, weak limits of solutions for rescaled equations and nonexistence of pattern formation. However, the higher dimensional mesenchymal transport models have significant difference compared to one dimensional case. The primary differ-

ence is the number of directions of fibre orientations. In higher dimension, there are infinite fibre orientations and hence the probability density $q(t, x, \theta)$ can be a delta function $q(\theta) = \delta_b(\theta)$ with respect to θ as the tissues are totally aligned in some direction b. Hence the analysis of L^∞ argument used in [17, 62] is no longer valid for mesenchymal transport models. In a forthcoming paper [58], we think of the orientation distribution q as a signed Borel measures on S^{n-1} and establish the existence of mild and classical solutions in the Banach space of regular signed real-valued Borel measures with total variation norm using semigroup theory of operators. The details are omitted since this work is still in preparation.

As I mentioned in the Introduction, the kinetic transport model can integrate microscopic level information on signal transduction into population level or tissue level models. In the transport equation, the turning kernel, plays a crucial role and determines the complexity and diversity that the macroscopic limits could be. Relying on on specific situation, the turning kernel can depend on the chemical concentration, and the spatial or temporal variation of the chemical concentration. In the model (1.2.6) and (1.2.7) derived by Dolak and Schemeiser [28], the temporal derivative is only formally included into the turning kernel due to the assumptions of uniform boundedness of turn kernel. In paper [117], we will truly include temporal derivative into the turn kernel and establish the global existence of weak solutions and rigorously derive the macroscopic limits in one dimension. For higher dimension, it is still an open question. From our analysis, the estimates for global bound of local solutions are optimally obtained and new techniques are need to be developed to treat higher dimensional case.

BIBLIOGRAPHY

[1] M. Aida, K. Osaki, T. Tsujikawa, A. Yagi, and M. Mimura. Chemotaxis and growth systems with singular sensitivity function. *Nonlinear. Anal. Real World Appl.*, 6:323–336, 2005.

[2] W. Alt. Biased random walk model for chemotaxis and related diffusion approximation. *J. Math. Biol.*, 9:147–177, 1980.

[3] W. Alt. Singular perturbation of differential integral equations describing biased random walks. *J. Reine Angew. Math.*, 322:15–41, 1981.

[4] H. Amann. Dynamic theory of quasilinear parabolic equations iii: Global existence. *Math. Z.*, 202:219–250, 1989.

[5] H. Amann. Dynamic theory of quasilinear parabolic equations ii: Reaction-diffusion systems. *Differential Integral Equations.*, 3:13–75, 1990.

[6] H. Amann. Nonhomogeneous linear and quasilinear elliptic and parabolic boundary value problems. *Function Spaces, Differential Oparators and Nonlinear Analysis, Teubner Texte zur Mathematik*, 133:9–126, 1993.

[7] N. Barkai and S. Leibler. Robustness in simple biochemical networks. *Nature.*, 387:913–917, 1997.

[8] V.M. Becerra. *Lecture notes on Advanced Nonlinear Control CY4A2.* The University of Reading, U.K., 2005.

[9] H.C. Berg. *Random Walks in Biology.* Princeton University Press, Princeton, N.J, 1983.

[10] H.C. Berg and D.A. Brown. Chemotaxis in escherichia coli. analysed by three-dimensional tracking. *Nature.*, 239:500–504, 1972.

[11] P. Biler. Local and global solvability of some parabolic system modeling chemotaxis. *Adv. Math. Sci. Appl.*, 8:715–743, 1998.

[12] P. Biler. Local and global solvability of some parabolic systems modelling chemotaxis. *Advances in Math. Sci. and Appl.*, 8(2):715–743, 1998.

[13] S. Block, J. Segall, and H. Berg. Adaption kinetics in bacterial chemotaxis. *J. Bacteriology*, 154:312–323, 1983.

[14] R. Bourret and A. Stock. Molecular information processing: lessons from bacterial chemotaxis. *J. Biological. Chemistry.*, 277:9625–9628, 2002.

[15] A. Bressan. *Hyperbolic System of Conservation Laws: the One-dimensional Cauchy Problem.* Oxford University Press, New York, 2001.

[16] H. Byren and M. Chaplain. Mathematical models for tumour angiogenesis-numerical simulations and nonlinear-wave equations. *Bull. Math. Biol.*, 57:461–485, 1995.

[17] F. Chalub, P.A. Markowich, B. Perthame, and C. Schmeiser. Kinetic models for chemotaxis and their drift-diffusion limits. *Monatsh. Math.*, 142:123–141, 2004.

[18] M. Chaplain and G. Logas. Mathematical modelling of cancer cell invasion of tissue: the role of the urokinase plasminogen activation system. *Math. Models Methods Appl. Sci.*, 15:1685–1734, 2005.

[19] K.C. Chen, R.M. Ford, and P.T. Cummings. Mathematical models for motile bacterial transport in cylindrical tubes. *J. Theor. Biol.*, 195:481–504, 1998.

[20] S. Childress. Chemotactic collapse in two dimensions. *Lecture Notes in Biomath.*, 55:61–68, 1984.

[21] S. Childress and J.K. Percus. Nonlinear aspects of chemotaxis. *Math. Biosci.*, 56:217–237, 1981.

[22] L. Corrias and B. Perthame. Critical space for the parabolic-parabolic keller-segel model in $\mathbb{R}^d$. *C. R. Math. Acad. Sci. Paris*, 342:745–750, 2006.

[23] L. Corrias, B. Perthame, and H. Zaag. Global solutions of some chemotaxis ans angiogenesis systems in high space dimensions. *Milan J. Math.*, 72:1–29, 2004.

[24] Q. Dautray and J.L. Lions. *Mathematical analysis and numerical methods for sciences and technology.* Springer, 1990.

[25] D. del Castillo-Negrete and B.A. Carreras. Stratified shear flows in a model of turbulence-shear interaction. *Phys. Plasmas*, 9:118–127, 2002.

[26] O. Diekmann and N.M. Temme. *Nonlinear Diffusion Problems.* Mathematisch Centrum Amsterdam, 1976.

[27] Y. Dolak and C. Schmeiser. The Keller-Segel model with logistic sensitivity function and small diffusivity. *SIAM J. Appl. Math.*, 66:286–308, 2005.

[28] Y. Dolak and C. Schmeiser. Kinetic models for chemotaxis: Hydrodynamic limits and spatio-temporal mechanics. *J. Math. Biol.*, 51:595–615, 2005.

[29] R. Erban and H.J. Hwang. Global existence results for complex hyperbolic models of bacterial chemotaxis. *Discrete Contin. Dyn. Syst. Ser. B*, 6:1239–1260, 2006.

[30] R. Erban, I. Kevrekidis, and H. Othmer. An equation free computational approach for extracting population level behavior from individual based models of biological dispersal. *Phys D.*, 215:1–24, 2006.

[31] R. Erban and H. Othmer. From individual to collective behavior in bacterial chemotaxis. *SIAM J. Appl. Math.*, 65(2):361–391, 2004.

[32] R. Erban and H. Othmer. From signal transduction to spatial pattern formation in *E. coli*: a paradigm for multiscale modeling in biology. *Multiscale Model. Simul.*, 3(3):362–394, 2005.

[33] R. Erban and H. Othmer. Taxis equations for amoeboid cells. *J. Math. Biol.*, 54:847–885, 2007.

[34] L.C. Evans. *Partial Differential Equations.* AMS, Providence, Rhode Island, 1997.

[35] E. Feireisl, P. Laurencot, and H. Petzeltova. On convergence to equilibria for the keller-segel chemotaxis mode. *J. Diff. Eqn*, 236:551–569, 2007.

[36] R. Firtel. Dictyostelium cinema. *http://www-biology.ucds.edu/~firtel/movies.html*, 1990.

[37] P. Friedl, S. Borgmann, and E. Brocker. Amoeboid leuckocyte crawling through extracelluer matrix: lessons from the *dictyostelium* paradigm of cell movement. *J. Leuk. Biol*, 38:359–375, 1999.

[38] P. Friedl and E.B. Bröcker. The biology of cell locomotion within three dimensional extracellular matrix. *Cell Motility Life Sci.*, 57:41–64, 2000.

[39] H. Gajewski and K. Zacharias. Global behavior of a reaction-diffusion system modelling chemotaxis. *Math. Nachr.*, 195:77–114, 1998.

[40] S. Goldstein. On diffusion by discontinuous movements and the telegraph equation. *Quart. J. Mech. Appl. Math.*, 4:129–156, 1951.

[41] K.P. Hadeler. Reaction transport systems in biological modelling. In V. Capasso and O. Diekmann, editors, *Mathematics Inspired by Biology*, Lect. Notes Math. 1714, pages 95–150, Heidelberg, 1999. Springer Verlag.

[42] M.A. Herrero and J.J.L. Velázeuez. Chemotactic collapse for the keller-segel model. *J. Math. Biol.*, 35:177–194, 1996.

[43] M.A. Herrero and J.J.L. Velázeuez. Singularity patterns in a chemotaxis model. *Math. Ann.*, 306:583–623, 1996.

[44] M.A. Herrero and J.J.L. Velázeuez. A blow-up mechanism for a chemotaxis model. *Ann. Scuola Norm. Sup. Pisa Cl. Sci.*, 24:633–683, 1997.

[45] J.P. Hespanha. Uniform stability of switched linear systems: Extensions of lasalle's invariant principle. *IEEE transactions on Automatic Control.*, 49(4):470–482, 2004.

[46] T. Hillen. Invariant principle for hyperbolic random walk systems. *J. Math. Anal. Appl*, 210:360–374, 1997.

[47] T. Hillen. M^5 mesoscopic and macroscopic models for mesenchymal motion. *J. Math. Biol.*, 53:585–616, 2006.

[48] T. Hillen, M. Chaplian, K. Painter, and Z. Wang. Mathematical analysis for merging and emerging patterns. *In preparation*, 2007.

[49] T. Hillen and L. Levine. Blow-up and pattern formation in hyperbolic models for chemotaxis in $1-D$. *Z. Angew. Math. Phys.*, 54:839–868, 2003.

[50] T. Hillen and H. Othmer. The diffusion limit of transport equations derived from velocity jump processes. *SIAM J. Appl. Math.*, 61(3):751–775, 2000.

[51] T. Hillen and K. Painter. Global existence for a parabolic chemotaxis model with prevention of overcrowding. *Adv. Appl. Math.*, 26:280–301, 2001.

[52] T. Hillen and K. Painter. A users guide to pde models for chemotaxis. *Submitted*, 2007.

[53] T. Hillen, K. Painter, and C. Schmeiser. Global existence for chemotaxis with finite sampling radius. *Discr. Cont. Dyn. Syst. B.*, 7(1):125–144, 2007.

[54] T. Hillen and A. Potapov. Global existence for the classical chemotaxis model in $1-D$. *Math. Meth. Appl. Sci.*, 27:1783–1801, 2004.

[55] T. Hillen, J. Renclawowicz, and Z. Wang. Analysis of an attraction-repulsion chemotaxis model. *In preparation*, 2007.

[56] T. Hillen, C. Rohde, and F. Lutscher. Existence of weak solutions for a hyperbolic model for chemosensitive movement. *J. Math. Anal. Appl.*, 260:173–199, 2001.

[57] T. Hillen and A. Stevens. Hyperbolic models for chemotaxis in $1-D$. *Nonlinear Analysis: Real World Applications*, 1(1):409–433, 2001.

[58] P. Hinow, T. Hillen, and Z. Wang. Analysis of the mesenchymal tranpsort model. *In preparation*, 2007.

[59] D. Hortsmann. The nonsymmetric case of the keller-segel model in chemotaxis: some recent results. *Nonlinear Differential Equations and Applications (NoDEA).*, 8:399–423, 2001.

[60] D. Hortsmann. From 1970 until present: the keller-segel model in chemotaxis and its consequences: I. *Jahresber. Deutsch. Math.-Verein*, 105:103–165, 2003.

[61] D. Hortsmann. From 1970 until present: the keller-segel model in chemotaxis and its consequences: II. *Jahresber. Deutsch. Math.-Verein*, 106:51–69, 2004.

[62] H.J. Hwang, K. Kang, and A. Stevens. Drift-diffusion limits of kinetic models for chemotaxis: a generalization. *Discrete Contin. Dyn. Syst. Ser. B*, 5:319–334, 2005.

[63] H.J. Hwang, K. Kang, and A. Stevens. Global solutions of nonlinear transport equations for chemosensitive movement. *SIAM J. Math. Anal.*, 36:1177–1199, 2005.

[64] H.J. Hwang, K. Kang, and A. Stevens. Global existence of classical solutions for a hyperbolic chemotaxis model and its parabolic limit. *Indiana Univ. Math. J.*, 55:289–316, 2006.

[65] W. Jäger and S. Luckhaus. On explosions of solutions to a system of partial differential equations modelling chemotaxis. *Trans. AMS*, 329:819–824, 1992.

[66] M. Kac. A stochastic model related to the telegrapher's equation. *Rocky Mountain J. Math.*, 4:497–509, 1956.

[67] E.F. Keller and L.A. Segel. Initiation of slime mold aggregation viewd as an instability. *J. Theor. Biol.*, 26:399–415, 1970.

[68] E.F. Keller and L.A. Segel. Model for chemotaxis. *J. Theor. Biol.*, 30:225–234, 1971.

[69] T. Kolokolnikov, T. Erneux, and J. Wei. Mesa-type patterns in the one-dimensional brusselator and their stability. *Physica D.*, 214:63–77, 2006.

[70] R. Kowalczyk. Preventing blow-up in a chemotaxis model. *J. Math. Anal. Appl.*, 305:566–588, 2005.

[71] O.A. Ladyžhenskaja, V.A. Solonnikov, and N.N. Ural'ceva. *Linear and Quasi-linear Equations of Parabolic Type.* AMS Providence, Rhode Island, 1968.

[72] J.P. LaSalle. *The Stability of Dynamical Systems, ser. Regional conference series in applied mathematics.* Society for Industrial and Applied Mathematics, 1976.

[73] P.G. LeFloch. *Hyperbolic System of Conservation Laws: the Theory of Classical and Nonclassical Shock Waves, Lectures in mathematics.* ETH Zürich, Birkhäuser Verlag, Basel-Boston-Berlin, 2002.

[74] R.J. LeVeque. *Numerical Methods for Conseravtion Laws.* Birkhäuser, Basel, 1992.

[75] H.A. Levine and B.D. Sleeman. A system of reaction diffusion equations arising in the theory of reinforced random walks. *SIAM J. Appl. Math.*, 57:683–730, 1997.

[76] G.M. Lieberman. *Second order parabolic differential equations.* World Scientific, Singapore, 1996.

[77] C.S. Lin, W.M. Ni, and I. Takagi. Large amplitude stationary solutions to a chemotaxis system. *J. Diff. Eqn.*, 72:1–27, 1988.

[78] M. Luca, A. Chavez-Ross, L. Edelstein-Keshet, and A. Mogilner. Chemotactic signaling, microglia, and Alzheimer's disease senile plaques: is there a connection? *Bull. Math. Biol.*, 65(4):693–730, 2003.

[79] H. Matano. Convergence of solutions of one-dimensional semilinear parabolic equations. *J. Math. Kyoto. Univ*, 18:221–227, 1978.

[80] J.B. Mcleod. Stability of the separable solution for fast diffusion. *Arch. Ration. Mech. Anal*, 74:379–388, 1980.

[81] T. Mimura and T. Tsujikawa. Aggregating pattern dynamics in a chemotaxis model including growth. *Physica D.*, 230:499–543, 1996.

[82] J.D. Murray. *Mathematical Biology.* Springer, 1989.

[83] T. Nagai. Blow-up of radially symmetric solutions to a chemotaxis system. *Adv. Math. Sci. Appl.*, 5:581–601, 1995.

[84] T. Nagai. Behavior of solutions to a parabolic-ellptic system modeling chemotaxis. *J. Korean Math. Soc*, 37:721–733, 2000.

[85] T. Nagai. Blow-up of nonradial solutions to parabolic-ellptic systems modeling chemotaxis in two-dimensioncal domains. *J. Inequal. Appl.*, 6:37–55, 2001.

[86] T. Nagai and T. Senba. Behavior of radially symmetric solutions of a system related to chemotaxis. *Nonlinear Analysis.*, 30:3837–3842, 1997.

[87] T. Nagai and T. Senba. Global existence and blow-up of radial solutions to a parabolic-elliptic system of chemotaxis. *Adv. Math. Sci. Appl.*, 8:145–156, 1998.

[88] T. Nagai, T. Senba, and T. Suzuki. Chemotaxis collapse in a parabolic system of mathematical biology. *Hiroshima Math. J.*, 30:463–497, 2000.

[89] T. Nagai, T. Senba, and K. Yoshida. Application of the Trudinger-Moser inequality to a parabolic system of chemotaxis. *Funkcialaj Ekvacioj.*, 40(3):411–433, 1997.

[90] V. Nanjundiah. Chemotaxis, signal relaying and aggregation morphology. *J. Theor. Biol.*, 42:63–105, 1973.

[91] K. Osaki, T. Tsujikawa, A. Yagi, and M. Mimura. Exponential attractor for a chemotaxis-growth system of equations. *Nonlinear Anal.*, 51:119–144, 2002.

[92] K. Osaki and A. Yagi. Finite dimensional attractor for one-dimensional Keller-Segel equations. *Funkcialaj Ekvacioj*, 44:441–469, 2001.

[93] H. Othmer, S.R. Dunbar, and W. Alt. Models of dispersal in biological systems. *J. Math. Biol.*, 26:263–298, 1988.

[94] H. Othmer and T. Hillen. The diffusion limit of transport equations II: Chemotaxis equations. *SIAM J. Appl. Math.*, 62(4):1122–1250, 2002.

[95] H. Othmer and A. Stevens. Aggregation, blowup and collapse: The ABC's of taxis in reinforced random walks. *SIAM J. Appl. Math.*, 57:1044–1081, 1997.

[96] W. Page. Personal communication. *Department of Biology, University of Alberta*, 2007.

[97] K. Painter. Multiscale modeling of individual cell migration strategies in the extracelluar matrix. *In preparation*, 2007.

[98] K. Painter and T. Hillen. Volume-filling and quorum-sensing in models for chemosensitive movement. *Canadian Appl. Math. Quart.*, 10(4):501–543, 2002.

[99] K. Painter, P.K. Maini, and H. Othmer. Development and application of a model of cellular response to multiple chemical cues. *J. Math. Biol.*, 41(4):285–314, 2000.

[100] K. Painter, H. Othmer, and P.K. Maini. Stripe formation in juvenile pomacanthus via chemotactic response to a reaction-diffusion mechanism. *Proc. Natl. Acad. Sci. USA.*, 96:5549–5554, 1999.

[101] C.S. Patlak. Random walk with persistence and external bias. *Bull. Math. Biophys.*, 15:311–338, 1953.

[102] B. Perthame. Mathematical tools for kinetic equations. *Bull. Amer. Math. Soc.*, 41(2):205–244, 2004.

[103] B. Perthame. *Transport equations in biology.* Birkhäuser Verlag, Basel, 2007.

[104] A. Potapov and T. Hillen. Metastability in chemotaxis models. *J. Dynamics Diff. Eq.*, 17, 2005.

[105] W. Rascle. Sur une eqúation integro-differentielle non lineaire issue de la biologie. *J. Diff. Eqn.*, 32:420–453, 1979.

[106] M.A. Rivero, R.T. Tranquillo, H.M. Buettner, and D.A. Lauffenburger. Transport models for chemotactic cell populations based on individual cell behavior. *Chem. Eng. Sci.*, 44:1–17, 1989.

[107] J.C. Robinson. *Infinite-Dimesnsional Dynamical Systems: an introduction to dissipative parabolic PDEs and the theory of global attractors.* Cambridge University Press, Cambridge, 2001.

[108] J. Salyers and D. Whitt. *Microbiology, Diversity, Disease and the Environment.* Fitzgerald Science Press, 2001.

[109] R. Schaaf. Stationary solutions of chemotaxis systems. *Trans. AMS*, 292(2):531–556, 1985.

[110] T. Senba and T. Suzuki. Local and norm behavior of blow-up solutions to a parabolic system of chemotaxis. *J. Korean Math. Soc.*, 37:929–941, 2000.

[111] T. Senba and T. Suzuki. Some structures of the solution set for a statioanry system of chemotaxis. *Adv. Math. Sci. Appl.*, 10:191–224, 2000.

[112] R.D. Skeel and M. Berzins. A method for the spatial discretization of parabolic equations in one space variable. *SIAM J. Sci. Statist. Comput*, 11:1–32, 1990.

[113] B.D. Sleeman, M. Ward, and J. Wei. Existence, stability, and dynamics of spike patterns in a chemotaxis model. *SIAM J. Appl. Math.*, 65:790–817, 2005.

[114] J. Smoller. *Shock Waves and Reaction–Diffusion Equations.* Springer-Verlag, Berlin, 1983.

[115] P. Spiro, J. Parkinson, and H. Othmer. A model of excitation and adaption in bacterial chemotaxis. *Proceedings of the Natioanl Academy of Sciences, USA.*, 94:7263–7268, 1997.

[116] A. Stevens. Derivation of chemotaxis-equations as limit dynamics of moderately interacting stochastic many particle systems. *SIAM J. Appl. Math.*, 61:183–212, 2000.

[117] A. Stevens and Z. Wang. Global existence and macrocsopic limits of a kinetic model chamotaxis with internal state. *In preparation*, 2007.

[118] M. Struwe and G. Tarantello. On multivortex solutions in chern-simons gauge theory. *Bull. U. M. I.*, 8:109–121, 1998.

[119] T. Suzuki. *Free energy and self-interaction particles.* Birkhäuser, Boston, 2005.

[120] R Tyson, S.R. Lubkin, and J. Murray. A minimum mechanism for bacterial pattern formation. *Proc. Roy. Soc. Lond. B. Bio.*, 266:299–304, 1999.

[121] R. Tyson, S.R. Lubkin, and J. Murray. Models and analysis of chemotactic bacterial patterns in a liquid medium. *J. Math. Biol.*, 266:299–304, 1999.

[122] G. Wang and J. Wei. Steady state solutions of a reaction-diffusion syatem modeling chemotaxis. *Math. Nachr.*, 233/234:221–236, 2002.

[123] D.D. Woodward, R. Tyson, M.R. Myerscough, J.D. Murray, E. Budrene, and H.C. Berg. Spatio-temporal patterns generated by *Salmonella typhimurium. Biophys. J.*, 68:2181–2189, 1995.

[124] D. Wrzosek. Global attractor for a chemotaxis model with prevention of overcrowding. *Nonlinear Anal.*, 59:1293–1310, 2004.

[125] D. Wrzosek. Long time behaviour of solutions to a chemotaxis model with volume filling effect. *Proc. Roy. Soc. Edinburgh Sect. A*, 136:431–444, 2006.

[126] Y. Yang, H. Chen, and W. Liu. On existence of global solutions and blow-up to a system of the reaction-diffusion equations modelling chemotaxis. *SIAM J. Math. Anal.*, 33:763–785, 2001.

[127] Y. Yang, H. Chen, W. Liu, and B.D. Sleeman. The solvability of some chemotaxis systems. *J. Diff. Eqn.*, 212:432–451, 2005.